Title

Characterization of a Pharmacological Tool for Functional Studies of KV2 Channels

Author

Marquis, Matthew James

Publication Date

2024

Peer reviewed|Thesis/dissertation

Characterization of a Pharmacological Tool for Functional Studies of K_V2 Channels

By

MATTHEW JAMES MARQUIS
DISSERTATION

Submitted in partial satisfaction of the requirements for the degree of

DOCTOR OF PHILOSOPHY

in

Biochemistry, Molecular, Cellular, and Developmental Biology

in the

OFFICE OF GRADUATE STUDIES

of the

UNIVERSITY OF CALIFORNIA

DAVIS

Approved:

Jon Sack, Chair

Jie Zheng

Tsung-Yu Chen

Committee in Charge

2024

Acknowledgments and Dedication

The findings presented here were made possible by the kind mentorship of Dr. Jon Sack and Dr. Vladimir Yarov-Yarovoy.

This dissertation is dedicated to my grandparents: Dr. David Maley Marquis, Dr. Marilyn Grace Alder, Robert Francis Miller, and Dolores “Cookie” Jean Hidalgo.

Permissions

Licenses for reproduction of previously published work can be found in Appendix II.

Abstract

Voltage-gated K^+ channels are widely expressed controllers of cellular behavior. Each channel has a gate between the cytosol and its K^+ conductive pore to control the flow of potassium. Small molecules that enter through this gate can block the pore. The interface between a channel and its blocker may change during pore closure, producing channel-state-biased blocker affinity or, equivalently, bias of channel state by bound blockers. My findings suggest that RY785, a small molecule which inhibits $K_V2.1$ voltage-gated K^+ channels, enters through the cytosolic gate and has biased affinity for closed channels. $K_V2.1$ channels may include $K_V8.1$ subunits which affect the structure and gating of the pore. I also find that RY785 exhibits a similar mechanism of inhibition for $K_V2.1/K_V8.1$ channels but with much lower affinity. Interestingly, the voltage dependence of RY785 inhibition suggests opening the cytosolic gate of $K_V2.1$ is not sufficient to permit K^+ conduction and that heteromerization with $K_V8.1$ reduces closure of this gate.

In addition to my work on potassium channel pharmacology, I include as an appendix a reflection on my experience designing and teaching an undergraduate seminar on modern ion channel research. This reflection was composed in partial satisfaction of the requirements for obtaining a graduate academic certificate in undergraduate education. This scholarly effort yielded proof-of-concept that undergraduate students benefit from instruction on how to locate and analyze original scientific research articles and produced template instructional materials.

Table of Contents

Chapter 1: Mechanisms of Ion Channel Inhibitors

Foreword

This chapter introduces general principles of voltage-gated and state-biased blockade of ion channels and alternative mechanisms by which channel activity can be modulated. These principles are critical in the following chapters which will present evidence that RY785 has gated access to its binding site and acts via state-biased blockade. This chapter is a reproduction of a chapter that I co-authored with my mentor, Jon Sack, for a reference text[1] on fundamental principles of ion channel function and the study thereof. It is a substantial revision of a chapter from an earlier reference text[2]. I contributed figures numbered 6.4 and 6.5, much of the text in sections 6.6 and 6.9, and various edits throughout the other figures and text. This material covers topics including gated inhibitor access to the pore lumen, state-biased affinity while blocking, and allosteric inhibition.

6

Ion Channel Inhibitors

Matthew J. Marquis and Jon T. Sack

CONTENTS

6.1 Mechanisms of Inhibition

Ion channel inhibitors can test a hypothesis or save a life. There is a broad chemical palette of ion channel inhibitors: metal ions, alkaloids, synthetic drugs, venom peptide toxins and endogenous modulatory proteins. These inhibitors act by various mechanisms. Blocker is scientific vernacular for inhibitor. In the context of ion channels, the term blocker can conjure up the imagery of a plugged pore, and many channel inhibitors act in such a fashion. However, not all ion channel inhibitors block the pore, and the term lends itself to imprecise use. To avoid semantic confusion here, the term pore blocker connotes a drug that itself occludes the ionic conduction pathway. A mechanistic alternative to pore blockade is allosteric inhibition, where an inhibitor causes a channel to close itself. Allosteric inhibition is also referred to as gating modification or self block. These two mechanisms, depicted in Figure 6.1, describe the fundamental workings of many ion channel inhibitors.

Inhibitors can work by a combination of both pore blockade and allosteric inhibition. An additional inhibitory mechanism involves prevention of a stimulus from acting on a channel, e.g., competitive steric displacement of an agonist by an antagonist. Competitive inhibition is not addressed explicitly in this chapter, as it is comprehensively treated in many other texts (Hilal-Dandan, Brunton, and Goodman 2013; Wyman and Gill 1990). Topics more unique to ion channels are considered here: the physics of pore blockade and gating modulation, with particular focus on how the transmembrane voltage can influence inhibitor efficacy.

DOI: 10.1201/9781003096214-7

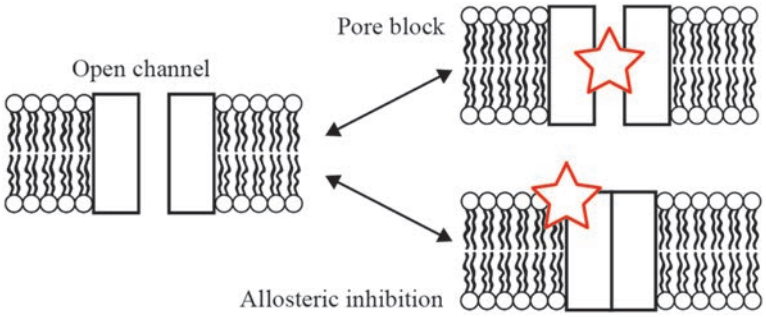

FIGURE 6.1
Types of inhibitors. Pore block results from inhibitors binding in the pore to occlude ion permeation. Allosteric inhibition results from inverse agonists that cause an open channel to close.

6.2 Pore Blockers

The inhibitory mechanism of pore blockers is intuitive: occlusion of the permeant ion path. Ion channel pore blockers play important roles in research and medicine. Tetrodotoxin is produced by symbiotic bacteria in poisonous creatures including puffer fish and newts. Tetrodotoxin blocks the pore of sodium channels and is used in physiology research to suppress sodium currents. Many venomous creatures make pore-blocking peptide toxins that researchers use to identify ion channel types. A peptide toxin from cone snail venom, ziconotide, is a pain therapeutic. The anesthetics phencyclidine and ketamine are NMDA receptor pore blockers. Inadvertent pore block of the hERG potassium channel by drugs such as terfenadine can trigger sudden cardiac death. The expanding pharmacopeia of ion channel pore blockers is far too large to be discussed in a single chapter, so we concern ourselves here with the mechanism of inhibition, which for all pore blockers is essentially the same: binding of the blocker blocks the ion conduction path.

In its simplest form, the concentration–inhibition relation of pore block is described by the physics of classical ligand–receptor interaction. To many physiologists, the relevant term is the fraction of channels that remain conducting at equilibrium, $f_{unblocked}$. For the simple process of an inhibitor blocking the pore of a channel, depicted in Figure 6.2a, this fraction is determined by the inherent dissociation rate, k_{off}, and an association rate constant, k_{on}, that is first-order with respect to the chemical activity of the inhibitor, which we will refer to as the inhibitor concentration, [X]:

$$\frac{f_{unblocked}}{f_{blocked}} = \frac{k_{off}}{k_{on}[X]} \tag{6.1}$$

The rate constants k_{off} and k_{on} differ for each inhibitor–channel pair and in some cases can be measured directly. The ratio of the dissociation and association rate constants yields the dissociation constant, K_D:

$$K_D = \frac{k_{off}}{k_{on}[X]} \tag{6.2}$$

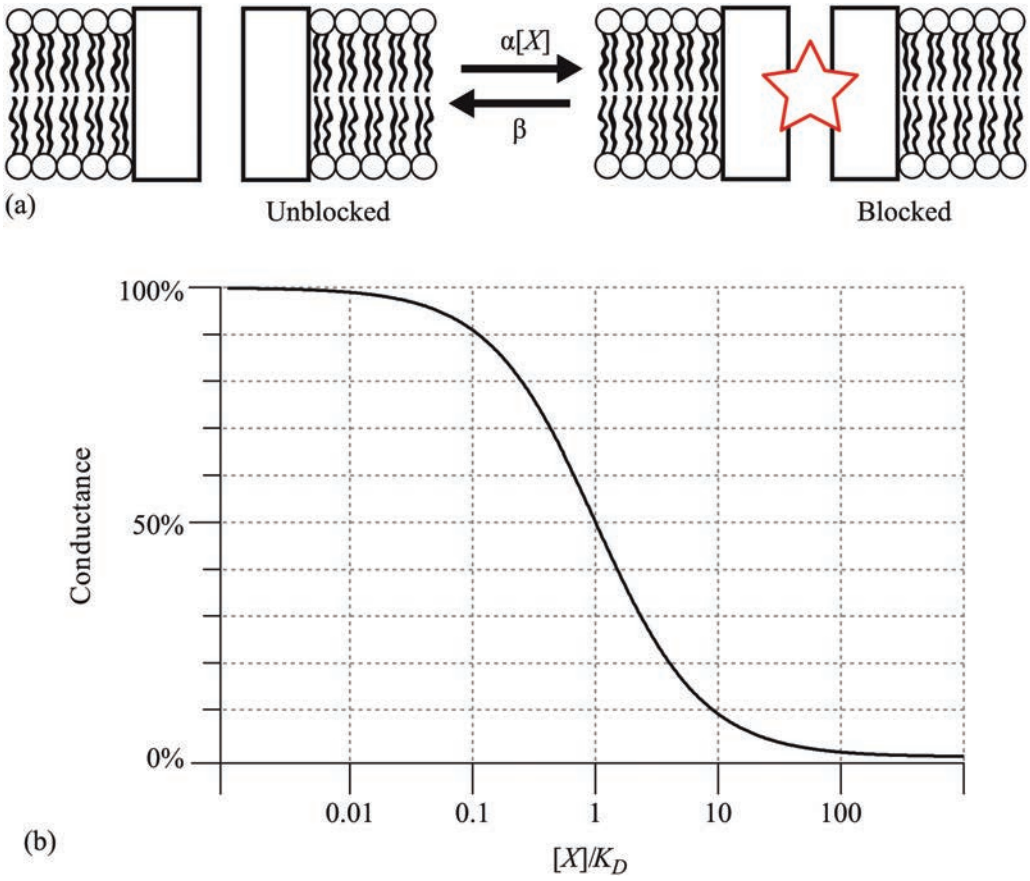

FIGURE 6.2
Pore blocker dose–response. (a) The fraction of channels blocked is determined by an association rate dependent on inhibitor concentration and an intrinsic dissociation rate. (b) When at equilibrium with a single binding site, a pore blocker will inhibit ionic conductance as a function of its concentration, [X]; and dissociation constant, K_D. Curve is plot of Equation 6.3.

The K_D has units of concentration and is a useful value to develop intuition about concentration dependence. In the case of a pore blocker that binds channels in a 1:1 fashion, the K_D is the concentration where 50% of channels will be inhibited, or IC_{50}, making it a straightforward measurable quantity. The K_D is sufficient to describe the concentration–response of the system at equilibrium.

$$\text{Conductance} = \frac{f_{\text{unblocked}}}{f_{\text{unblocked}} + f_{\text{blocked}}} = \frac{1}{1+\left([X]/K_D\right)} \tag{6.3}$$

A plot of Equation 6.3 demonstrates the dependence of channel block on the concentration of inhibitor (Figure 6.2b). Equation 6.3 is variously referred to as the law of mass action, a Langmuir binding isotherm or Hill logistic with a coefficient of 1. Note that there is a broad concentration range of inhibitor action, with five orders of magnitude increase in inhibitor concentration to span the conductance decrement from 1% inhibition to 99% inhibition (Figure 6.2b). One can never fully inhibit a current, but only approach a saturating

value. Thus, when determining what inhibitor concentration to use, consideration needs to be given to how much remaining current is tolerable.

6.3 Perturbation of Pore Block

Structural analyses of blocked ion channels have illuminated atomic-level details of the pore blockade mechanism. These details include which features of the inhibitor form stabilizing interactions with the channel as well as where the inhibitor sits relative to the ions that permeate the channel pore. Structurally, pore blockers are indeed found to be blocking the ion path (Figure 6.3a–c). Consequently, the binding of pore blockers is impacted by permeant ions. The interactions between permeant ions and pore blockers can be quite complex. Importantly, the effects of permeant ions are dynamic. Ion channels open and close, changing the access of permeant ions in solution to blocker sites and hence modulating their effects on inhibitors. Additionally, transmembrane voltage change impacts permeant ions and can exert force on charged blockers directly. The effects of permeant ions and voltage change can dramatically alter the degree of inhibition by an ion channel blocker.

To quantitate the impact of a physical perturbation on the binding of a pore blocker, it is useful to calculate changes in binding energy. Permeant ions and voltage change the energy of the blocked state to make it more or less favorable. The amount of binding energy for a simple pore block is described by Equation 6.4:

$$\Delta G_{blocked} = -k_B T \ln\left(\frac{[X]}{K_D}\right) \tag{6.4}$$

where

$\Delta G_{blocked}$ is the Gibbs free energy for binding
k_B is the Boltzmann constant.
T is the absolute temperature.
ln is a logarithm with base e.

Note that binding energy does not saturate at any concentration. This is due to the binding rates of the blocker continuing to increase as concentration is increased.

When a blocker's binding is altered by a change of some kind, its binding energy will change. We can call ΔG_p a perturbation of inhibitor binding energy, and determine its impact on $\Delta G_{blocked}$:

$$\Delta G_{blocked} = \Delta G^0_{blocked} + \Delta G_p \tag{6.5}$$

$\Delta G^0_{blocked}$ is the energy of inhibitor binding before perturbation. This energetic formulation can describe the effect of many perturbations: voltage changes, ionic concentration, effects of temperature and other factors. Under physiological conditions, voltage and ionic concentration can be relevant perturbations. Effects of the concentration of competitive ligands are treated comprehensively elsewhere (Hilal-Dandan, Brunton, and Goodman 2013; Wyman and Gill 1990). The effect of voltage on block of ion □ow is a phenomenon unique to ion channels and is considered further here.

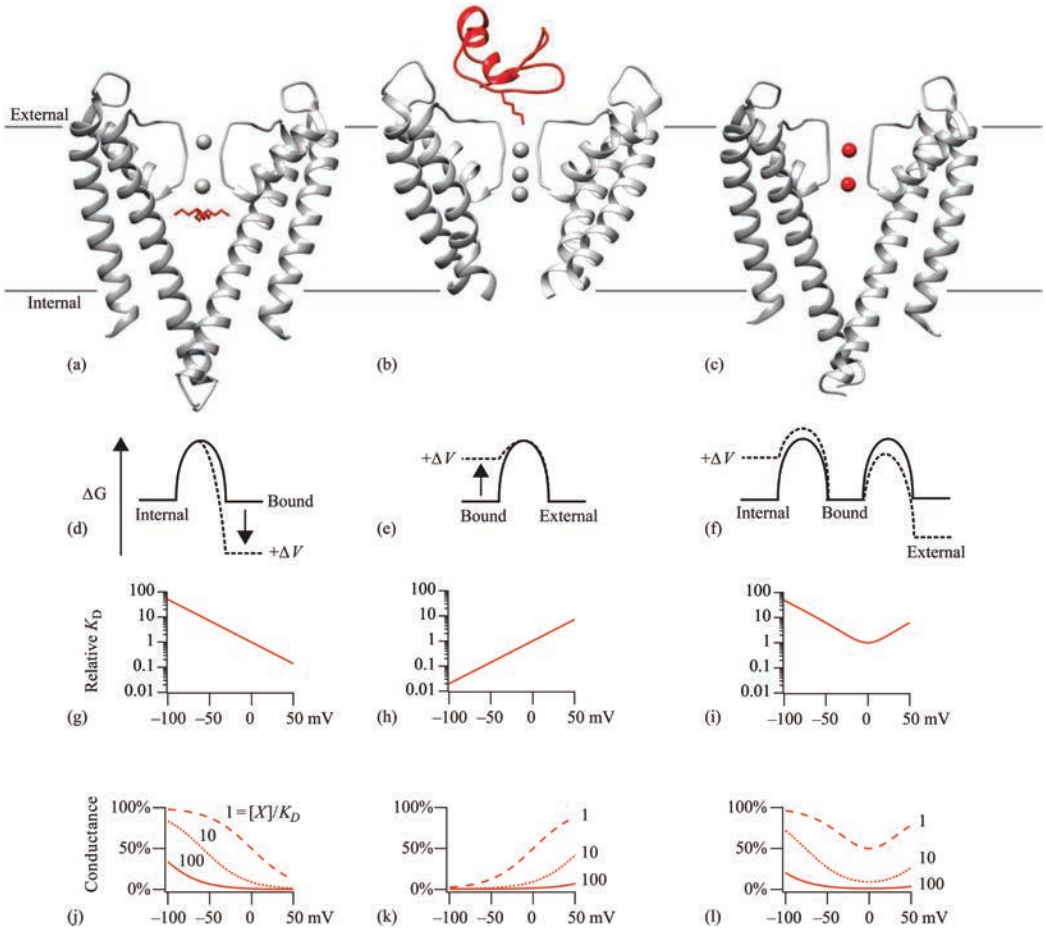

FIGURE 6.3
Pore blockers and voltage-dependent block. (a–c) Crystal structures of K^+ channels (gray) with pore blockers bound (red). Balls indicate permeant ions. (Renderings by Drew Tilley.) The blockers shown in panels (a) and (b) are described in Section 6.4. The blocker shown in panel (c) is described in Section 6.5. (a) Rendering of tetrabutylammonium blocking the pore of the KcsA channel, PDB ID 2HVJ. (b) Charybdotoxin blocking the pore of a Kv channel, PDB ID 4JTA. (c) Ba^{2+} blocking the pore of the KcsA channel, PDB ID 2ITD. (d–f) Reaction coordinate cartoons illustrating the voltage dependence of pore blocker binding. The ordinate represents increasing free energy. Dotted curves indicate energetic changes resulting from an intracellular voltage increase. (g–i) Relative K_D–voltage relation of theoretical pore blockers. Voltage dependence of K_D from Equation 6.8, with $z = 1\ e_0$ (g), $z = -1\ e_0$ (h), or Equation 6.9 (i) with $z_{off,in} = 1\ e_0$, $z_{off,out} = -1\ e_0$, $k_{off,0mV,in} = k_{off,0mV,out}$, $z_{on,in} = 1\ e_0$, $z_{on,out} = 0$, $k_{on,0mV,in} = k_{on,0mV,out}$. (j–l) Conductance–voltage relation of theoretical pore blockers. Curves are plots of Equation 6.3 with voltage dependence of K_D from (g–i). Dashed curve indicates an inhibitor concentration equal to the K_D at 0 mV. Dotted curve is $10 \times K_D$, solid curve $100 \times K_D$.

The K_D of a pore blocker can depend on voltage. The physical origins of voltage-dependent inhibition can be complex, especially when impacted by permeant ions. In the most simple, theoretical case, the voltage dependence of a pore blocker can be conveyed with a single parameter, z, the partial charge value that leads to voltage dependence (Woodhull 1973). Measurements of the degree of inhibition at different voltages can empirically constrain z. From z, how the concentration–response of a pore blocker will be affected by

voltage can be predicted. With a simple dependence of pore block on z, the binding energy derived from a voltage change, Δ V, can be easily calculated with Faraday's constant, F:

$$\Delta G_V = \Delta V z F \tag{6.6}$$

Hence,

$$\Delta G_{blocked} = \Delta G^0_{blocked} + \Delta G_V \tag{6.7}$$

and the voltage dependence of the K_D is

$$K_D = K^0_D e^{-\Delta V z F} \tag{6.8}$$

The full mechanism of voltage-dependent pore blockade may not be as simple as the theoretical case discussed here, but the preceding equations can serve as reasonable approximations under many conditions. The exact nature of the voltage dependence of inhibition is determined by the geometry of the blocking interaction. A few speci□c examples are discussed later to elaborate how voltage-dependent interactions can originate.

6.4 One-Sided Pore Blockers

Many pore blockers can reach their binding site from only one side of the cell membrane. For example, in Figure 6.3a, the inhibitor can reach its binding site only from the internal side of the pore; while in Figure 6.3b, the pore-blocking peptide can bind and dissociate only from the extracellular side. The sidedness of inhibitor binding determines the voltage dependence of its inhibition.

One of the best-studied types of pore blockers are the quaternary ammonium (QA) ions that inhibit K^+ channels from the intracellular side (Armstrong 1969). The QA ion was found to □t nicely into the hydrophobic cavity of a K^+ channel, just internal to the selectivity □lter, where a permeant ion normally resides (Zhou et al. 2001) (Figure 6.3a). QA ions are too large to squeeze through the narrow selectivity □lter of K^+ channels. To dissociate, they must exit inward, and their voltage dependence arises from this dissociation to the intracellular side of the channel. As the voltage inside a cell is decreased, QA ions, being positively charged, can be directly affected by a transmembrane electric □eld. Additionally, K^+ ions are electrostatically forced through the channel, displacing the pore blocker from its binding site. The more rapid dissociation leads to a decreased af□nity (larger K_D) for the pore blocker at more negative voltages. This effect is schematized in the energy diagram of Figure 6.3d. When voltage increases, an internal blocker of a cation channel is liable to be more stable in the bound con□guration. The kinetics of QA ion interactions with K^+ channels can be complex. For the purposes of demonstration, however, it is useful to discuss an idealized simple scenario predicted by Equation 6.8 (Figure 6.3g). Note that within the physiologically relevant voltage range, of –100 to 50 mV, the percent conductance inhibited is altered dramatically. A concentration of pore blocker that inhibits only a small fraction of the conductance at a negative resting potential may inhibit the majority of the current if the cell is brought to a positive potential. The voltage dependence

of an internal blocker can be far steeper than that depicted in Figure 6.3g. This type of voltage dependence forms the basis of inward rectification of inward-rectifier K^+ channels, where endogenous polyamines inhibit the outward flow of ions (Lu 2004). Given the dramatic changes in inhibition with cell potential, it is worth carefully considering the voltage changes in any experimental preparation with voltage-dependent inhibitors.

Pore blockers that act from the external side of the pore will have the opposite voltage dependence to internal blockers. Some ion channel inhibitors are pore-blocking toxins that bind the extracellular side of the pore. One of these is the scorpion peptide charybdotoxin, which has been crystallized bound to a K^+ channel (Banerjee et al. 2013). The resultant structure provides an example of how a peptide can physically occlude the conducting pore (Figure 6.3b). Akin to the internal pore blockers discussed earlier, the peptide mimics the chemistry of the channel's permeant ions to bind tightly to the extracellular side of the channel pore. Charybdotoxin displaces a K^+ ion from its binding site with a positively charged lysine residue. Interactions with permeant ions enhance the voltage dependence of toxin dissociation from the channel (Park and Miller 1992). As the voltage inside a cell is increased, the force driving K^+ ions through the channel out of the cell leads to a decreased affinity for the toxin, which is pushed out to the external solution by the flow of K^+ ions (Figure 6.3e). Hence, the voltage dependence is opposite of blockers that exit to the intracellular solution (Figure 6.3g, h). Interestingly, this opposing voltage dependence of extracellular dissociation has been harnessed by NMDA receptors to allow conduction only when block by external Mg^{2+} has been relieved by positive cellular voltage (Mayer, Westbrook, and Guthrie 1984). Akin to inward-rectifier K^+ channels, pore block of NMDA forms a voltage-dependent gate important for normal physiological function.

6.5 Slowly Permeating Blocking Ions

Some inhibitors are ions that more slowly pass through the channel pore. A common class of inhibitors used in electrophysiology experiments is small metal ions that block pores. In experimental preparations, many Ca^{2+} channels can be blocked with Cd^{2+} or Co^{2+}, and K^+ channels with Cs^+ or Ba^{2+}. Ba^{2+} ion block of K^+ channels has been carefully investigated (Neyton and Miller 1988) and serves as an excellent case study of a slowly permeating blocker. Crystal structures have revealed the location of Ba^{2+} in K^+ channels (Jiang and MacKinnon 2000), where it can be seen replacing K^+ in the selectivity filter (Figure 6.3c). The Ba^{2+} ion is nearly the same size as K^+, allowing it to fit snugly into these sites. Yet, due to its greater charge, Ba^{2+} dynamics differ, and it remains in the channel pore for long periods of time, preventing the flux of other ions. Ba^{2+} eventually dissociates, and like K^+, it can exit from its binding site to either the internal or external solution.

The ability of permeant ions to enter and exit the pore from both sides of the channel can lead to biphasic voltage dependence. In addition to interactions with permeant ions, slowly permeating ions have an innate voltage dependence. As voltage is increased inside the cell, cationic blocking ions are driven into the channel from the internal solution and bound ions punch through to exit the external side (Figure 6.3f). Thus, the rate of dissociation of a slowly permeating blocker to opposing sides of the membrane have opposing polarity. For this situation, voltage dependence has multiple components, and different steps in the slow permeation process can dominate at different voltages. A description of such behavior is as follows:

$$K_D = \frac{k^0_{off,internal} \cdot e^{-\Delta V z_{off,internal} F} + k^0_{off,external} \cdot e^{-\Delta V z_{off,external} F}}{k^0_{on,internal}[X]e^{-\Delta V z_{off,internal} F} + k^0_{on,external}[X]e^{-\Delta V z_{on,external} F}} \quad (6.9)$$

The multiple voltage-sensitive components lead to multiphasic voltage dependence. This is depicted in Figure 6.3i, where at negative voltages, inhibition decreases because ions exit to the internal side, and at positive voltages, the inhibition also decreases because ions exit to the external side. Multiphasic voltage dependence is a hallmark of slowly permeating blockers that was identified in careful studies of the proton block of sodium channels (Woodhull 1973).

Voltage-dependent inhibition can be problematic for researchers seeking to pharmacologically eliminate a current, as an inhibitor that produces near-complete inhibition at some voltages can be ineffective at others. This variable inhibition is due to voltage dependence alone, and the efficacy of inhibitors becomes even more complicated when effects of channel conformation are considered.

6.6 Gated Inhibitor Access

The ability of a pore blocker to inhibit can depend on the conformational state of the channel. Block kinetics can exhibit state dependence when a blocker binds in the interior of a channel, to a site that is only accessible when the protein adopts certain conformations. This is often referred to as gated access. A common form of gated access is when inhibitors are only able to enter open channels (Figure 6.4a). Open channel block of K^+ channels was classically described by Clay Armstrong (Armstrong and Hille 1972). A prominent example of open channel block is N-type or ball-and-chain inactivation of K^+ channels, where a protein amino terminus acts as an inhibitor (Zagotta, Hoshi, and Aldrich 1990). A feature of N-termini and some other open channel blockers is that channels cannot close their access gate when the blocker is bound. Other blockers that require channel opening to access an interior blocking site can become trapped inside the channel when it closes. The gate that controls inhibitor access is not necessarily the gate that controls ion permeation. Channels can undergo many conformational changes prior to opening and, when inhibitor access is gated differently than ion permeation, blockers may enter partially activated closed conformations in addition to the open ones (Figure 6.4b). This has been demonstrated for the block of BK channels by intracellular QA compounds (Tang, Zeng, and Lingle 2009). Blockers can also have multiple access pathways that are gated differently. For example, lidocaine can access Na^+ channels through the cytoplasmic Na^+ gate and can also access the same blocking site from the lipid bilayer through a fenestration in the side of the channel (Nguyen et al. 2019; Hille 1977) (Figure 6.4c).

A hallmark of gated inhibitor access is that channel conductance activates, then decays as blockers enter and inhibit channels (Figure 6.4d, e). While gated access necessarily affects the rate of inhibitor binding, it does not necessarily affect binding affinity. However, if the channel does not close normally with the inhibitor bound, the inhibitor will affect gating, and channel gating will affect binding affinity. Such allosteric effects on channel conformation are discussed further next.

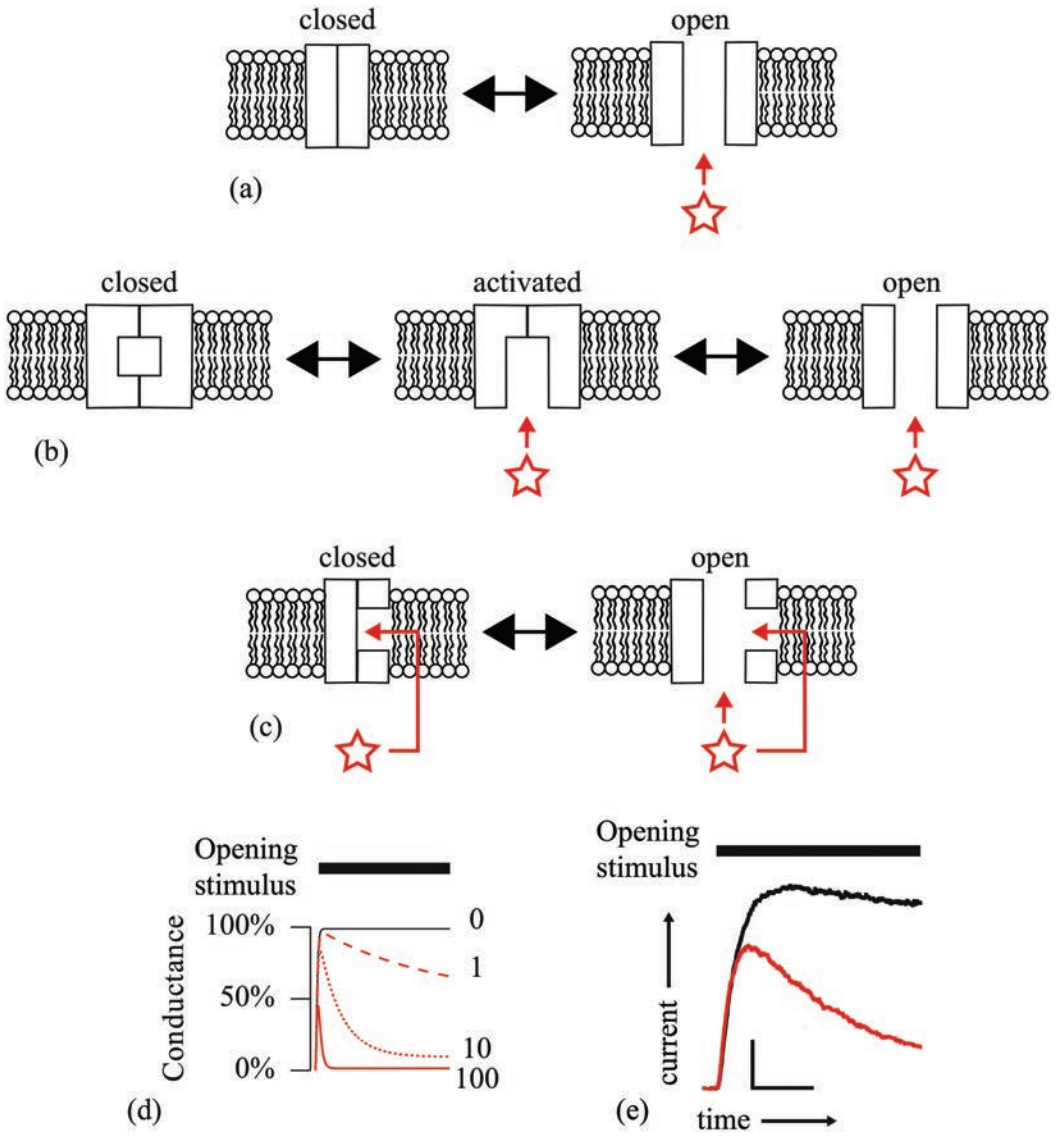

FIGURE 6.4
Gated inhibitor access. (a) An open channel blocker can only occlude the pore when the channel opens. (b) Blocker access may be gated differently than ion conduction. (c) There may be multiple paths, gated differently, to an inhibitor binding site. (d) Time dependence of pore blockade in a kinetic model of an open channel block. Black curve indicates opening in the absence of inhibitor. Dashed red curve indicates an inhibitor concentration equal to the K_D of the open state. Dotted red curve is $10 \times K_D$, solid red curve $100 \times K_D$. (e) Block of the voltage-gated K^+ channel Kv2.1 by the blocker RY785. To access its binding site, RY785 requires voltage stimulation but not channel opening.

6.7 Allosteric Inhibition

Not all ion channel inhibitors block the pore. Many act by inducing the channel to close. This mechanism is fundamentally distinct from pore blockade, as the inhibitory action is not due to the inhibitor obstructing the flow of ions, but to the inhibitor stabilizing channels in nonconducting conformations (Figure 6.5). Despite these very different mechanisms, distinguishing pore blockade from allosteric inhibition can be difficult.

Inhibitors can act by a variety of physical means, such as membrane perturbation, surface charge screening or direct binding to channels. Direct binding can competitively inhibit channels by preventing binding of an activating ligand or act by an allosteric mechanism. The fundamental concept of allostery is that a modulatory molecule can selectively stabilize protein conformations, shifting the equilibrium between conformational states. A molecule that stabilizes nonconducting conformations is a negative allosteric modulator.

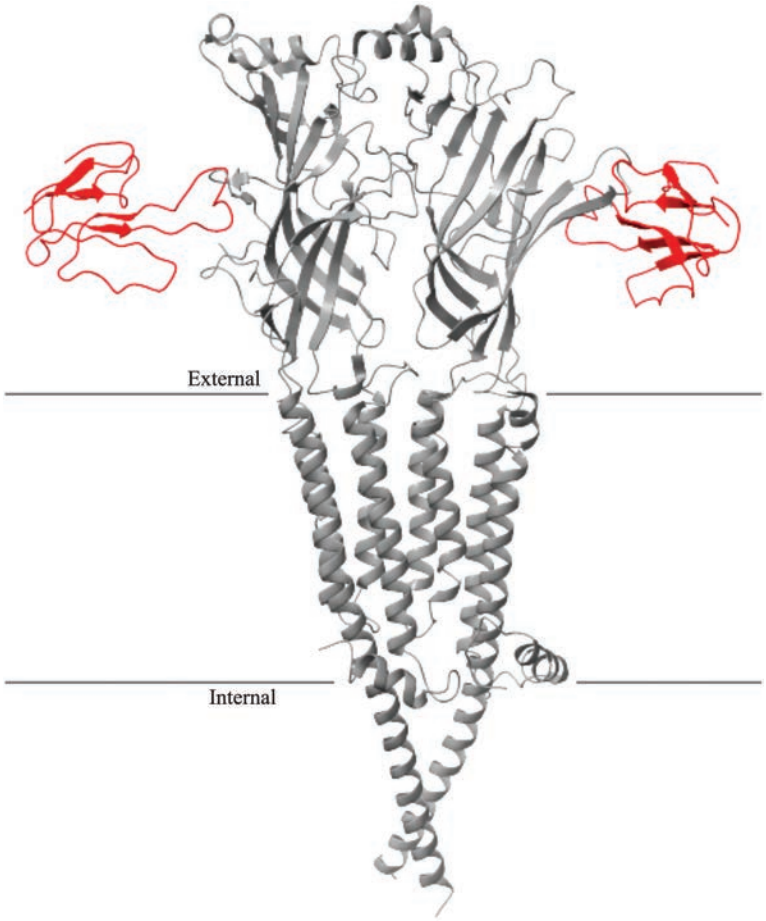

FIGURE 6.5
α-bungarotoxin inhibits acetylcholine receptors by an allosteric mechanism while binding far from the ion conduction pathway. Cryo-EM structure of the nicotinic acetylcholine receptor from Tetronarce californica (gray) with bound α-bungarotoxin (red), PDB ID 6UWZ. For clarity, only two of five channel subunits are shown. (Renderings made in ChimeraX; Pettersen et al. 2021.)

By shifting the equilibrium of a channel to nonconducting, the channel will open less often and be inhibited.

Allosteric inhibitors act by energetically stabilizing closed states relative to open ones. In the simplest case, an inhibitor binds to a single site and prevents a channel from opening (Figure 6.6a). This type of allosteric inhibition is technically inverse agonism, as the channel cannot open with the inhibitor bound. For an inverse agonist, the fraction of channel current inhibited is the fraction bound, with the remaining conductance determined by

$$\text{Conductance} = \frac{f_{\text{unbound}}}{f_{\text{unbound}} + f_{\text{bound}}} = \frac{1}{1 + \left([X] / K_D \right)} \tag{6.10}$$

The thermodynamics of this type of inhibition can make the concentration–response indistinguishable from pore block (note that Equation 6.3 is identical). However, other aspects of the response to the inhibitor can distinguish between pore block and allostery. The differences can be subtle or radical. In many cases, the binding of an allosteric inhibitor is sensitive to the conformational changes associated with channel gating. Changing the stimulus that opens the channel will change the binding of the inhibitor. Figure 6.6c depicts alleviation of inverse agonism in response to increasing opening stimulus. The inverse agonist □ghts the opening stimulus (Figure 6.6b), and the greater the concentration of inhibitor applied, the more stimulus energy is needed to open the channel. The effects of a full inverse agonist saturate only with complete inhibition: otherwise, more inhibitor produces more inhibition. The opening stimuli for many channels are ligands or voltage. As the interactions of inhibitors with ligand-gated proteins are discussed in great detail elsewhere (Wyman and Gill 1990; Hilal-Dandan, Brunton, and Goodman 2013), we here discuss the particular interactions of allosteric inhibitors with voltage-gating processes.

In the case of many voltage-gated channels, voltage increase leads to more channel opening, and inverse agonists modulate these voltage-gating processes. Since voltage alters the probability that a channel will be closed, the fraction of channels with inhibitors bound will change with voltage. The fact that voltage can also affect pore blocker binding can make these two types of inhibition even tougher to distinguish and requires careful interpretation of inhibition data.

An example of an inverse agonist can be found in the defensive mucus of a marine snail. The gastropod Calliostoma canaliculatum secretes 6-bromo-2-mercaptotryptamine (BrMT) to deter predators. BrMT is an inverse agonist of voltage-gated K^+ channels (Sack, Aldrich, and Gilly 2004). BrMT acts by selectively binding to closed channels, as in Figure 6.6a, to prevent channels from opening. Its effects are consistent with full inverse agonism where the inhibitor must dissociate from the channel before it can open. In the presence of BrMT, the more positive voltage is required for activation. Increasing concentrations require progressively more positive voltages to open the channels (Figure 6.6d). The major effect of inverse agonists can be due to kinetic rather than equilibrium properties. It can be shown with a reaction coordinate diagram (Figure 6.6b) that a full inverse agonist that requires unbinding before opening will increase the total activation barrier, $\Delta G^{\ddagger}_{\text{opening}}$, by an amount equal to the free energy change of its binding to the closed state of the channel, $\Delta G_{\text{closed binding}}$. Thus, if the inhibitor prevents rate-limiting steps in channel opening, a full inverse agonist will slow the time course of channel opening by a factor of at least

$$\frac{\tau_{\text{inhibited}}}{\tau_{\text{control}}} = 1 + \frac{[X]}{K_{D\ \text{closed}}} \tag{6.11}$$

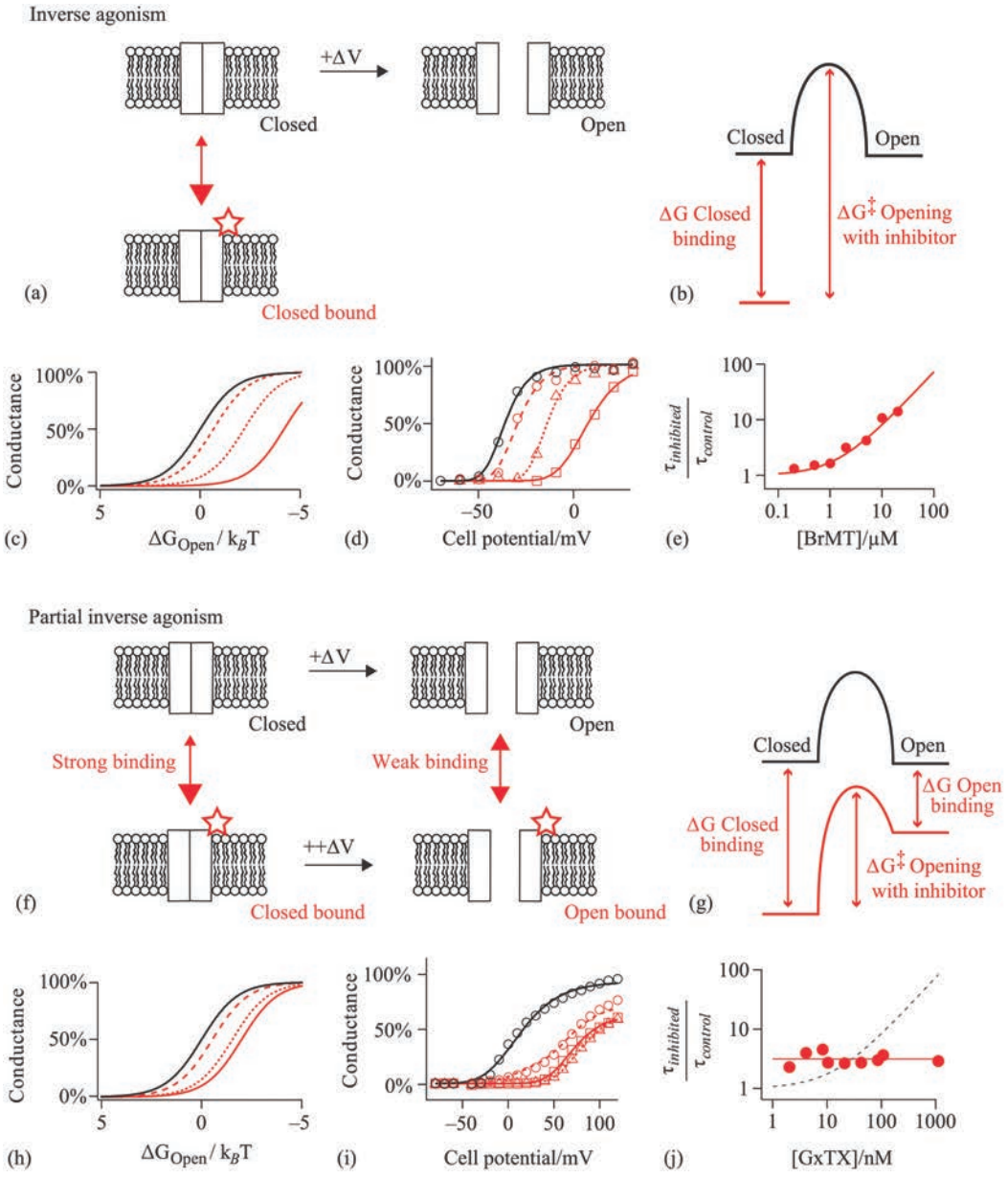
Inverse agonism
+ΔV
Closed
Open
Closed bound
(a)
Closed
Open
ΔG Closed binding
ΔG‡ Opening with inhibitor
(b)
Conductance
100%
50%
0%
5
0
−5
ΔG_Open / k_BT
(c)
Conductance
100%
50%
0%
−50
0
Cell potential/mV
(d)
τ_inhibited / τ_control
100
10
1
0.1
1
10
100
[BrMT]/μM
(e)
Partial inverse agonism
+ΔV
Closed
Open
Strong binding
Weak binding
++ΔV
Closed bound
Open bound
(f)
Closed
Open
ΔG Open binding
ΔG Closed binding
ΔG‡ Opening with inhibitor
(g)
Conductance
100%
50%
0%
5
0
−5
ΔG_Open / k_BT
(h)
Conductance
100%
50%
0%
−50
0
50
100
Cell potential/mV
(i)
τ_inhibited / τ_control
100
10
1
1
10
100
1000
[GxTX]/nM
(j)

where τ represents the time constant of the rate-limiting kinetic process in activation. With increasing concentrations of an inhibitor, channel opening will be progressively slowed (Figure 6.6e). This progressive alteration of kinetics with increasing dose is a hallmark of a full inverse agonist.

6.8 Partial Inverse Agonism

Some allosteric inhibitors will allow channels to open while the inhibitor remains bound. Inhibitors that act in such a way are partial inverse agonists (Figure 6.6f). A partial inverse agonist lowers the probability that a channel will be in a fully open state. The degree to which the binding of a partial inverse agonist leads to channel closing is the coupling between binding and inhibition. This can be quanti□ed as a coupling energy, $\Delta G_{coupling}$, which can be understood as the amount of energy the inhibitor uses to close the channel. But where does $\Delta G_{coupling}$ arise from? The □rst law of thermodynamics demands that energy cannot just appear. It must be accounted for. It turns out that $\Delta G_{coupling}$ is derived from the binding energy of the inhibitor. When channels open with an inverse agonist bound, it weakens inhibitor binding (Figure 6.6f).

An energy diagram for this type of inhibition is given in Figure 6.6g. It depicts a general model of allosteric interaction where a portion of an inhibitor's binding energy is used to keep the channel from opening. How much coupling energy will arise from a change in binding can be calculated from the binding energies to the different channel states. The coupling energy comes from the difference in binding energy of the open and closed states:

$$\Delta G_{coupling} = \Delta G_{open\,binding} - \Delta G_{closed\,binding} \tag{6.12}$$

FIGURE 6.6 (CONTINUED)
Allosteric inhibition. (a) A full inverse agonist needs to dissociate before the channel can open. Cartoon depicts a voltage activated ion channel that only binds inhibitor in its closed state. (b) Inverse agonist binding energetically stabilizes the closed state. (c) The dose–response of a full inverse agonist does not saturate. Each curve is a Boltzmann distribution of conductance arising from increasing open probability. The black curve is control condition. The dashed curve indicates an inhibitor concentration equal to the K_D for the closed conformation. The dotted curve is $10 \times K_D$; solid red curve $100 \times K_D$. (d) Shift of conductance–voltage relation of Shaker K^+ channels does not saturate with increasing concentrations of the inverse agonist BrMT (Sack, Aldrich, and Gilly 2004). The black curve is Boltzmann distribution □t to control data points. The dashed curve is 1 μM BrMT, dotted curve 5 μM, solid curve 20 μM. (e) Increasing inverse agonist concentration progressively slows channel opening. Data points are time constants of channel opening in indicated concentrations of BrMT relative to control. The curve is Equation 6.11 with K_D set to 0.8 μM. (f) A partial inverse agonist can remain bound while the channel opens. The cartoon depicts a voltage-activated ion channel that strongly binds inhibitor in its closed state and more weakly in its open conformation. (g) Open-state binding of partial inverse agonists allow the activation barrier for opening to be reduced. (h) The dose–response of a partial inverse agonist saturates. Each curve is a Boltzmann distribution of conductance arising from increasing open probability. The black curve is the control condition. The dashed curve indicates an inhibitor concentration equal to $K_{D\,closed}$ where $K_{D\,open}$ is 10 $\times$ $K_{D\,closed}$. Dotted curve is $10 \times K_{D\,closed}$, solid red curve $100 \times K_{D\,closed}$. (i) Shift of conductance–voltage relation of Kv2.1 channels saturates at high concentrations of the partial inverse agonist GxTX (Tilley et al. 2019). The black curve is the Boltzmann distribution □t to control data points. The dashed curve is 10 μM GxTX, dotted curve 100 μM, solid curve 1 μM. (j) The rate of channel opening with partial inverse agonist is concentration-independent. Data points are time constants of channel opening in indicated concentrations of GxTX relative to control. The solid line is 3.1-fold slowing of opening. The dashed curve is Equation 6.11 with K_D set to 13 nM, $K_{D\,closed}$; poor □t indicates GxTX is not a full inverse agonist.

As binding affinities are related by dissociation constants, it can be seen that

$$\Delta G_{coupling} = -k_B T \ln\left(\frac{1+\left([X]/K_{D\,open}\right)}{1+\left([X]/K_{D\,closed}\right)}\right) \tag{6.13}$$

and at high concentrations of inhibitor, the effect of the inhibitor saturates:

$$\lim_{[X]\to\infty} \Delta G_{coupling} = -k_B T \ln\left(\frac{K_{D\,closed}}{K_{D\,open}}\right) \tag{6.14}$$

Therefore, the ratio of the dissociation constants for the open and closed conformations limits the potential of a partial inverse agonist to close a channel. This is demonstrated by the simulation in Figure 6.6h; the effects of partial inverse agonists saturate with increasing inhibitor concentration.

An example of a partial inverse agonist is the tarantula toxin guangxitoxin-1E (GxTX). When bound by GxTX, K^+ channels require more stimulus voltage to open, but increasing the toxin concentration fails to completely inhibit the channels (Figure 6.6i). This is due to channels opening with the partial inverse agonist bound. As depicted in Figure 6.6g, a channel opening with an inhibitor bound can have a $\Delta G^{\ddagger}_{opening}$ that is less than an opening pathway that first requires inhibitor dissociation. Because channels can open in the presence of inhibitors, the opening rate saturates and becomes insensitive to higher concentrations of toxin (Figure 6.6j). Due to limited efficacy, a partial inverse agonist mechanism may limit consequences of drug overdose.

6.9 Use-Dependent Pore Block

Pore blockers can also allosterically modulate channels. An open channel blocker may prevent a channel from closing, like a foot in a door jamb, and could be considered a full agonist if it did not also block the permeation pathway. Other blockers that enter through the channel permeation gate can stabilize closed channels. For example, the "closed channel blocker," 4-aminopyridine, destabilizes the fully activated conformations of K^+ channel voltage sensors while bound in the pore (Armstrong and Loboda 2001). A wide variety of sodium channel inhibitors used to treat pain, arrhythmias and epilepsy are state-dependent pore blockers. In the case of these sodium channel inhibitors, state dependence is referred to as use dependence because the degree of inhibition of the channel increases when the channel is stimulated. Upon repetitive stimulus, such as a train of action potentials, open channel blockers or other use-dependent inhibitors will progressively inhibit their targets (Courtney 1975). This is thought to be an important property of drugs that mitigate excitotoxic pathologies, such as epilepsy (Rogawski and Loscher 2004).

6.10 Inhibition by Lipid Bilayer Effects

The preceding treatments of inhibition mechanism assume that the inhibitor interacts directly with the ion channel. However, inhibitors can act without binding to channels.

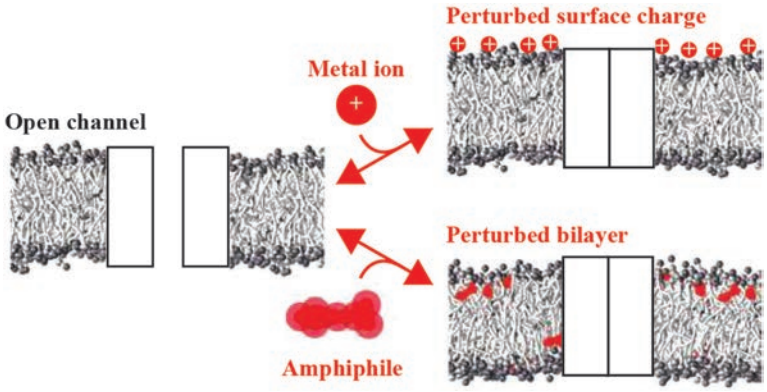

FIGURE 6.7
Membrane perturbation can alter channel function. Illustrations represent allosteric inhibition of channels by perturbing the surrounding membrane. Membrane images are molecular dynamics simulation snapshots of a phospholipid bilayer ±10 mol% resveratrol, an amphiphilic phytochemical. (Simulation and rendering by Helgi I. Ingólfsson.)

All ion channels are suspended in a sheet of lipid bilayer that forms the cell membrane. The bilayer is intimately involved in channel function. Some inhibitors do not appear to bind the ion channels they affect at all, but rather act by perturbing the membrane that surrounds them (Figure 6.7).

A classically studied mechanism of inhibitor action is the surface charge effect. This is where ions adsorb to the surface of membranes, perturbing the electric field near the membrane, and hence the activity of channels in the membrane (Frankenhaeuser and Hodgkin 1957). Multivalent metal ions such as Mg^{2+} can induce classical surface charge effects. The degree of surface charge effect varies from channel to channel and is dependent on the precise conformation of each voltage sensor. Molecules with surface charge effects can also modulate channels by mechanisms distinct from surface charge. For example, Mg^{2+} can also be a pore blocker.

Inhibitors that are hydrophobic or amphipathic in their physical chemistry can partition into the cell membrane. Membrane-partitioning molecules are everywhere and include detergents, lipids, a wide variety of phytochemicals and most clinically used small molecule drugs. By changing the physical properties of the membrane itself, bilayer-perturbing molecules can change equilibria between open and closed channels (Andersen and Koeppe 2007). These changes in equilibria can resemble the effects of directly bound inverse agonists, but may have unusual concentration-response profiles. Membrane perturbing inhibitors have promiscuous effects on many different membrane proteins (Ingolfsson et al. 2014). Whenever working with molecules that are soluble in organic solvents or poorly soluble in water, it is wise to consider their potential to alter ion channel gating by membrane perturbation.

6.11 Concluding Remarks

We have discussed mechanisms by which inhibitors decrease the conductance of ion channels. Inhibitors can bind in the pore and block ion flow, or act allosterically by closing

the channel either by direct binding or perturbing the surrounding membrane. Different types of inhibitors are well suited for specific tasks. In attempting to dissect the role of a channel in a complex physiological situation, a selective and complete inhibitor of a specific channel type is called for. In this case, a pore blocker may be preferable. A partial inverse agonist can partially inhibit a channel with a therapeutic window spanning a wide range of concentrations. To inhibit channels only under hyperexcitable pathophysiological conditions, a use-dependent inhibitor may be most appropriate. In any case, understanding how inhibitor efficacy is affected by voltage changes, channel activity and the membrane bilayer allows one to choose ion channel inhibitor doses and interpret results of experiments more wisely.

Acknowledgments

The authors' research on inhibitors has been supported by National Institutes of Health (NIH) grants NS096317, NS114956 and HL128537.

Suggested Readings

Andersen, O. S., and R. E. Koeppe, 2nd. 2007. "Bilayer thickness and membrane protein function: an energetic perspective." Annu Rev Biophys Biomol Struct 36:107–30. doi:10.1146/ annurev.biophys.36.040306.132643.

Armstrong, C. M. 1969. "Inactivation of the potassium conductance and related phenomena caused by quaternary ammonium ion injection in squid axons." J Gen Physiol 54 (5):553–75.

Armstrong, C. M., and B. Hille. 1972. "The inner quaternary ammonium ion receptor in potassium channels of the node of Ranvier." J Gen Physiol 59 (4):388–400. doi:10.1085/ jgp.59.4.388.

Armstrong, C. M., and A. Loboda. 2001. "A model for 4-aminopyridine action on K channels: similarities to tetraethylammonium ion action." Biophys J 81 (2):895–904. doi:10.1016/ S0006-3495(01)75749-9.

Banerjee, A., A. Lee, E. Campbell, and R. Mackinnon. 2013. "Structure of a pore-blocking toxin in complex with a eukaryotic voltage-dependent K(+) channel." Elife 2:e00594. doi:10.7554/ eLife.00594.

Courtney, K. R. 1975. "Mechanism of frequency-dependent inhibition of sodium currents in frog myelinated nerve by the lidocaine derivative GEA." J Pharmacol Exp Ther 195 (2):225–36.

Frankenhaeuser, B., and A. L. Hodgkin. 1957. "The action of calcium on the electrical properties of squid axons." J Physiol 137 (2):218–44.

Hilal-Dandan, R., L. L. Brunton, and L. S. Goodman. 2013. Goodman and Gilman's manual of pharmacology and therapeutics. 2nd ed. New York: McGraw-Hill.

Hille, B. 1977. "Local anesthetics: hydrophilic and hydrophobic pathways for the drug-receptor reaction." J Gen Physiol 69 (4):497–515. doi:10.1085/ jgp.69.4.497.

Ingolfsson, H. I., P. Thakur, K. F. Herold, E. A. Hobart, N. B. Ramsey, X. Periole, D. H. de Jong, M. Zwama, D. Yilmaz, K. Hall, T. Maretzky, H. C. Hemmings, Jr., C. Blobel, S. J. Marrink, A. Kocer, J. T. Sack, and O. S. Andersen. 2014. "Phytochemicals perturb membranes and promiscuously alter protein function." ACS Chem Biol 9 (8):1788–98. doi:10.1021/ cb500086e.

Jiang, Y., and R. MacKinnon. 2000. "The barium site in a potassium channel by x-ray crystallography." J Gen Physiol 115 (3):269–72.

Lu, Z. 2004. "Mechanism of recti□cation in inward-recti□er K+ channels." Annu Rev Physiol 66:103–29. doi:10.1146/ annurev.physiol.66.032102.150822.
Mayer, M. L., G. L. Westbrook, and P. B. Guthrie. 1984. "Voltage-dependent block by Mg2+ of NMDA responses in spinal cord neurones." Nature 309 (5965):261–3.
Neyton, J., and C. Miller. 1988. "Discrete Ba2+ block as a probe of ion occupancy and pore structure in the high-conductance Ca2+ -activated K+ channel." JGen Physiol 92 (5):569–86.
Nguyen, P. T., K. R. DeMarco, I. Vorobyov, C. E. Clancy, and V. Yarov-Yarovoy. 2019. "Structural basis for antiarrhythmic drug interactions with the human cardiac sodium channel." Proc Natl Acad Sci U S A 116 (8):2945–54. doi:10.1073/ pnas.1817446116.
Park, C. S., and C. Miller. 1992. "Interaction of charybdotoxin with permeant ions inside the pore of a K+ channel." Neuron 9 (2):307–13.
Pettersen, E. F., T. D. Goddard, C. C. Huang, E. C. Meng, G. S. Couch, T. I. Croll, J. H. Morris, and T. E. Ferrin. 2021. "UCSF ChimeraX: structure visualization for researchers, educators, and developers." Protein Sci 30 (1):70–82. doi:10.1002/ pro.3943.
Rogawski, M. A., and W. Loscher. 2004. "The neurobiology of antiepileptic drugs." Nat Rev Neurosci 5 (7):553–64. doi:10.1038/ nrn1430.
Sack, J. T., R. W. Aldrich, and W. F. Gilly. 2004. "A gastropod toxin selectively slows early transitions in the Shaker K channel's activation pathway." JGen Physiol 123 (6):685–96.
Tang, Q. Y., X. H. Zeng, and C. J. Lingle. 2009. "Closed-channel block of BK potassium channels by bbTBA requires partial activation." JGen Physiol 134 (5):409–36. doi:10.1085/ jgp.200910251.
Tilley, D. C., J. M. Angueyra, K. S. Eum, H. Kim, L. H. Chao, A. W. Peng, and J. T. Sack. 2019. "The tarantula toxin GxTx detains K(+) channel gating charges in their resting conformation." JGen Physiol 151 (3):292–315. doi:10.1085/ jgp.201812213.
Woodhull, A. M. 1973. "Ionic blockage of sodium channels in nerve." JGen Physiol 61 (6):687–708.
Wyman, J., and S. J. Gill. 1990. Binding and linkage: functional chemistry of biological macromolecules. Mill Valley, CA: University Science Books.
Zagotta, W. N., T. Hoshi, and R. W. Aldrich. 1990. "Restoration of inactivation in mutants of Shaker potassium channels by a peptide derived from ShB." Science 250 (4980):568–71. doi:10.1126/ science.2122520.
Zhou, M., J. H. Morais-Cabral, S. Mann, and R. MacKinnon. 2001. "Potassium channel receptor site for the inactivation gate and quaternary amine inhibitors." Nature 411 (6838):657–61.

Chapter 2: The Mechanism of State-Biased Blockade of Kv2.1 Channels by RY785

Foreword

This chapter presents my findings on the mechanism by which RY785 inhibits Kv2.1. These results support a model in which RY785 requires voltage sensor activation to reach its binding site and allosterically affects the gating of Kv2.1. RY785 exhibits closed state-bias and traps itself in its binding site which, putatively, is in the central cavity of the channel. Voltage sensor activation allows RY785 access to this binding site at lower voltage than is required for channels to adopt their conductive state. This suggests that two gates, activated by different voltages, regulate K^+ conduction through Kv2.1. This chapter is a reproduction of an article[3] that I wrote describing work I performed under the mentorship of my co-author, Jon Sack. These findings were honored with an editorial summary[4] in the *Journal of General Physiology*.

JGP Journal of General Physiology

ARTICLE

Mechanism of use-dependent Kv2 channel inhibition by RY785

Matthew James Marquis[1] and Jon T. Sack[1,2]

Understanding the mechanism by which ion channel modulators act is critical for interpretation of their physiological effects and can provide insight into mechanisms of ion channel gating. The small molecule RY785 is a potent and selective inhibitor of Kv2 voltage-gated K^+ channels that has a use-dependent onset of inhibition. Here, we investigate the mechanism of RY785 inhibition of rat Kv2.1 (*Kcnb1*) channels heterologously expressed in CHO-K1 cells. We find that 1 µM RY785 block eliminates Kv2.1 current at all physiologically relevant voltages, inhibiting ≥98% of the Kv2.1 conductance. Both onset of and recovery from RY785 inhibition require voltage sensor activation. Intracellular tetraethylammonium, a classic open-channel blocker, competes with RY785 inhibition. However, channel opening itself does not appear to alter RY785 access. Gating current measurements reveal that RY785 inhibits a component of voltage sensor activation and accelerates voltage sensor deactivation. We propose that voltage sensor activation opens a path into the central cavity of Kv2.1 where RY785 binds and promotes voltage sensor deactivation, trapping itself inside. This gated-access mechanism in conjunction with slow kinetics of unblock supports simple interpretation of RY785 effects: channel activation is required for block by RY785 to equilibrate, after which trapped RY785 will simply decrease the Kv2 conductance density.

Introduction

Ion channel inhibitors are used to investigate the physiological functions of their target proteins. Each ion channel inhibitor has a characteristic mechanism of action which determines whether the degree of inhibition will vary with local conditions such as membrane potential or permeant ion concentration (Sack and Eum, 2015; Dilly et al., 2011). To interpret the impact of an inhibitor in a physiological experiment, it is important to understand the mechanism of the inhibitor. Here, we investigate the mechanism of a small molecule that potently and selectively inhibits Kv2 voltage-gated K^+ channels.

Kv2 channels are conserved from Cnidaria to Chordata (Li et al., 2015), suggesting they serve unique and fundamental purposes. Mammals have two Kv2 orthologs, Kv2.1 and Kv2.2, which are pore-forming protein subunits that can assemble as homotetramers or heterotetramers to form voltage-gated Kv2 channels (Frech et al., 1989; Kihira et al., 2010). Kv2 channels are expressed in nervous, muscular, and endocrine cell types (Bocksteins, 2016; Vacher et al., 2008). Kv2.1 is notably important in the brain, where it is highly and widely expressed in central neurons and forms the principal delayed rectifier current of many neuron types (Trimmer, 1991; Liu and Bean, 2014; Guan et al., 2007; Mandikian et al., 2014; Malin and Nerbonne, 2002; Du et al., 2000; Murakoshi and Trimmer, 1999; Pathak et al., 2016; Kimm et al., 2015). In mice and humans, mutations of Kv2.1 (*KCNB1*) result in severe neuropathologies, suggesting a fundamental importance in neuronal function (Bar et al., 2020; Speca et al., 2014; Hawkins et al., 2021; Thiffault et al., 2015; Torkamani et al., 2014). In neurons, Kv2 channels can mediate or suppress sustained, high-frequency action potential generation (Hönigsperger et al., 2017; Liu and Bean, 2014; Romer et al., 2019). In smooth muscle, Kv2.1 modulates myogenic tone (O'Dwyer et al., 2020; Amberg and Santana, 2006; Zhong et al., 2010). In pancreatic β cells, Kv2 channels suppress insulin secretion (Li et al., 2013; Jacobson et al., 2007). In photoreceptors, Kv2.1 contributes to the outward dark current (Fortenbach et al., 2021). Kv2.1 is subject to complex regulation by phosphorylation (Misonou et al., 2005; Murakoshi et al., 1997; Cerda and Trimmer, 2011; McCord and Aizenman, 2013; Misonou et al., 2004), SUMOylation (Dai et al., 2009; Plant et al., 2011), assembly with pore-forming KvS and auxiliary subunits (Bocksteins and Snyders, 2012; Bocksteins, 2016; Peltola et al., 2016, 2011), and membrane lipid composition (Delgado-Ramírez et al., 2018; Milescu et al., 2009; Ramu et al., 2006). These complex regulations make the voltage responses of Kv2 channels

[1]Department of Physiology & Membrane Biology, University of California, Davis, Davis, CA; [2]Department of Anesthesiology and Pain Medicine, University of California, Davis, Davis, CA.

Correspondence to Jon T. Sack: jsack@ucdavis.edu.

difficult to predict, highlighting the importance of inhibitors for determining the contributions of Kv2 channels to the wide range of physiological functions they participate in.

Recently, the contributions of Kv2 channels to electrical signaling have been identified using peptide toxins from spiders (Pathak et al., 2016; Kimm et al., 2015; Liu and Bean, 2014; Newkirk et al., 2021; Romer et al., 2019; Speca et al., 2014). Especially useful toxins include stromatoxin-1 and guangitoxin-1E (GxTX), with GxTX being more selective for Kv2 channels (Escoubas et al., 2002; Herrington et al., 2006). However, these peptides are not uniformly efficacious. Both stromatoxin-1 and GxTX are partial inverse agonists. GxTX acts by preferentially binding to resting voltage sensors on the channel, thereby stabilizing closed channels (Tilley et al., 2019). An aspect of this mechanism is that depolarization promotes toxin dissociation. GxTX inhibition can thus be overcome at more depolarized potentials or during high-frequency stimuli, and this negative use dependence can complicate interpretation (Tilley et al., 2014). Because of the difficulties of interpretation that stem from the allosteric mechanism of spider toxins, a Kv2-selective inhibitor without the complications of use dependence and gating modulation could enable more definitive physiology experiments.

A class of Kv2-selective inhibitors were developed in a small-molecule medicinal chemistry project at Merck (Herrington et al., 2011). Of these, an uncharged molecule, RY785, was the most potent Kv2.1 inhibitor, with a half-maximal inhibitory concentration (IC_{50}) of 50 nM. Depolarization from a negative holding potential was required for the onset of inhibition by RY785, leading us to wonder whether this apparent use dependence would impact RY785's performance as an inhibitor. Here, we determine how voltage activation of Kv2.1 interacts with inhibition by RY785.

Two mechanisms that can create use dependence are allosteric modulation and gated access to a binding site. Allosteric modulation can inhibit ion channels via stabilization of nonconducting conformations (Hille, 1977; Hondeghem and Katzung, 1977). This can result in modification of conductance kinetics or voltage dependence. A hallmark of allosteric inhibition is that channels in nonconducting conformations bind their ligands with higher affinity. A gated-access mechanism involves a conformational change that allows an inhibitor to access and exit its binding site. A gated-access mechanism controls intracellular quaternary ammonium ion block of voltage-gated K^+ channels (Armstrong, 1971; Armstrong and Hille, 1972). Use dependence can also be produced by a combination of allosteric modulation and gated access, as with lidocaine block of voltage-gated Na^+ channels (Nguyen et al., 2019; Hille, 1977; Vedantham and Cannon, 1999) or dofetilide block of hERG K^+ channels (Wang et al., 2016; Wu et al., 2015; Ficker et al., 1998). Here, we investigate whether allosteric modulation or gated-access mechanisms undergird the use-dependent inhibition of Kv2.1 by RY785.

Materials and methods

Cell culture

A Chinese hamster ovary (CHO)-K1 cell line stably transfected with vectors enabling tetracycline-induced expression of the rat Kv2.1 channel (Trapani and Korn, 2003) was maintained in cell culture–treated polystyrene dishes (130180; Thermo BioLite) at 37°C in a 5% CO_2 atmosphere in growth medium composed of Ham's F-12 medium (11765-054; Gibco) containing 10% FBS (100-500; GemCell) and 1% penicillin–streptomycin solution (15140-122; Life Technologies). The CHO cell line was a gift from Stephen Korn, University of Connecticut, Storrs, CT. It was validated by tetracycline induction of Kv2.1-like delayed rectifier K^+ currents and tested negative for mycoplasma (Lonza MycoAlert). Cells were cultured with 1 µg/ml blasticidin S HCl (A11139-03; Gibco) and 25 µg/ml zeocin (46-0509; Invitrogen) to retain transfected vectors. 1–2 h before experiments, 1 µg/ml minocycline HCl (ALX-380-109-M050; Enzo) was added to medium to induce channel expression. For voltage-clamp recording, cells were harvested by manual scraping in PBS with 0.48 mM EDTA (15040-066; Gibco) and pelleted by centrifugation at 1,000 *g* for 2 min. For K^+ current experiments, cells were resuspended in the growth medium. For gating current experiments, cells were resuspended and pelleted three times in gating current external solution. Cells were slowly rotated in a polypropylene tube (05-408-134; Fisher) at room temperature until use. For K^+ current experiments, aliquots of cell suspension were added to a recording chamber containing external solution, allowed to settle, and rinsed with external solution before recording. For gating current experiments, aliquots of cell suspension in gating current external solution were added to a dry recording chamber.

K^+ current measurements

Patch-clamp experiments were performed at room temperature (22.0–23.5°C). Voltage clamp was achieved with an Axopatch 200B amplifier (Axon Instruments) run by Patchmaster v2x90.5 software (HEKA). The external bath solution contained (in mM) 155 NaCl, 10 HEPES, 1.5 $CaCl_2$, 1 $MgCl_2$, and 3.5 KCl, adjusted to pH 7.2 with NaOH. External solution was supplemented with 1:1,000 vol:vol DMSO as a vehicle control or, when indicated, 1 µM RY785 (19813; Cayman) as 1:1,000 1 mM RY785 in DMSO. In some experiments, 5 µM tetrodotoxin was added to suppress endogenous voltage-gated Na^+ channels. We did not see any suggestion that tetrodotoxin or the rapidly inactivating endogenous Na^+ channels impacted analyses of Kv2.1 currents, and results with and without tetrodotoxin were pooled. The internal pipette solution contained (in mM) 50 KF, 70 KCl, 35 KOH, 5 EGTA, and 50 HEPES, adjusted to pH 7.4 with KOH. Internal solution osmolarity was adjusted with sucrose in some experiments. Data with and without sucrose are pooled. Recording pipettes were pulled from thin-walled borosilicate glass (1.5-mm outer diameter, 1.1-mm inner diameter, with filament; Sutter Instrument) on a horizontal micropipette puller (Sutter P-87) using five or more heating cycles to achieve a taper to the tip over minimal length. Pipettes were typically coated with a silicone elastomer (Dow Corning Sylgard 184) and heat-cured. Data with and without Sylgard are pooled. Pipette-tip resistances with the above solutions were 0.96–2.41 MΩ with positive pressure applied to pipette.

CHO cells with a round shape and smooth surface were selected for whole-cell voltage clamp. To minimize voltage errors

at the cell membrane due to series resistance, several measures were taken. To control the magnitude of K^+ currents, Kv2.1 expression was induced by incubation with minocycline for 128–155 min (experiments with tetraethylammonium [TEA]) and 42–110 min (other experiments). Series resistances were estimated by manual nulling of capacitance and were <11 MΩ. The series resistance compensation correction circuit was set to 60–90%. Lag was 10 µs. Data were excluded from analysis if the product of current amplitude and estimated series resistance remaining after compensation was >10 mV. The largest current analyzed in this dataset was 11.3 nA. Cell capacitances were 1.9–17.7 pF, resulting in cell membrane charging time constants of <54 µs before compensation, at least two orders of magnitude faster than time constants fitted to ionic currents. Currents for I–V relations were low-pass filtered at 10 kHz and digitized at 100 kHz. Currents for drug association/dissociation experiments were low-pass filtered at 5 kHz and digitized at 10 kHz. The holding potential was −100 mV. Remaining capacitance and Ohmic leak were subtracted offline using traces recorded during P/5 voltage protocols from holding potential. In sequences of voltage steps, at least 2 s elapsed between the start times of each recording. For vehicle and RY785 wash-in, solution was exchanged by flushing a volume of ≥200 µl through a recording chamber of <100 µl (Warner RC-24N). RY785 was applied after vehicle. Time courses of current inhibition (detailed below) were analyzed for artifacts resulting from solution exchange. We observed that, following wash-in of RY785 or vehicle, Kv2.1 current amplitudes would increase by 5.0 ± 2.9% (mean ± SEM, n = 32 cells) or 5.32 ± 0.70% (mean ± SEM, n = 4 cells), respectively. Current amplitudes in vehicle-washed cells would then slowly decay by as much as 23% (Fig. 3 B). This variability was deemed too minor to alter our interpretation or conclusions and therefore tolerated.

Gating current measurements

The following modifications from the whole-cell protocol were applied during gating-current recordings. Channel expression was induced by incubation with minocycline for 36–60 h. The external bath solution contained (in mM) 140 NMDG, 60 HEPES, 2 $CaCl_2$, 2 $MgCl_2$, 0.1 EDTA, 0.01 CsCl, and 84 methanesulfonic acid at pH 7.3. When indicated, the external solution was mixed 1,000:1 with DMSO or 1 mM RY785 in DMSO. The internal solution contained (in mM) 90 NMDG, 50 NMDG hydrofluoride, 1 NMDG hydrochloride, 60 HEPES, 5 EGTA, 5 sucrose, and 29 methanesulfonic acid at pH 7.3. Pipette-tip resistances with the above solutions were 2.7–7.7 MΩ with positive pressure applied to the pipette. All pipettes were coated with Sylgard and fire-polished. Series resistances were 5.5–13.8 MΩ, except for one 47-MΩ cell that responded well to compensation circuitry. Cell capacitances were 3.1–13.0 pF. To exclude artifacts of membrane charging, data were not analyzed until 200 µs after a voltage step. The series resistance prediction circuit was set to 70%, resulting in predicted membrane charging time constants of <45 µs. The series resistance compensation correction circuit was set to 70–75% with 10-µs lag. Currents were low-pass filtered at 10 kHz and digitized at 50 kHz. In sequences of voltage steps, 4 s elapsed between the start times of each recording. Vehicle or RY785 were manually added to a 200-µl recording chamber with a 5-min wait before recording. Vehicle and RY785 were applied in a blinded and randomized fashion with unblinding after completion of data analysis.

Monitoring current inhibition and recovery

The voltage protocols for determining the voltage dependence of Kv2.1 inhibition by and recovery from RY785 consisted of 10-s cycles containing two voltage steps from the holding potential of −100 mV. The first voltage step is a 20-ms test pulse to +40 mV to gauge the proportion of conductive channels. Afterward, the cell is returned to −100 mV holding potential for 30 ms, then given a postpulse to a voltage between −80 and +40 mV. The 30-ms interval between a test pulse and subsequent postpulse is 10 times the 3-ms deactivation time constant of Kv2.1 at −100 mV (Tilley et al., 2019), so deactivation is expected to be >99% complete by the end of the step. The postpulse was 500 ms for the inhibition protocols and 4 s for the recovery protocols. Testing of each cell went as follows: (1) a baseline was established in vehicle by recording 10 cycles of the inhibition protocol; (2) during a 2-min gap, the recording chamber solution was exchanged with 1 µM RY785 or vehicle control; (3) the inhibition protocol resumed until currents stabilized (15–80 cycles); (4) 10 cycles of the recovery protocol were recorded while the bath still contained 1 µM RY785; (5) during a 1-min gap, continuous flow was started of a solution without RY785; and (6) recording of the recovery protocol resumed with continuous solution flow until currents stabilized (71–155 cycles).

Analysis

Electrophysiology analysis, curve fitting, and plotting were performed with Igor Pro 8 (Wavemetrics), which uses a Levenberg–Marquardt algorithm for least-squares curve fitting. For presentation, gating current traces were Gaussian-filtered at 2 kHz.

Conductance (G) was calculated as ionic current divided by the K^+ driving force:

$$V_{cell} = V_{command} - \left[\left(1-f_{compensated}\right) \times R_{series} \times I\right] - V_{LJ}, \quad (1)$$

where V_{cell} is membrane voltage; $V_{command}$ is command voltage; $f_{compensated}$ is fraction of series resistance compensated; R_{series} is measured series resistance; I is measured current; V_{LJ} is liquid-junction potential; and V_{LJ} of 12 mV was calculated using Patchers Power Tools v2.15 (Mendez and Wurriehausen, 2009).

For the conductance–voltage (G–V) relation, conductance values were determined from current levels in the final 2 ms of 100-ms steps to the indicated voltage. Kv2.1-mediated currents were isolated by subtraction of currents remaining in 1 µM RY785. Kv2.1-mediated currents were divided by the driving force for K^+ relative to the calculated Nernst potential of −97.4 mV. Conductance levels were plotted against command voltage and normalized to their mean from +80 to +100 mV. G–V relations were fitted with a Boltzmann function:

$$f(V) = A\left\{1 + e^{\left[\frac{(V_{half} - V)zF}{RT}\right]}\right\}^{-x}, \quad (2)$$

where A is maximum amplitude, z is valence in units of elementary charge (e_0), F is the Faraday constant, R is the ideal gas constant, and T is absolute temperature. The variable x is the power, or order, of the Boltzmann function. When fitting the G–V, x was set to 4 (Tilley et al., 2019). V_{half} is the activation midpoint in units of millivolts. In Eq. 2, the voltage that produces half-maximal conductance, V_{mid}, when $x = 4$ is

$$V_{mid} = V_{half} - \left[\frac{\ln\left(2^{\frac{1}{x}} - 1\right)RT}{zF}\right] = V_{half} + \left(\frac{42.39}{z}\right). \quad (3)$$

Inhibition and recovery rate calculations

Rates of channel inhibition by RY785 for Fig. 3 were determined from the test pulses of the two-voltage-step protocol described above. The amplitudes of test pulse current were fitted with an exponential function (Eq. 4), starting with the first record after RY785 wash-in:

$$I = I_0 + Ae^{\frac{(x_0 - x)}{\tau}}, \quad (4)$$

where I is current, I_0 is current at time zero, A is equilibrium current amplitude, x is time, x_0 is time 0, and τ is the time constant. The apparent inhibition rate ($k_{apparent}$) is τ^{-1}. To estimate an inhibition rate during the variable-potential postpulses (k_{post}), we assumed that no significant inhibition occurs when holding at −100 mV (Fig. 2 B) and applied a correction to account for inhibition during test pulses to +40 mV (k_{test}), weighted by pulse durations (d_{test} and d_{post}):

$$k_{apparent} = \frac{k_{test} \times d_{test} + k_{post} \times d_{post}}{d_{cycle}}, \quad (5)$$

where d_{cycle} is the length of one protocol cycle. k_{test} was determined from the mean $k_{apparent}$ with postpulses and test pulses to +40 mV such that $k_{test} = k_{post}$. For the estimates of inhibition rate during a single pulse ($k_{single\ step}$) presented in Fig. 4, Eq. 4 was fitted to current decay during the first postpulse in RY785. As an attempt to correct for current decay in vehicle due to inactivation, current decay in vehicle was fitted with Eq. 4, and τ^{-1} in vehicle was subtracted from τ^{-1} in RY785.

Current recovery after RY785 wash-out with test pulses and postpulses to +40 mV was fitted with Eq. 4, yielding apparent recovery rates from which recovery rates ($k_{recover}$) were determined using Eq. 5 as above, where $k_{test} = k_{post} = k_{recover}$. For recovery experiments with postpulses to −80 mV, limited recovery occurred, and $k_{apparent}$ was estimated by linear regression. To calculate $k_{recover}$ using Eq. 5, k_{test} from the +40-mV recovery protocol was used. In one experiment, current did not recover following RY785 wash-out, and this cell was excluded from analysis.

Estimation of K_d

Rates of channel inhibition and recovery were used in Eq. 6 to estimate a dissociation constant (K_d) for RY785 binding to Kv2.1 at +40 mV:

$$K_d = \frac{k_{off}}{k_{on}}, \quad (6)$$

where $k_{off} = k_{recover}$ with postpulses to +40 mV and $k_{on} = k_{post}/[\text{RY785}]$ when k_{post} measured the rate of inhibition at +40 mV. The contribution of k_{off} to the kinetics of inhibition at +40 mV was ignored as $k_{post} \gg k_{off}$. The parent compound from which RY785 was derived inhibits human Kv2.1 with a Hill coefficient of close to 1 (1.2; Herrington et al., 2011), suggesting that it is reasonable to ignore the possibility of cooperative binding in a K_d estimate.

Activation rate

Channel activation time constants were determined by fitting single-exponential functions (Eq. 4) to current amplitude time courses during the final 15 ms of the 20-ms test pulse to +40 mV. We did this for a randomly selected sample of 10 of the above inhibition rate experiments. Time constants were excluded if SD of fit was >15 ms. In Fig. S2 B, peak currents were means of the final 0.5 ms of the test pulse and were normalized to the first record after RY785 wash-in.

Gating current analyses

Charge (Q) movement was quantified by integrating gating currents. ON gating currents were integrated from 0.2 to 6 ms after the start of the voltage step. OFF gating currents were integrated from 0.2 to 20 ms after the start of the voltage step. Currents were baseline-subtracted from 20 to 30 ms after the start of the voltage step. Charge movement data as functions of voltage were fitted with a Boltzmann function (Eq. 2) with $f(V) = Q$ and the order, x, set to 1. Time constants were determined by fitting Eq. 4 to the decay phase of gating current traces. The voltage dependence of ON gating charge movement was determined by fitting gating current decay time constants as a function of voltage:

$$\tau = \tau_{0mV}\left(e^{\frac{-VzF}{RT}}\right), \quad (7)$$

where τ is the time constant of ON gating current decay, $\tau_{0\ mV}$ is the time constant of ON gating current decay at 0 mV, V is voltage, z is valence in units of elementary charge (e_0), F is the Faraday constant, R is the ideal gas constant, and T is absolute temperature. Traces with obvious leak artifacts were excluded from analysis.

Statistics

Statistical tests were performed in Igor Pro 8. Uncertainties reported with fit parameters are SDs. Arithmetic means and SEMs are reported for current amplitudes and charge movement. Geometric means and positive SEMs are reported for time constants and rates. Wilcoxon rank tests were performed assuming independent samples unless otherwise noted. Two-tailed P values are reported for the hypothesis that samples have identical medians.

Online supplemental material

Fig. S1 compares currents from untransfected CHO cells and Kv2.1-CHO cells in 1 µM RY785. Fig. S2 compares Kv2.1

activation kinetics during onset of inhibition by RY785. Fig. S3 is an alignment of expected cavity-lining residues of Kv2 and KvS channel subunits.

Results

At all physiological voltages, block by RY785 appears complete

Knowing how completely a drug can inhibit channels is important for interpretation of experiments and can reveal clues about the drug's mechanism of action. We asked how completely RY785 inhibits Kv2 K^+ currents. To study RY785 inhibition, we voltage-clamped homomeric channels composed of rat Kv2.1 subunits expressed in a stably transfected CHO-K1 cell line (Trapani and Korn, 2003). When 1 µM RY785 was applied and depolarizing steps were given until currents stabilized, RY785 eliminated voltage-activated outward currents (Fig. 1 A). Block by RY785 appeared complete, as currents with activation kinetics resembling Kv2.1 were no longer discernable. At +40 mV, 1 µM RY785 blocked 98.3 ± 0.4% (mean ± SEM) of outward current (Fig. 1 B). CHO-K1 cells have been found to lack endogenous voltage-gated K^+ channel expression (Gamper et al., 2005), yet in untransfected CHO-K1 cells, endogenous outward currents were apparent above +40 mV. These endogenous CHO currents were not blocked by 1 µM RY785 and appeared similar to the residual currents of Kv2.1-CHO cells in 1 µM RY785 (Fig. S1 A). A comparison of current amplitudes at +90 mV, where endogenous CHO currents were detectable in all cells, revealed that the magnitude of residual currents of Kv2.1-CHO cells in 1 µM RY785 were within SEM of CHO cells without a Kv2.1 plasmid (Fig. S1 B). This suggests that most, if not all, residual outward current from Kv2.1-CHO cells in 1 µM RY785 (Fig. 1 C) is attributable to endogenous CHO currents, not Kv2.1. These findings indicate that 1 µM RY785 eliminates the Kv2.1 conductance in response to voltage steps up to at least +90 mV from a holding potential of −100 mV, a range spanning the physiologically relevant voltages set by typical Na^+ and K^+ reversal potentials.

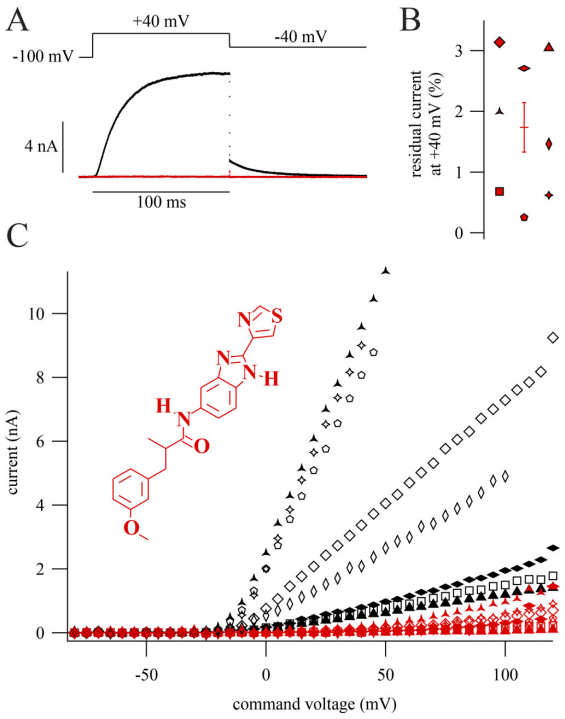

Figure 1. **RY785 blocks Kv2.1.** Displayed currents in 1 µM RY785 are following a train of depolarizations to allow RY785 to inhibit Kv2.1 currents. **(A)** Top: Voltage command. Bottom: Representative currents from a whole-cell voltage-clamped Kv2.1-CHO cell in vehicle (black) and RY785 (red). **(B)** Current remaining during inhibition by RY785 from eight cells (red symbols). Horizontal line is mean ± SEM. **(C)** Current as a function of command voltage. Currents are means 98–100 ms after the start of the activating voltage step. Symbols correspond to individual cells in vehicle (black) and RY785 (red). Points are excluded if the predicted voltage error of clamp is >10 mV. Inset: Structure of RY785.

RY785 inhibition requires voltage activation but not channel opening

After application of RY785 to human Kv2.1 channels, voltage activation is required for onset of inhibition, and K^+ current progressively declines during repeated positive voltage steps (Herrington et al., 2011). We characterized how inhibition of rat Kv2.1 by RY785 responds to voltage activation. To measure the voltage dependence of the rate of inhibition by RY785, we designed a two-pulse protocol containing a brief test pulse to +40 mV followed by longer postpulse to a voltage which we later varied between experiments. In the presence of 1 µM RY785, Kv2.1 current amplitudes in response to a two-pulse protocol decay over time (Fig. 2 A). No inhibition occurs when cells are held at −100 mV (Fig. 2 B). The simple exponential kinetics of block in response to +40-mV voltage steps (Fig. 2 B, red curve) suggests that a single RY785 binding event is sufficient to completely inhibit Kv2.1. Additionally, when K^+ conductance is only partially inhibited by RY785, the time constants associated with voltage activation do not vary (Fig. S2), consistent with all-or-nothing block of individual channels.

We next tested whether channel opening is required for RY785 inhibition. If so, then RY785 should inhibit Kv2.1 with a rate proportional to the channel's open probability. We used the whole-cell Kv2.1 G–V relationship as a proxy for Kv2.1 open probability. Although the occurrence of subconducting conformations of rat Kv2.1 single channels (Chapman et al., 1997) makes the G–V relationship an imperfect proxy, the fully conducting conformation of a rat Kv2.1 variant has been used to effectively characterize its G–V relationship (Islas and Sigworth, 1999), and we have found subconducting conformations to occur <10% as often as full openings in this Kv2.1-CHO cell line (Tilley et al., 2019), suggesting that the G–V relationship is reasonably proportionate to open probability. We monitored the decay of Kv2.1 current amplitudes in the presence of RY785 and varied the voltage of the postpulse step between cells (Fig. 3, A and B). We then fitted an exponential function (Eq. 4) to the decay of Kv2.1 currents during repeated cycles of the two-pulse protocol (Fig. 3 B). In these fits, the apparent rate of inhibition seems to saturate below −60 mV and above 0 mV (Fig. 3 C). We estimated rates of inhibition during the postpulse steps (k_{post}; Eq. 5). A

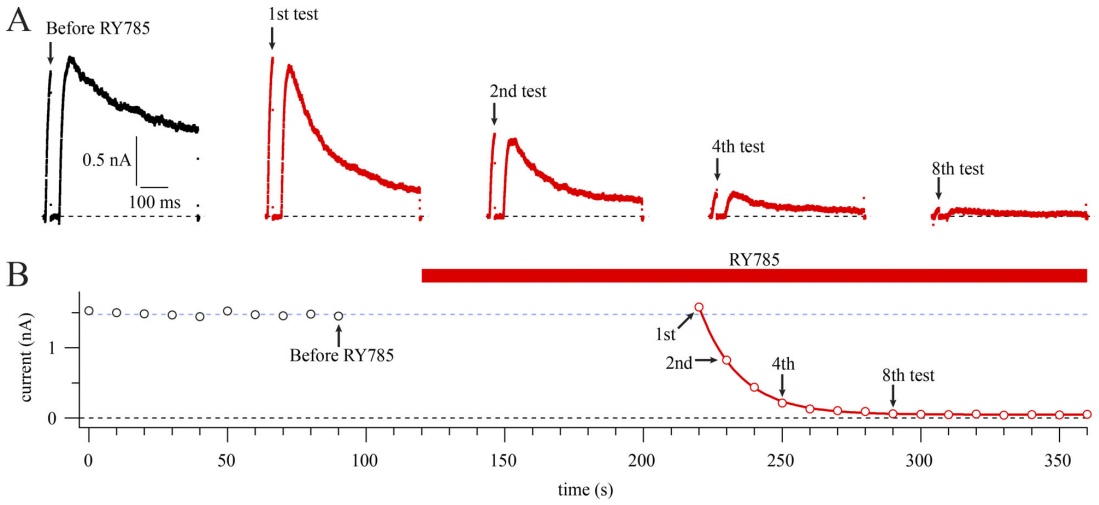

Figure 2. **Voltage stimuli are required for RY785 to inhibit Kv2.1. (A)** Current traces from a representative cell in vehicle (black) or 1 µM RY785 (red). Voltage protocol from a holding potential of −100 mV is a 20-ms step to +40 mV followed by a 30-ms step to −100 mV and then a 500-ms step to +40 mV. Arrows indicate time points labeled in B. **(B)** Mean current in the final 1 ms of the 20-ms test pulse (circles). Red bar indicates application of 1 µM RY785. Currents in RY785 are fitted with an exponential function (Eq. 4, red curve). Function variables ± SD, y_0 = 0.0482 ± 0.0039 nA, A = 1.533 ± 0.012 nA, τ = 14.40 ± 0.24 s. Dotted blue line indicates steady state current before RY785 application.

Boltzmann fit (Eq. 2) assigned half-maximal k_{post} at V_{mid} = −20.2 ± 4.9 mV (Fig. 3 D). However, G–V relations calculated from currents recorded in vehicle (Fig. 1) indicated that the voltage at which conductance was half maximal was V_{mid} = +23.8 ± 1.2 mV (Fig. 3 E), 44 mV more positive than the midpoint of the inhibition rate. It appears clear that the voltage dependence of block does not follow G. The coarse resolution and substantial cell-to-cell variability in the k_{post}–voltage relation precludes more detailed conclusions about the voltage dependence of the inhibition rate. Nevertheless, this finding is inconsistent with the hypothesis that RY785 binds only once channels open. To assess the validity of our estimates of k_{post}, we also determined RY785 inhibition rates by fitting exponential functions to current decay (Fig. 4 A). The inhibition rate was determined in this manner during 0-, +20-, and +40-mV pulses where Kv2.1 current decay could be reliably fitted. After applying a correction that attempts to account for current decay due to inactivation, the inhibition rates measured by fitting current decay during a single pulse ($k_{single\ pulse}$, Fig. 4 B) were about two times faster than values measured from repeated two-pulse cycles (k_{post}, Fig. 3 E), which we consider to be roughly similar. RY785 inhibition rates measured by the method of Fig. 4 were not significantly different at 0, +20, or +40 mV (one-way ANOVA, P = 0.39). However, Kv2.1 conductance increases between 0 and +40 mV (one-way ANOVA, P = 1.7 × 10^{-10}) by a factor of 3 (Fig. 3 E). Again, the onset of RY785 inhibition is responsive to voltage activation, but the rate is not correlated with the degree of channel opening. We noted that the V_{mid} of k_{post} was similar to the V_{mid} = −29.3 ± 2.8 mV of gating charge movement from Kv2.1 in the same CHO-K1 cell line (Fig. 3 E). This correlation suggests that the RY785 binding site is exposed by voltage-sensor activation, but not channel opening itself.

RY785 is trapped by the resting conformation of Kv2.1

We asked how membrane voltage affects relief of inhibition after wash-out of RY785 from the recording chamber. If RY785 is an allosteric modulator that simply prefers voltage-activated channel conformations, then channel deactivation at negative voltages would enhance drug dissociation. Alternatively, if voltage activation provides gated access to a binding site, channel deactivation could trap RY785 within the channel. To distinguish between these possibilities, we analyzed current recovery after drug wash-out as a proxy for RY785 dissociation and asked whether recovery from inhibition depends on voltage. Our recovery from inhibition protocol was performed following a subset of the 1 µM RY785 wash-in experiments of Fig. 3 (Fig. 5 A). During recovery experiments, we used a two-pulse protocol with 4-s postpulses and tested two postpulse voltages: −80 and +40 mV (Fig. 5 B). With a −80 mV postpulse, only 8.1 ± 1.9% (mean ± SEM) of current recovered after 600 s of pulsing (Fig. 5 C, left). However, with a +40 mV postpulse, 65.2 ± 8.3% of current recovered over the same duration (Fig. 5 C, right). Some current recovery time courses exhibited a delay before current amplitudes begin to rise. While this delay could be indicative of current recovery requiring multiple RY785 molecules to dissociate from each channel, the cell-to-cell variability in delay leads us to suspect that the delay results from a variable latency for RY785 to diffuse out from cells. From exponential fits (Eq. 4) of current recovery time courses, we estimate the rate of current recovery to be 0.0104 ± 0.0016 s^{-1} (mean ± SEM) during the pulses to +40 mV (Fig. 5 D). Current recovery was incomplete with postpulses to −80 mV. Using linear regression, we estimated the recovery rate to be 0.000134 ± 0.000031 s^{-1} (Fig. 5 D) during postpulses to −80 mV, 1% of the rate at +40 mV. These results suggest that dissociation of RY785 from Kv2.1 is highly

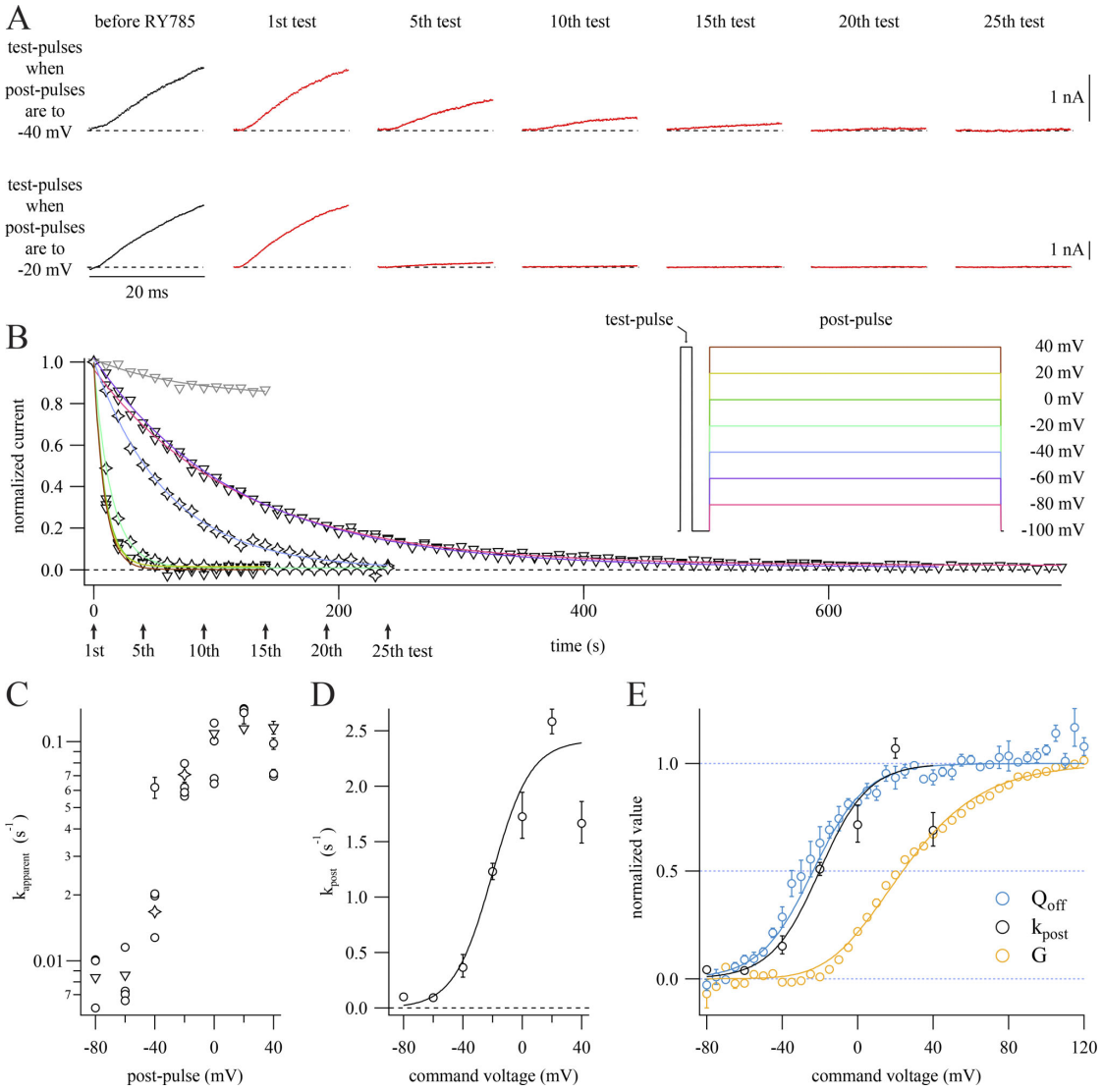

Figure 3. **RY785 inhibition rate is not proportional to K⁺ conductance. (A)** Representative current traces from two cells subjected to the voltage protocol inset in B. Cells held at −100 mV were given a 20-ms step to +40 mV followed by a 30-ms step to −100 mV and then a 500-ms step to a voltage which varied between cells. 10 s elapsed during each cycle. Dashed lines indicate 0 current. Data from these exemplars are represented as stars in B and C. **(B)** Time courses of current inhibition from representative cells with postpulses to the indicated voltages. Mean currents from the final 1 ms of each test pulse (symbols) are normalized to the first test pulse in RY785. Stars correspond to exemplars shown in A. Arrows indicate time points shown in A. Function variables from fitted exponential function (Eq. 4, curves) ± SD; −80 mV, τ = 119.0 ± 01.2 s^{-1}, I_0 = 0.0211 ± 0.0016; −60 mV, τ = 116.0 ± 1.0 s^{-1}, I_0 = 0.0123 ± 0.0016; −40 mV, τ = 59.7 ± 02.0 s^{-1}, I_0 = 0.0034 ± 0.0085; −20 mV, τ = 14.13 ± 00.16 s^{-1}, I_0 = 0.0093 ± 0.0013; 0 mV, τ = 09.168 ± 00.063 s^{-1}, I_0 = 0.01323 ± 0.00083; +20 mV, τ = 08.71 ± 00.18 s^{-1}, I_0 = 0.0162 ± 0.0024; +40 mV, τ = 08.62 ± 00.59 s^{-1}, I_0 = 0.0017 ± 0.0080; vehicle control (gray), +20 mV, τ = 74 ± 21 s^{-1}, I_0 = 0.832 ± 0.023. **(C)** Apparent rates of inhibition ($k_{apparent}$) plotted against postpulse voltage. $k_{apparent}$ ± SD from fits to individual cells. Stars and triangles correspond to exemplars shown in A and B. **(D)** Relation of RY785 inhibition rate during the postpulse (k_{post}) to postpulse voltage. Geometric mean rate ± SEM (circles) calculated from cells in C. Boltzmann function fitted to RY785 inhibition rates (curve). Function variables ± SD: *x* held at 1. V_{half} = −20.2 ± 4.9 mV, *z* = 1.97 ± 0.30 e_0, *A* = 2.41 ± 0.24 s^{-1}. **(E)** Comparison of RY785 inhibition rates to Kv2.1 G–V relation (yellow) and OFF gating charge–voltage (Q_{OFF}–*V*) relation (blue). Means ± SEM. G–V from cells in vehicle, *n* = 4 cells. Q_{OFF}–*V* replotted from a prior publication (Tilley et al., 2019). Amplitudes normalized to fitted Boltzmann functions (Eq. 2), shown as solid curves. Function variables ± SD; Q_{OFF}, *x* set to 1, V_{half} = −23.7 ± 1.6 mV, *z* = 1.81 ± 0.12 e_0; G, *x* set to 4, V_{half} = −19.95 ± 0.73 mV, *z* = 0.968 ± 0.020 e_0.

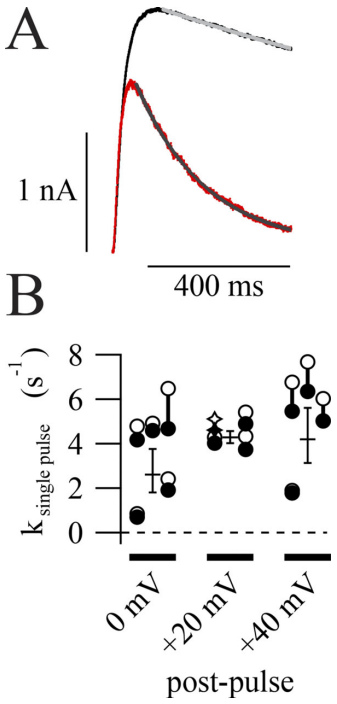

Figure 4. **Rates of inhibition determined from single voltage steps. (A)** Representative current decay during postpulses. First pulse in 1 µM RY785 (red) fitted with an exponential function (Eq. 4, gray curve). Function variables ± SD, I_0 = 34.6 ± 1.4 pA, τ = 0.19591 ± 0.00051 s. Average of 10 traces in vehicle (black) and fit (light gray curve), τ ± SD = 7.4 ± 1.2 s, I_0 held at 34.6 pA. **(B)** Category plot showing inhibition rates at three voltages. Hollow symbols represent rates of current decay in RY785 from individual cells. Filled symbols represent rates of current decay in RY785 corrected by subtracting rate of current decay in vehicle from the same cell. Stars correspond to the exemplar shown in A. Geometric means ± SEM of corrected rates are shown as horizontal lines. n = 4 or 5 per voltage.

dependent on voltage activation of the channel, occurring at a lower rate when the channel is deactivated. This result is inconsistent with a simple allosteric mechanism in which RY785 dissociates more rapidly from resting channels. Our observations instead suggest that RY785 has better access to and from its inhibitory site when channels are voltage activated.

TEA competes with RY785

A gated-access mechanism was first used to explain open channel block by intracellular quaternary ammonium ions such as TEA (Armstrong and Hille, 1972). TEA binds within the central cavity of voltage-gated K^+ channels, with access to the intracellular solution gated by the protein's sixth transmembrane helix (S6; Armstrong and Hille, 1972; Choi et al., 1993; Zhou et al., 2001). If RY785 binds in the central cavity, then we would expect it to compete for its binding site with TEA. To test this, we asked whether the rate of inhibition by RY785 could be reduced by intracellular TEA. At +20 mV, the predicted IC_{50} of internally applied TEA against rat Kv2.1 is 0.25 mM (Taglialatela et al., 1991). We supplemented our pipette solution with 2 mM TEA, which is predicted to occupy the central cavity 89% of the time at +20 mV, then applied 1 µM RY785 and stimulated with a two-pulse protocol with postpulses to +20 mV. We found that pretreatment with TEA slowed RY785 inhibition by a factor of 4 (Fig. 6). Thus, although RY785 is not exclusively an open channel blocker, occupancy of the intracellular TEA binding site prevents RY785 from binding in the channel.

RY785 alters gating charge movement

To search for evidence of allosteric modulation by RY785, we measured Kv2.1 gating currents. After treatment with 1 µM RY785, both ON and OFF gating currents appeared to be altered (Fig. 7, A and B). RY785 diminished the amount of ON gating charge movement compared with vehicle controls (Fig. 7 C) and, to a greater extent, diminished OFF gating charge (Fig. 7 D), indicating that RY785 inhibits components of voltage sensor movement. We suspect that the discrepancy between the magnitude of diminishment of the ON and OFF gating charges is an artifact of our current integration procedures. While we were able to reliably integrate a fast component of ON gating charge movement, the final steps of Kv2.1 voltage activation are much slower, and these small gating currents were difficult to reliably differentiate from integration noise. Consequently, more charge is apparent in OFF gating charge movements after these slow steps have occurred, leading to an apparent Q_{OFF}/Q_{ON} ratio >1 (Tilley et al., 2019). Here, the average apparent Q_{OFF}/Q_{ON} ratio from 0 to +80 mV in vehicle controls was 1.6 ± 0.1 (SEM, n = 8). However, the Q_{OFF}/Q_{ON} ratio drops to near unity in 1 µM RY785, 0.9 ± 0.2 (SEM, n = 4), indicating that that, in addition to the diminishment of fast ON charge movement, a slower component of ON charge movement is eliminated by RY785. To probe how gating charge dynamics are modulated by RY785, we analyzed gating current kinetics. The kinetics and voltage dependence of the decay of ON gating current remaining in RY785 are similar to vehicle controls (Fig. 7 E). However, RY785 accelerates OFF gating charge kinetics (Fig. 7 F), indicating that deactivation of channels inhibited by RY785 is accelerated. Altogether, the gating current modifications indicate that RY785 prevents movement of a component of gating charge and accelerates deactivation of the gating charge that remains mobile.

Discussion

The mechanism of inhibition

We conclude that intracellular TEA competes with RY785, that RY785 binds to and dissociates from an inhibitory site only accessible when voltage sensors are activated, that channel opening itself has little impact on access, and that RY785 binding prevents some gating charge movement and promotes voltage sensor deactivation. A physical model that might explain our observations is RY785 binding within a central cavity, with access available in activated-not-open and open states. Further, the accelerated OFF gating currents suggest that RY785 binding closes the cavity, trapping RY785 within the channel. Together,

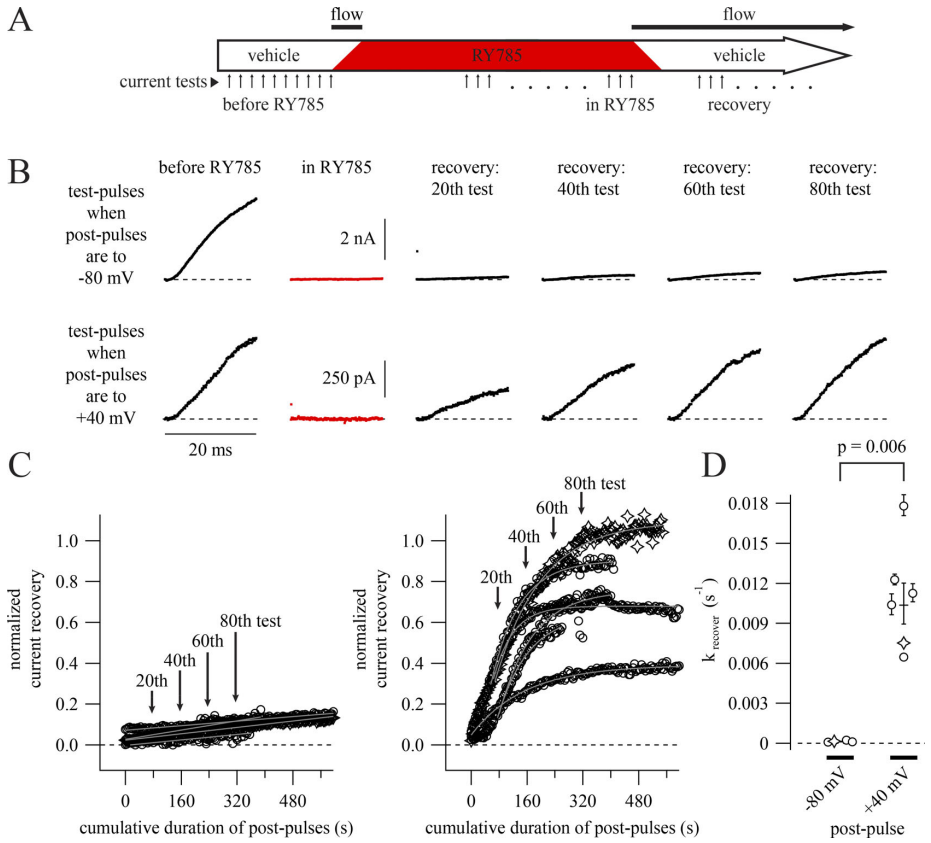

Figure 5. **Negative membrane potential slows RY785 dissociation. (A)** Cartoon timeline of experiments. The number of voltage protocol cycles used to inhibit and recover Kv2.1 currents varied between cells. **(B)** Representative current traces from two cells. Dashed lines indicate zero current. Data from these cells are represented as stars in C and D. **(C)** Time courses of current recovery with postpulses to −80 (left) or +40 (right) mV. Mean currents from the final 1 ms of each test pulse, normalized to before RY785 wash-in, are shown as symbols. Arrows indicate time points shown in B. Time courses at −80 mV (left, n = 4) are fitted with gray lines. Time courses at +40 mV (right, n = 6) are fitted with single exponential functions (Eq. 4, gray curves). **(D)** Category plot showing current recovery rates at two voltages. Rates were calculated from the fits in C. Geometric means ± SEM are shown as horizontal lines.

these results suggest that RY785 may act as a "closed-channel blocker" similar to 4-aminopyridine in Kv1 channels (Armstrong and Loboda, 2001). Trapping of blockers has been documented for Kv channels including Shaker Kv1 (Holmgren et al., 1997), and mammalian Kv3.1 (Kirsch and Drewe, 1993). When Kv channels close their intracellular gate, a constriction is formed that prevents access of molecules as small as Ag^+ (del Camino and Yellen, 2001) and exit of blockers including quaternary ammonium ions and 4-aminopyridine (Kirsch and Drewe, 1993; Holmgren et al., 1997). We have found that RY785 bears the hallmarks of trapping: requirement for voltage activation for block or unblock. RY785 appears unique among these trapped blockers in that it eliminated the majority of OFF gating current, by 64 ± 15% in our experiments. Trapping of 4-aminopyridine in Shaker channels or TEA in Shaker I470C does not eliminate gating charge, but shifts charge movement to more positive voltages and accelerates OFF gating current (Loboda and Armstrong, 2001; Melishchuk and Armstrong, 2001).

Alternate interpretations

The observation that RY785 becomes trapped by negative membrane potentials is incompatible with a simple allosteric mechanism in which RY785 merely stabilizes voltage-activated channel conformations, and RY785 destabilizes activated conformations, as evidenced by diminished ON gating currents. While physical trapping of RY785 within the channel seems the most parsimonious explanation for our results, we cannot exclude more complicated models. Kv2.1 channels adopt inactivated and other nonconducting states (O'Connell et al., 2010; Fox et al., 2013; VanDongen et al., 1990). While it is possible that RY785 induces one of these states, this would offer no obvious explanation for RY785's voltage dependence of inhibition or its effects on gating currents.

We interpreted RY785's effects on gating current kinetics under the simplifying assumption that residual gating currents correspond to conformation changes that also occur in the unbound channel. However, multiple other possibilities exist if

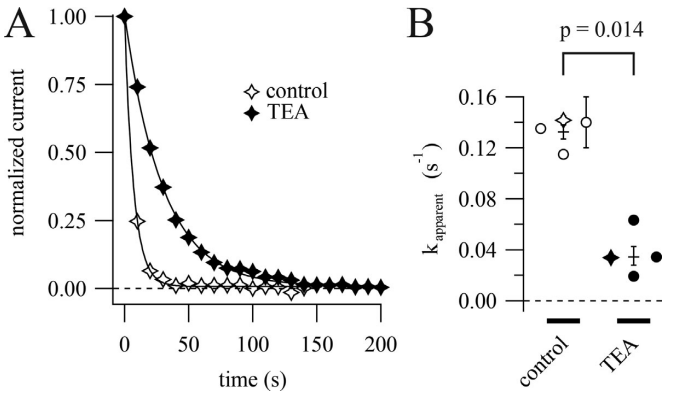

Figure 6. **Intracellular TEA competes with RY785. (A)** Time courses of current inhibition by 1 µM RY785 from cells with postpulses to +20 mV. Mean currents from the final 1 ms of each test pulse (symbols), normalized to the first test pulse in RY785. Time courses from a representative control cell (open symbols) and a representative cell pretreated with 2 mM intracellular TEA (closed symbols). Time courses are fitted with exponential functions (Eq. 4). Data from these cells are represented as stars in B. **(B)** Apparent RY785 inhibition rates ± TEA. Rates ± SD from fits to individual cells (symbols). Geometric means ± SEM are shown as horizontal lines.

RY785 binding generates new voltage sensor conformations. Furthermore, differences in the solutions for K^+ and gating current recordings could alter interactions with RY785. For example, intracellular $NMDG^+$ is an open-channel blocker of Shaker K^+ channels (Melishchuk and Armstrong, 2001), and if $NMDG^+$ interacts similarly with Kv2.1, then acceleration of OFF gating current following RY785 application could be due to RY785 displacing $NMDG^+$ from the channel cavity.

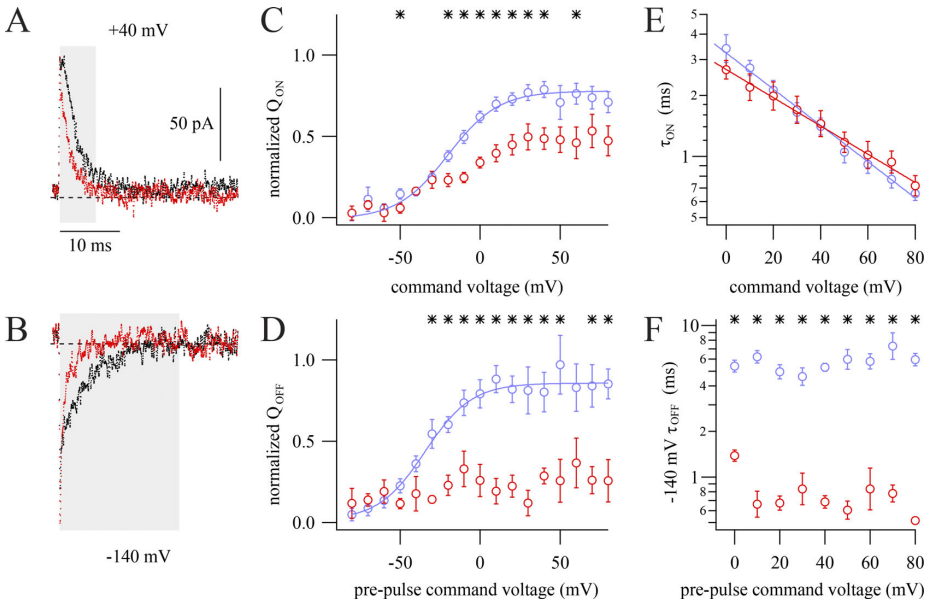

Figure 7. **RY785 modifies gating currents.** Kv2.1 gating currents were elicited in K^+-free solutions with 100-ms steps to voltages between −80 and +80 mV from a holding potential of −100 mV (ON gating currents) and during subsequent 50-ms steps to −140 mV (OFF gating currents). **(A)** Exemplar ON gating currents at +40 mV before (black) and after (red) application of RY785. Integration windows used for the analysis in C (highlighted) were 0.2–6 ms after the voltage step. **(B)** Exemplar OFF gating currents at −140 mV following the steps shown in A before (black) and after (red) application of RY785. Integration windows used for the analysis in D (highlighted) were 0.2–20 ms after the voltage step. **(C)** Mean ON gating charge transfer (Q_{ON}) as a function of voltage from n = 8 vehicle-treated cells (blue) and n = 4 RY785-treated cells (red). Mean ± SEM. *, P < 0.05. Curve is fit of Eq. 2 with x held at 1. Function variables ± SD, vehicle: V_{half} = −20.1 ± 5.8 mV, z = 1.62 ± 0.57 e_0, A = 0.79 ± 0.11. RY785 data was not well fitted by Eq. 2. **(D)** Mean OFF gating charge (Q_{OFF}) transfer as a function of voltage from vehicle-treated cells (blue) and RY785-treated cells (red). Mean ± SEM. *, P < 0.05. Vehicle: n = 7 overall, ≥6 at each voltage; RY785: n = 4 overall, ≥2 at each voltage. Curve is a fit of Eq. 2 with x held at 1. Function variables ± SD: V_{half} = −34.4 ± 9.0 mV, z = 1.7 ± 1.0 e_0, A = 0.84 ± 0.21. RY785 was not well fitted by Eq. 2. **(E)** Mean time constants of activation (τ_{ON}) determined by fitting Eq. 4 to the decay phase of ON gating current traces from n = 8 vehicle-treated cells (blue) and n = 4 RY785-treated cells (red). Mean ± SEM. Lines are fits of Eq. 7. Function variables ± SD; vehicle, τ = 3.2 ± 0.6 ms, z = 0.52 ± 0.09 e_0; RY785, τ = 2.7 ± 0.5 ms, z = 0.41 ± 0.09 e_0. **(F)** Mean time constants of deactivation (τ_{OFF}) determined by fitting Eq. 4 to the decay phase of OFF gating current traces from vehicle-treated cells (blue) and RY785-treated cells (red). Mean ± SEM. *, P < 0.05. Vehicle, n = 8 overall, ≥6 at each voltage; RY785, n = 4 overall, ≥2 at each voltage.

Implications regarding channel gating

Taken together, competition with TEA and the requirement of voltage sensor activation for block imply that the channel creates a pathway for RY785 to enter the central cavity of activated-not-open channels. What might this activated-not-open conformation be? When Kv2.1 activates in response to positive voltage steps, pore opening is far slower than voltage-sensor activation, and the G–V is shifted to voltages more positive than the fourth power of the Q–V (Tilley et al., 2019; Islas and Sigworth, 1999; Scholle et al., 2004). This behavior resembles that of the ILT mutant of the Shaker voltage-gated K^+ channel (Smith-Maxwell et al., 1998; Ledwell and Aldrich, 1999). However, the central cavity of the activated-not-open Shaker ILT channel is not open to the cytosol (del Camino et al., 2005). If the S6 gate in activated-not-open Kv2.1 is also closed, and RY785 indeed binds within the central cavity, then RY785 would need to gain access through a voltage-dependent gate which is distinct from the intracellular S6 movements that gate access to K^+ and TEA. Such a gate exists in voltage-gated Na^+ channels that have membrane-buried fenestrations in their pores through which lipophilic drug molecules may enter (Hille, 1977; Nguyen et al., 2019). However, no fenestrations are apparent in the open state of Kv1.2, the closest relative of Kv2.1 with a high-resolution structure (Long et al., 2005). As such, RY785 access to the central cavity with a closed S6 intracellular gate seems unlikely.

It seems more plausible that Kv2.1 adopts an activated-not-open conformation with the central cavity open to the cytosol, providing RY785 and intracellular TEA a route of access and subsequent egress. It is not clear whether widening of the intracellular S6 gate is the final opening step in the Kv2.1 activation path. BK and CNG channels, which are structurally related to Kv channels, gate access of blocking molecules to the intracellular cavity, yet gate ionic permeation with the selectivity filter (Wilkens and Aldrich, 2006; Contreras et al., 2008; Contreras and Holmgren, 2006; Tang et al., 2009; Thompson and Begenisich, 2012; Yan et al., 2016). If selectivity filter opening is the final step in the Kv2.1 activation pathway, then intracellular S6 movements could gate access of RY785. This mechanism would also explain voltage-gated access of 4-aminopyridine to closed states of Kv2.1 (Kirsch and Drewe, 1993). Selectivity filter gating in Kv2.1 channels has been studied in the context of inactivation and operates differently than in Kv1 channels (Klemic et al., 1998; Cheng et al., 2011; Coonen et al., 2020; Immke et al., 1999; Andalib et al., 2004). We note that a selectivity filter mutation that abolishes selectivity filter gating also abolishes the slow step in Kv2.1 activation gating and shifts the G–V to more negative voltages (Coonen et al., 2020). These behaviors are consistent with gating at the selectivity filter underlying the separation of gating-charge movement from conductance in both time and voltage. Considering these features of Kv2 gating, we propose an explanation for gated access of RY785: upon voltage sensor activation, Kv2.1 adopts an activated-not-open conformation in which the intracellular S6 gate has opened to the cytosol, yet the selectivity filter is in a nonconducting state (Scheme 1). The gating current modifications could potentially be accounted for by RY785 accelerating deactivation from the activated-not-open conformation

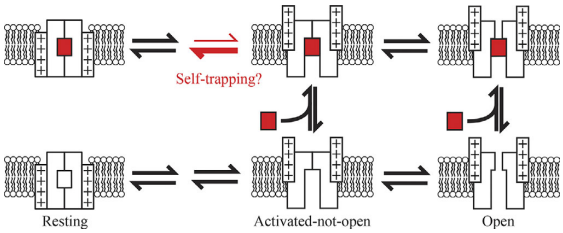

Scheme 1. **Proposed mechanism of inhibition.** State diagram depicting a Kv2.1 channel gating in the presence of RY785 (red rectangle). RY785 has access only to voltage-activated conformations of the channel. RY785 promotes deactivation and is trapped by deactivation of voltage sensors to a resting state.

(red arrows) or other modifications to gating kinetics. As deactivation traps RY785 and RY785 accelerates voltage sensor deactivation, the slow unblock kinetics may result from "self-trapping" upon RY785 binding.

Pharmacological implications

We find that 1 μM RY785 almost completely inhibits the K^+ conductance mediated by rat Kv2.1 channels heterologously expressed in CHO-K1 cells. Extrapolating from the block and recovery kinetics with 1 μM RY785 and postpulses to +40 mV, we estimate a K_d of 6.2 ± 1.2 nM (SEM) for the rat Kv2.1 channels expressed in CHO-K1 cells. This appears more potent than the reported IC_{50} of 50 nM for RY785 against human Kv2.1 expressed in CHO-K1 cells (Herrington et al., 2011). However, we do not know whether there is a difference in affinities between human and rat Kv2.1 or whether the difference is due to distinct measurement methods or other differences in experiments, e.g., temperature, voltage clamp configuration, or voltage protocols. We did not measure an IC_{50} from concentration-effect experiments and note that slow kinetics of block at nanomolar concentrations, slow kinetics of unblock, time-dependent changes in Kv2.1 gating after whole-cell break, voltage dependence of RY785 access, and allosteric effects all pose challenges to accurate measurement of a meaningful IC_{50}.

The process of RY785 block appears to simply decrease K^+ conductance density, and a simple decrease in Kv2 conductance density is the expected effect of RY785 in other experimental conditions. As RY785 appears to alter gating charge equilibria, the principle of coupled equilibria requires that RY785 affinity for Kv2.1 be affected by gating. As such, the extensive regulation of Kv2 channel gating in vivo could alter the affinity and dynamics of RY785 inhibition. Because RY785 stabilizes a deactivated conformation, more positive membrane potentials could weaken RY785 affinity. However, any changes in membrane potential within the physiological voltage range would be expected to only slowly impact RY785 blockade. The estimated dissociation rates at −80 mV and +40 mV, of 0.0001 s^{-1} and 0.01 s^{-1}, respectively, suggest that any unblock induced by more positive voltages would equilibrate far too slowly to impact K^+ conductance kinetics on the millisecond timescale of a typical action potential.

As TEA competes with RY785, it is possible that residues of the intracellular cavity, in which TEA binds, also form the RY785 binding site. If so, sequence similarities suggest that RY785 will be effective at blocking the Kv2 channels of many animals. Residues lining the intracellular cavity are identical between Kv2.1 and Kv2.2 and among several deuterostome species with divergence occurring among protostomes (Fig. S3 A). Consistent with this sequence conservation, human Kv2.1 and Kv2.2 have similar affinities for the parent compound from which RY785 was derived (Herrington et al., 2011). Kv1.2 is inhibited by this parent compound with 61-times lower affinity and no apparent use dependence (Herrington et al., 2011). The apparent lack of use dependence could result from a separate mechanism of inhibition, or use dependence could be obscured by rapid equilibration of RY785 with its Kv1.2 binding site. Kv2 subunits can heteromultimerize with Kv5, Kv6, Kv8, and Kv9 subunits, which are collectively known as KvS or silent subunits. The pore regions of KvS subunits are poorly conserved with Kv2 (Fig. S3 B). Some, but not all, Kv2/KvS heteromers have altered TEA pharmacology (Moreno-Domínguez et al., 2009; Zhu et al., 1999), leaving open the question of how Kv2/KvS heteromers will be affected by RY785.

While Kv2 channel heterogeneity may complicate how RY785 impacts endogenous Kv2 currents, we expect the fundamentals of the RY785 gated-access trapping mechanism to apply generally. We suggest that understanding the trapping mechanism presented here could aid interpretation of experiments using RY785 to block endogenous Kv2 channels: channel activation is required for block by RY785 to equilibrate, after which, trapped RY785 will simply decrease the Kv2 conductance density.

Acknowledgments

Christopher J. Lingle served as editor.

We thank Rebecka Sepela, Tsung-Yu Chen, Jie Zheng, Bruce Bean, and Sooyeon Jo for critical feedback.

This research was supported by US National Institutes of Health grants R01NS096317 and R01HL128537.

The authors declare no competing financial interests.

Author contributions: M.J. Marquis: Conceptualization, Formal analysis, Investigation, Methodology, Visualization, Writing - original draft, Writing - reviewing & editing. J.T. Sack: Conceptualization, Formal analysis, Funding acquisition, Investigation, Methodology, Project administration, Supervision, Visualization, Writing - original draft, Writing - reviewing & editing.

Submitted: 10 June 2021
Revised: 1 March 2022
Accepted: 30 March 2022

References

Amberg, G.C., and L.F. Santana. 2006. Kv2 channels oppose myogenic constriction of rat cerebral arteries. *Am. J. Physiol. Cell Physiol.* 291: C348–C356. https://doi.org/10.1152/ajpcell.00086.2006

Andalib, P., J.F. Consiglio, J.G. Trapani, and S.J. Korn. 2004. The external TEA binding site and C-type inactivation in voltage-gated potassium channels. *Biophys. J.* 87:3148–3161. https://doi.org/10.1529/biophysj.104.046664

Armstrong, C.M. 1971. Interaction of tetraethylammonium ion derivatives with the potassium channels of giant axons. *J. Gen. Physiol.* 58:413–437. https://doi.org/10.1085/jgp.58.4.413

Armstrong, C.M., and B. Hille. 1972. The inner quaternary ammonium ion receptor in potassium channels of the node of ranvier. *J. Gen. Physiol.* 59: 388–400. https://doi.org/10.1085/jgp.59.4.388

Armstrong, C.M., and A. Loboda. 2001. A model for 4-aminopyridine action on K channels: Similarities to tetraethylammonium ion action. *Biophys. J.* 81:895–904. https://doi.org/10.1016/S0006-3495(01)75749-9

Bar, C., G. Barcia, M. Jennesson, G. Le Guyader, A. Schneider, C. Mignot, G. Lesca, D. Breuillard, M. Montomoli, B. Keren, et al. 2020. Expanding the genetic and phenotypic relevance of KCNB1 variants in developmental and epileptic encephalopathies: 27 new patients and overview of the literature. *Hum. Mutat.* 41:69–80. https://doi.org/10.1002/humu.23915

Bocksteins, E. 2016. Kv5, Kv6, Kv8, and Kv9 subunits: No simple silent bystanders. *J. Gen. Physiol.* 147:105–125. https://doi.org/10.1085/jgp.201511507

Bocksteins, E., and D.J. Snyders. 2012. Electrically silent Kv subunits: Their molecular and functional characteristics. *Physiology* 27:73–84. https://doi.org/10.1152/physiol.00023.2011

Cerda, O., and J.S. Trimmer. 2011. Activity-dependent phosphorylation of neuronal Kv2.1 potassium channels by CDK5. *J. Biol. Chem.* 286: 28738–28748. https://doi.org/10.1074/jbc.M111.251942

Chapman, M.L., H.M. VanDongen, and A.M. VanDongen. 1997. Activation-dependent subconductance levels in the drk1 K channel suggest a subunit basis for ion permeation and gating. *Biophys. J.* 72:708–719. https://doi.org/10.1016/s0006-3495(97)78707-1

Cheng, Y.M., J. Azer, C.M. Niven, P. Mafi, C.R. Allard, J. Qi, S. Thouta, and T.W. Claydon. 2011. Molecular determinants of U-type inactivation in Kv2.1 channels. *Biophys. J.* 101:651–661. https://doi.org/10.1016/j.bpj.2011.06.025

Choi, K.L., C. Mossman, J. Aubé, and G. Yellen. 1993. The internal quaternary ammonium receptor site of shaker potassium channels. *Neuron.* 10: 533–541. https://doi.org/10.1016/0896-6273(93)90340-W

Contreras, J.E., and M. Holmgren. 2006. Access of quaternary ammonium blockers to the internal pore of cyclic nucleotide-gated channels: Implications for the location of the gate. *J. Gen. Physiol.* 127:481–494. https://doi.org/10.1085/jgp.200509440

Contreras, J.E., D. Srikumar, and M. Holmgren. 2008. Gating at the selectivity filter in cyclic nucleotide-gated channels. *Proc. Natl. Acad. Sci. USA.* 105: 3310 LP–3314. https://doi.org/10.1073/pnas.0709809105

Coonen, L., E. Mayeur, N. De Neuter, D.J. Snyders, L.G. Cuello, and A.J. Labro. 2020. The selectivity filter is involved in the U-type inactivation process of Kv2.1 and Kv3.1 channels. *Biophys. J.* 118:2612–2620. https://doi.org/10.1016/j.bpj.2020.03.032

Dai, X.Q., J. Kolic, P. Marchi, S. Sipione, and P.E. MacDonald. 2009. SUMOylation regulates Kv2.1 and modulates pancreatic β-cell excitability. *J. Cell Sci.* 122:775–779. https://doi.org/10.1242/jcs.036632

del Camino, D., and G. Yellen. 2001. Tight steric closure at the intracellular activation gate of a voltage-gated K^+ channel. *Neuron.* 32:649–656. https://doi.org/10.1016/S0896-6273(01)00487-1

del Camino, D., M. Kanevsky, and G. Yellen. 2005. Status of the intracellular gate in the activated-not-open state of shaker K^+ channels. *J. Gen. Physiol.* 126:419–428. https://doi.org/10.1085/jgp.200509385

Delgado-Ramírez, M., J.J. De Jesús-Pérez, I.A. Aréchiga-Figueroa, J. Arreola, S.K. Adney, C.A. Villalba-Galea, D.E. Logothetis, and A.A. Rodríguez-Menchaca. 2018. Regulation of Kv2.1 channel inactivation by phosphatidylinositol 4,5-bisphosphate. *Sci. Rep.* 8:1769. https://doi.org/10.1038/s41598-018-20280-w

Dilly, S., C. Lamy, N. V Marrion, J.F. Liégeois, J. Liégeois, and V. Seutin. 2011. Ion-channel modulators: More diversity than previously thought. *ChemBioChem.* 12:1808–1812. https://doi.org/10.1002/cbic.201100236

Du, J., L.L. Haak, E. Phillips-Tansey, J.T. Russell, and C.J. McBain. 2000. Frequency-dependent regulation of rat hippocampal somato-dendritic excitability by the K^+ channel subunit Kv2.1. *J. Physiol.* 522 Pt 1:19–31. https://doi.org/10.1111/j.1469-7793.2000.t01-2-00019.xm

Escoubas, P., S. Diochot, M.L. Célérier, T. Nakajima, and M. Lazdunski. 2002. Novel tarantula toxins for subtypes of voltage-dependent potassium channels in the Kv2 and Kv4 subfamilies. *Mol. Pharmacol.* 62:48–57. https://doi.org/10.1124/mol.62.1.48

Ficker, E., W. Jarolimek, J. Kiehn, A. Baumann, and A.M. Brown. 1998. Molecular determinants of dofetilide block of HERG K^+ channels. *Circ. Res.* 82:386–395. https://doi.org/10.1161/01.RES.82.3.386

Fortenbach, C., G.P. Allina, C.M. Shores, S.J. Karlen, E.B. Miller, H. Bishop, J.S. Trimmer, M.E. Burns, and E.N. Pugh. 2021. Loss of the K+ channel Kv2.1 greatly reduces outward dark current and causes ionic dysregulation and degeneration in rod Photoreceptors. *J. Gen. Physiol.* 153:e202012687. https://doi.org/10.1085/JGP.202012687

Fox, P.D., R.J. Loftus, and M.M. Tamkun. 2013. Regulation of Kv2.1 K+ conductance by cell surface channel density. *J. Neurosci.* 33:1259 LP–1270. https://doi.org/10.1523/JNEUROSCI.3008-12.2013

Frech, G.C., A.M. VanDongen, G. Schuster, A.M. Brown, and R.H. Joho. 1989. A novel potassium channel with delayed rectifier properties isolated from rat brain by expression cloning. *Nature*. 340:642–645. https://doi.org/10.1038/340642a0

Gamper, N., J.D. Stockand, and M.S. Shapiro. 2005. The use of Chinese hamster ovary (CHO) cells in the study of ion channels. *J. Pharmacol. Toxicol. Methods*. 51:177–185. https://doi.org/10.1016/j.vascn.2004.08.008

Guan, D., T. Tkatch, D.J. Surmeier, W.E. Armstrong, and R.C. Foehring. 2007. Kv2 subunits underlie slowly inactivating potassium current in rat neocortical pyramidal neurons. *J. Physiol.* 581:941–960. https://doi.org/10.1113/jphysiol.2007.128454

Hawkins, N.A., S.N. Misra, M. Jurado, S.K. Kang, N.C. Vierra, K. Nguyen, L. Wren, A.L. George, J.S. Trimmer, and J.A. Kearney. 2021. Epilepsy and neurobehavioral abnormalities in mice with a dominant-negative KCNB1 pathogenic variant. *Neurobiol. Dis.* 147:105141. https://doi.org/10.1016/j.nbd.2020.105141

Herrington, J., Y.P. Zhou, R.M. Bugianesi, P.M. Dulski, Y. Feng, V.A. Warren, M.M. Smith, M.G. Kohler, V.M. Garsky, M. Sanchez, et al. 2006. Blockers of the delayed-rectifier potassium current in pancreatic β-cells enhance glucose-dependent insulin secretion. *Diabetes*. 55:1034 LP–1042. https://doi.org/10.2337/diabetes.55.04.06.db05-0788

Herrington, J., K. Solly, K.S. Ratliff, N. Li, Y.P. Zhou, A. Howard, L. Kiss, M.L. Garcia, O.B. McManus, Q. Deng, et al. 2011. Identification of novel and selective Kv2 channel inhibitors. *Mol. Pharmacol.* 80:959–964. https://doi.org/10.1124/mol.111.074831

Hille, B. 1977. Local anesthetics: Hydrophilic and hydrophobic pathways for the drug-receptor reaction. *J. Gen. Physiol.* 69:497–515. https://doi.org/10.1085/jgp.69.4.497

Holmgren, M., P.L. Smith, and G. Yellen. 1997. Trapping of organic blockers by closing of voltage-dependent K+ channels: Evidence for a trap door mechanism of activation gating. *J. Gen. Physiol.* 109:527–535. https://doi.org/10.1085/jgp.109.5.527

Hondeghem, L.M., and B.G. Katzung. 1977. Time- and voltage-dependent interactions of antiarrhythmic drugs with cardiac sodium channels. *Biochim. Biophys. Acta*. 472:373–398. https://doi.org/10.1016/0304-4157(77)90003-x

Hönigsperger, C., M.J. Nigro, and J.F. Storm. 2017. Physiological roles of Kv2 channels in entorhinal cortex layer II stellate cells revealed by guangxitoxin-1E. *J. Physiol.* 595:739–757. https://doi.org/10.1113/JP273024

Immke, D., M. Wood, L. Kiss, and S.J. Korn. 1999. Potassium-dependent changes in the conformation of the Kv2.1 potassium channel pore. *J. Gen. Physiol.* 113:819–836. https://doi.org/10.1085/jgp.113.6.819

Islas, L.D., and F.J. Sigworth. 1999. Voltage sensitivity and gating charge in shaker and shab family potassium channels. *J. Gen. Physiol.* 114:723–742. https://doi.org/10.1085/jgp.114.5.723

Jacobson, D.A., A. Kuznetsov, J.P. Lopez, S. Kash, C.E. Ämmälä, and L.H. Philipson. 2007. Kv2.1 ablation alters glucose-induced islet electrical activity, enhancing insulin secretion. *Cell Metab.* 6:229–235. https://doi.org/10.1016/j.cmet.2007.07.010

Kihira, Y., T.O. Hermanstyne, and H. Misonou. 2010. Formation of heteromeric Kv2 channels in mammalian brain neurons. *J. Biol. Chem.* 285:15048–15055. https://doi.org/10.1074/JBC.M109.074260

Kimm, T., Z.M. Khaliq, and B.P. Bean. 2015. Differential regulation of action potential shape and burst-frequency firing by BK and Kv2 channels in substantia nigra dopaminergic neurons. *J. Neurosci.* 35:16404–16417. https://doi.org/10.1523/JNEUROSCI.5291-14.2015

Kirsch, G.E., and J.A. Drewe. 1993. Gating-dependent mechanism of 4-aminopyridine block in two related potassium channels. *J. Gen. Physiol.* 102:797–816. https://doi.org/10.1085/jgp.102.5.797

Klemic, K.G., C.C. Shieh, G.E. Kirsch, and S.W. Jones. 1998. Inactivation of Kv2.1 potassium channels. *Biophys. J.* 74:1779–1789. https://doi.org/10.1016/S0006-3495(98)77888-9

Ledwell, J.L., and R.W. Aldrich. 1999. Mutations in the S4 region isolate the final voltage-dependent cooperative step in potassium channel activation. *J. Gen. Physiol.* 113:389–414. https://doi.org/10.1085/jgp.113.3.389

Lenaeus, M.J., D. Burdette, T. Wagner, P.J. Focia, and A. Gross. 2014. Structures of KcsA in complex with symmetrical quaternary ammonium compounds reveal a hydrophobic binding site. *Biochemistry*. 53:5365–5373. https://doi.org/10.1021/bi500525s

Li, X.N., J. Herrington, A. Petrov, L. Ge, G. Eiermann, Y. Xiong, M.V. Jensen, H.E. Hohmeier, C.B. Newgard, M.L. Garcia, et al. 2013. The role of voltage-gated potassium channels Kv2.1 and Kv2.2 in the regulation of insulin and somatostatin release from pancreatic islets. *J. Pharmacol. Exp. Therapeut.* 344:407 LP–416. https://doi.org/10.1124/jpet.112.199083

Li, X., H. Liu, J.C. Luo, S.A. Rhodes, L.M. Trigg, D.B. Van Rossum, A. Anishkin, F.H. Diatta, J.K. Sassic, D.K. Simmons, et al. 2015. Major diversification of voltage-gated K+ channels occurred in ancestral parahoxozoans. *Proc. Natl. Acad. Sci. USA*. 112:E1010–E1019. https://doi.org/10.1073/pnas.1422941112

Liu, P.W., and B.P. Bean. 2014. Kv2 channel regulation of action potential repolarization and firing patterns in superior cervical ganglion neurons and hippocampal CA1 pyramidal neurons. *J. Neurosci.* 34:4991–5002. https://doi.org/10.1523/JNEUROSCI.1925-13.2014

Loboda, A., and C.M. Armstrong. 2001. Resolving the gating charge movement associated with late transitions in K channel activation. *Biophys. J.* 81:905–916. https://doi.org/10.1016/S0006-3495(01)75750-5

Long, S.B., E.B. Campbell, and R. MacKinnon. 2005. Crystal structure of a mammalian voltage-dependent shaker family K+ channel. *Science*. 309:897–903. https://doi.org/10.1126/science.1116269

Malin, S.A., and J.M. Nerbonne. 2002. Delayed rectifier K+ currents, IK, are encoded by Kv2 alpha-subunits and regulate tonic firing in mammalian sympathetic neurons. *J. Neurosci.* 22:10094–10105. https://doi.org/10.1523/JNEUROSCI.22-23-10094.2002

Mandikian, D., E. Bocksteins, L.K. Parajuli, H.I. Bishop, O. Cerda, R. Shigemoto, and J.S. Trimmer. 2014. Cell type-specific spatial and functional coupling between mammalian brain Kv2.1 K+ channels and ryanodine receptors. *J. Comp. Neurol.* 522:3555–3574. https://doi.org/10.1002/cne.23641

McCord, M.C., and E. Aizenman. 2013. Convergent Ca^{2+} and Zn^{2+} signaling regulates apoptotic Kv2.1 K+ currents. *Proc. Natl. Acad. Sci. USA*. 110:13988–13993. https://doi.org/10.1073/pnas.1306238110

Melishchuk, A., and C.M. Armstrong. 2001. Mechanism underlying slow kinetics of the OFF gating current in Shaker potassium channel. *Biophys. J.* 80:2167–2175. https://doi.org/10.1016/S0006-3495(01)76189-9

Mendez, F., and F. Wurriehausen. 2009. Patcher's Power Tools. Max-Planck-Institut für biophysikalische Chemie, Göttingen, Germany. http://www3.mpibpc.mpg.de/groups/neher/index.php?page=aboutppt

Milescu, M., F. Bosmans, S. Lee, A.A. Alabi, J.I. Kim, and K.J. Swartz. 2009. Interactions between lipids and voltage sensor paddles detected with tarantula toxins. *Nat. Struct. Mol. Biol.* 16:1080–1085. https://doi.org/10.1038/nsmb.1679

Misonou, H., D.P. Mohapatra, E.W. Park, V. Leung, D. Zhen, K. Misonou, A.E. Anderson, and J.S. Trimmer. 2004. Regulation of ion channel localization and phosphorylation by neuronal activity. *Nat. Neurosci.* 7:711–718. https://doi.org/10.1038/nn1260

Misonou, H., D.P. Mohapatra, and J.S. Trimmer. 2005. Kv2.1: A voltage-gated K+ channel critical to dynamic control of neuronal excitability. *NeuroToxicology*. 26:743–752. https://doi.org/10.1016/j.neuro.2005.02.003

Moreno-Domínguez, A., P. Cidad, E. Miguel-Velado, J.R. López-López, and M.T. Pérez-García. 2009. De novo expression of Kv6.3 contributes to changes in vascular smooth muscle cell excitability in a hypertensive mice strain. *J. Physiol.* 587:625–640. https://doi.org/10.1113/jphysiol.2008.165217

Murakoshi, H., and J.S. Trimmer. 1999. Identification of the Kv2.1 K+ channel as a major component of the delayed rectifier K+ current in rat hippocampal neurons. *J. Neurosci.* 19:1728–1735. https://doi.org/10.1523/JNEUROSCI.19-05-01728.1999

Murakoshi, H., G. Shi, R.H. Scannevin, and J.S. Trimmer. 1997. Phosphorylation of the Kv2.1 K+ channel alters voltage-dependent activation. *Mol. Pharmacol.* 52:821 LP–828. https://doi.org/10.1124/mol.52.5.821

Newkirk, G.S., D. Guan, N. Dembrow, W.E. Armstrong, R.C. Foehring, and W.J. Spain. 2022. Kv2.1 potassium channels regulate repetitive burst firing in extratelencephalic neocortical pyramidal neurons. *Cereb. Cortex*. 32:1055–1076. https://doi.org/10.1093/cercor/bhab266

Nguyen, P.T., K.R. DeMarco, I. Vorobyov, C.E. Clancy, and V. Yarov-Yarovoy. 2019. Structural basis for antiarrhythmic drug interactions with the human cardiac sodium channel. *Proc. Natl. Acad. Sci. USA*. 116:2945–2954. https://doi.org/10.1073/pnas.1817446116

O'Connell, K.M.S., R. Loftus, and M.M. Tamkun. 2010. Localization-dependent activity of the Kv2.1 delayed-rectifier K+ channel. *Proc.*

Natl. Acad. Sci. USA. 107:12351–12356. https://doi.org/10.1073/pnas.1003028107

O'Dwyer, S.C., S. Palacio, C. Matsumoto, L. Guarina, N.R. Klug, S. Tajada, B. Rosati, D. McKinnon, J.S. Trimmer, and L.F. Santana. 2020. Kv2.1 channels play opposing roles in regulating membrane potential, Ca^{2+} channel function, and myogenic tone in arterial smooth muscle. *Proc. Natl. Acad. Sci. USA*. 117:3858–3866. https://doi.org/10.1073/pnas.1917879117

Pathak, D., D. Guan, and R.C. Foehring. 2016. Roles of specific Kv channel types in repolarization of the action potential in genetically identified subclasses of pyramidal neurons in mouse neocortex. *J. Neurophysiol.* 115:2317–2329. https://doi.org/10.1152/jn.01028.2015

Peltola, M.A., J. Kuja-Panula, S.E. Lauri, T. Taira, and H. Rauvala. 2011. AMIGO is an auxiliary subunit of the Kv2.1 potassium channel. *EMBO Rep.* 12:1293–1299. https://doi.org/0.1038/embor.2011.204

Peltola, M.A., J. Kuja-Panula, J. Liuhanen, V. Võikar, P. Piepponen, T. Hiekkalinna, T. Taira, S.E. Lauri, J. Suvisaari, N. Kulesskaya, et al. 2016. AMIGO-Kv2.1 potassium channel complex is associated with schizophrenia-related phenotypes. *Schizophrenia Bull.* 42:191–201. https://doi.org/10.1093/schbul/sbv105

Plant, L.D., E.J. Dowdell, I.S. Dementieva, J.D. Marks, and S.A.N. Goldstein. 2011. SUMO modification of cell surface Kv2.1 potassium channels regulates the activity of rat hippocampal neurons. *J. Gen. Physiol.* 137:441–454. https://doi.org/10.1085/jgp.201110604

Ramu, Y., Y. Xu, and Z. Lu. 2006. Enzymatic activation of voltage-gated potassium channels. *Nature*. 442:696–699. https://doi.org/10.1038/nature04880

Romer, S.H., A.S. Deardorff, and R.E.W. Fyffe. 2019. A molecular rheostat: Kv2.1 currents maintain or suppress repetitive firing in motoneurons. *J. Physiol.* 597:3769–3786. https://doi.org/10.1113/JP277833

Sack, J.T., and K.S. Eum. 2015. Ion channel inhibitors. In Handbook of Ion Channels. J. Zheng, and M.C. Trudeau, editors. 1st ed. Florida: Taylor & Francis Group, Boca Raton. https://doi.org/10.1201/b18027

Scholle, A., S. Dugarmaa, T. Zimmer, M. Leonhardt, R. Koopmann, B. Engeland, O. Pongs, and K. Benndorf. 2004. Rate-limiting reactions determining different activation kinetics of Kv1.2 and Kv2.1 channels. *J. Membr. Biol.* 198:103–112. https://doi.org/10.1007/s00232-004-0664-0

Smith-Maxwell, C.J., J.L. Ledwell, and R.W. Aldrich. 1998. Uncharged S4 residues and cooperativity in voltage-dependent potassium channel activation. *J. Gen. Physiol.* 111:421–439. https://doi.org/10.1085/jgp.111.3.421

Speca, D.J., G. Ogata, D. Mandikian, H.I. Bishop, S.W. Wiler, K. Eum, H.J. Wenzel, E.T. Doisy, L. Matt, K.L. Campi, et al. 2014. Deletion of the Kv2.1 delayed rectifier potassium channel leads to neuronal and behavioral hyperexcitability. *Gene Brain Behav.* 13:394–408. https://doi.org/10.1111/gbb.12120

Taglialatela, M., A.M. Vandongen, J.A. Drewe, R.H. Joho, A.M. Brown, and G.E. Kirsch. 1991. Patterns of internal and external tetraethylammonium block in four homologous K^+ channels. *Mol. Pharmacol.* 40:299–307

Tang, Q.Y., X.H. Zeng, and C.J. Lingle. 2009. Closed-channel block of BK potassium channels by BbTBA requires partial activation. *J. Gen. Physiol.* 134:409–436. https://doi.org/10.1085/jgp.200910251

Thiffault, I., D.J. Speca, D.C. Austin, M.M. Cobb, K.S. Eum, N.P. Safina, L. Grote, E.G. Farrow, N. Miller, S. Soden, et al. 2015. A novel epileptic encephalopathy mutation in KCNB1 disrupts Kv2.1 ion selectivity, expression, and localization. *J. Gen. Physiol.* 146:399–410. https://doi.org/10.1085/jgp.201511444

Thompson, J., and T. Begenisich. 2012. Selectivity filter gating in large-conductance Ca^{2+}-activated K^+ channels. *J. Gen. Physiol.* 139:235–244. https://doi.org/10.1085/jgp.201110748

Tilley, D.C., K.S. Eum, S. Fletcher-Taylor, D. C Austin, C. Dupré, L.A. Patrón, R.L. Garcia, K. Lam, V. Yarov-Yarovoy, B.E. Cohen, and J.T. Sack. 2014. Chemoselective tarantula toxins report voltage activation of wild-type ion channels in live cells. *Proc. Natl. Acad. Sci. USA*. 111:E478–E4796. https://doi.org/10.1073/pnas.1406876111

Tilley, D.C., J.M. Angueyra, K.S. Eum, H. Kim, L.H. Chao, A.W. Peng, and J.T. Sack. 2019. The tarantula toxin GxTx detains K^+ channel gating charges in their resting conformation. *J. Gen. Physiol.* 151:292 LP–315. https://doi.org/10.1085/jgp.201812213

Torkamani, A., K. Bersell, B.S. Jorge, R.L. Bjork Jr., J.R. Friedman, C.S. Bloss, J. Cohen, S. Gupta, S. Naidu, C.G. Vanoye, et al. 2014. De novo KCNB1 mutations in epileptic encephalopathy. *Ann. Neurol.* 76:529–540. https://doi.org/10.1002/ana.24263

Trapani, J.G., and S.J. Korn. 2003. Control of ion channel expression for patch clamp recordings using an inducible expression system in mammalian cell lines. *BMC Neurosci.* 4:15. https://doi.org/10.1186/1471-2202-4-15

Trimmer, J.S. 1991. Immunological identification and characterization of a delayed rectifier K^+ channel polypeptide in rat brain. *Proc. Natl. Acad. Sci. USA*. 88:10764–10768. https://doi.org/10.1073/pnas.88.23.10764

Vacher, H., D.P. Mohapatra, and J.S. Trimmer. 2008. Localization and targeting of voltage-dependent ion channels in mammalian central neurons. *Physiol. Rev.* 88:1407–1447. https://doi.org/10.1152/physrev.00002.2008

VanDongen, A.M.J., G.C. Frech, J.A. Drewe, R.H. Joho, and A.M. Brown. 1990. Alteration and restoration of K^+ channel function by deletions at the N- and C-termini. *Neuron*. 5:433–443. https://doi.org/10.1016/0896-6273(90)90082-Q

Vedantham, V., and S.C. Cannon. 1999. The position of the fast-inactivation gate during lidocaine block of voltage-gated Na^+ channels. *J. Gen. Physiol.* 113:7–16. https://doi.org/10.1085/jgp.113.1.7

Wang, Y., J. Guo, L.L. Perissinotti, J. Lees-Miller, G. Teng, S. Durdagi, H.J. Duff, and S.Y. Noskov. 2016. Role of the PH in state-dependent blockade of HERG currents. *Sci. Rep.* 6:32536. https://doi.org/10.1038/srep32536

Waterhouse, A.M., J.B. Procter, D.M.A. Martin, M. Clamp, and G.J. Barton. 2009. Jalview version 2-A multiple sequence alignment editor and analysis workbench. *Bioinformatics*. 25:1189–1191. https://doi.org/10.1093/bioinformatics/btp033

Wilkens, C.M., and R.W. Aldrich. 2006. State-independent block of BK channels by an intracellular quaternary ammonium. *J. Gen. Physiol.* 128:347–364. https://doi.org/10.1085/jgp.200609579

Wu, W., A. Gardner, and M.C. Sanguinetti. 2015. The link between inactivation and high-affinity block of HERG1 channels. *Mol. Pharmacol.* 87:1042–1050. https://doi.org/10.1124/mol.115.098111

Yan, J., Q. Li, and R.W. Aldrich. 2016. Closed state-coupled C-type inactivation in BK channels. *Proc. Natl. Acad. Sci. USA*. 113:6991–6996. https://doi.org/10.1073/pnas.1607584113

Zhong, X.Z., K.S. Abd-Elrahman, C.H. Liao, A.F. El-Yazbi, E.J. Walsh, M.P. Walsh, and W.C. Cole. 2010. Stromatoxin-sensitive, heteromultimeric Kv2.1/Kv9.3 channels contribute to myogenic control of cerebral arterial diameter. *J. Physiol.* 588:4519–4537. https://doi.org/10.1113/jphysiol.2010.196618

Zhou, M., J.H. Morais-Cabral, S. Mann, and R. MacKinnon. 2001. Potassium channel receptor site for the inactivation gate and quaternary amine inhibitors. *Nature*. 411:657–661. https://doi.org/10.1038/35079500

Zhu, X.R., R. Netzer, K. Böhlke, Q. Liu, and O. Pongs. 1999. Structural and functional characterization of Kv6.2, a new γ-subunit of voltage-gated potassium channel. *Recept. Channel*. 6:337–350

Supplemental material

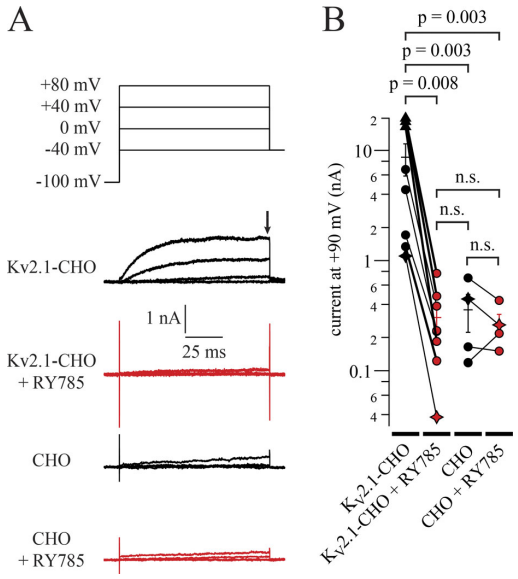

Figure S1. **Residual currents in 1 µM RY785 resemble endogenous CHO currents. (A)** Top: Voltage command. Bottom: Representative currents from Kv2.1-CHO cells or CHO cells without heterologous Kv2.1, in vehicle (black) and RY785 (red). Black arrow indicates time point used for current amplitude quantification in B. **(B)** Current amplitudes at +90 mV. Currents from 98 to 100 ms after stepping to +90 mV from a holding potential of −100 mV (symbols). Exemplars from A are shown as stars. Three cells had voltage clamp errors exceeding 10 mV at +90 mV (triangles). For these three cells, currents were analyzed from +20 to +30 mV, where voltage clamp errors were <10 mV, and extrapolated to +90 mV using the Boltzmann fit to the Kv2.1 G–V (Fig. 3 E). *n* = 8 Kv2.1-CHO cells and *n* = 4 CHO cells. Bars are arithmetic means ± SEM.

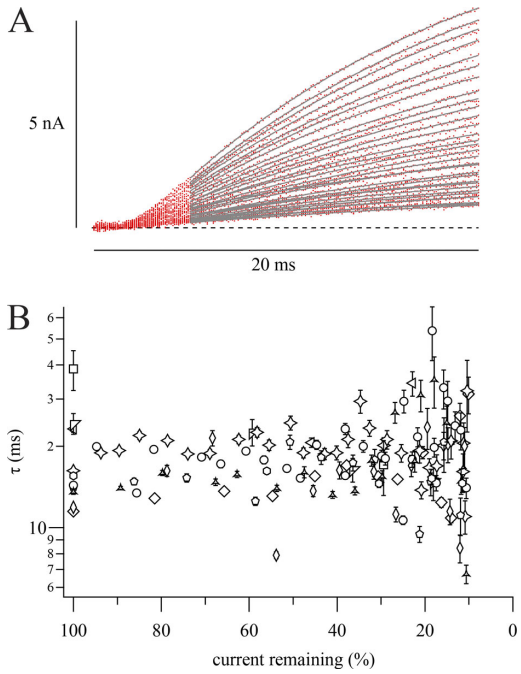

Figure S2. **RY785 does not affect Kv2.1 K^+ current activation kinetics. (A)** Representative K^+ current traces during our two-pulse protocol in the presence of RY785. Overlaid traces from a representative cell during sequential steps to +40 mV from −100 mV (red traces), fitted with a single exponential function (Eq. 4, gray curves). Later traces are smaller in amplitude. Postpulse was to −60 mV in this cell. **(B)** Activation τ ± SD from fits as in A plotted against the corresponding trace's peak current relative to that recorded during the first +40-mV step in RY785. Different symbols represent n = 10 cells. Stars correspond to the cell in A. Only measurements with >10% remaining current are presented, as fitted time constants became noisier at smaller current amplitudes.

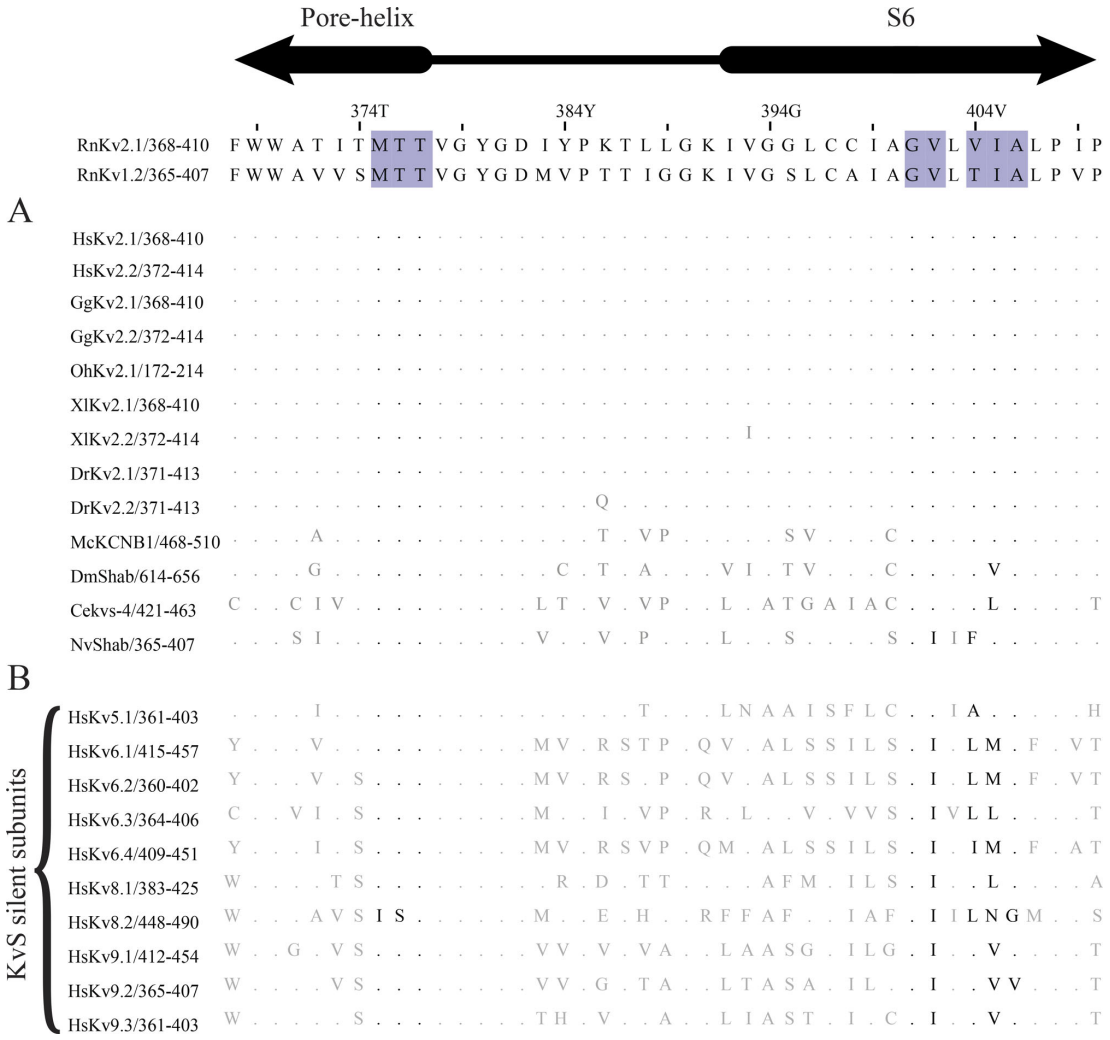

Figure S3. **Conservation of pore-lining residues of Kv2 orthologs and paralogs.** The *Rattus norvegicus* Kv2.1 (RnKv2.1) sequence is used for residue numbering at top. Homology to Kv1.2 was used to infer the locations of pore-lining residues (purple highlights) in RnKv2.1. **(A)** Conservation of pore-lining residues of RnKv2.1 with Kv2-family orthologs. Alignments created in Jalview 2.11.1.4 (Waterhouse et al., 2009). Dots represent residues in protein subunits that are identical to corresponding residues in RnKv2.1. Residues forming the tetraalkylammonium binding site in RnKv1.2 (Lenaeus et al., 2014; Long et al., 2005) are shown in black. Species: *Homo sapiens* (Hs), *Gallus gallus* (Gg), *Ophiophagus Hannah* (Oh), *Xenopus laevis* (Xl), *Danio rerio* (Dr), *Mytilus coruscus* (Mc), *Drosophila melanogaster* (Dm), *Caenorhabditis elegans* (Ce), *Nematostella vectensis* (Nv). **(B)** Conservation of pore-lining residues of mammalian Kv2.1 with KvS silent subunits.

Chapter 3: RY785 Resistance of Kv2.1 Channels with Heteromeric Pores and Neuronal Kv2 Channels

Foreword

This chapter presents a collaborative study investigating Kv2 channels containing regulatory pore subunits of the KvS superfamily. KvS subunits modulate channel gating and form part of the putative RY785 binding site. I found that heteromerization of Kv2.1 with the KvS subunit Kv8.1 produces channels that are ~1,000 times less sensitive to RY785. These heteromeric channels still require voltage activation to bind RY785 but recover from block at a voltage that closes channels. This could suggest that heteromerization reduces the RY785 affinity of the resting state or reduces is stability. RY785 is the only known compound that can selectively block homomeric Kv2 channels. Applying RY785 to human nociceptors revealed KvS-like Kv2 conductances, the first evidence of functional KvS-containing channels in these cells. This chapter is a reproduction of a manuscript[5] that has been submitted for peer review. My contributions to this manuscript are in Figures 2, 2 Supplement, 3, and 8 and their associated text. These define the concentration dependence of Kv2.1/Kv8.1 channel block by RY785, dissociation kinetics, effects of RY785 on gating, and effects of RY785 on Kv2 conductances in human neurons. I also contributed to the design of other electrophysiological experiments, general editing throughout the manuscript, and overall interpretation of data.

A Kv2 inhibitor combination reveals native neuronal conductances consistent with Kv2/KvS heteromers.

Robert G. Stewart[1,2,4], Matthew James Marquis[1], Sooyeon Jo[4], Aman Aberra[2,5], Verity Cook[2,6], Zach Whiddon[2], Michael Ferns[1,3], Jon T. Sack[1,2,3]

Affiliations:
[1] Department of Physiology and Membrane Biology, University of California Davis
[2] Neurobiology Course, Marine Biological Laboratory, Woods Hole, Massachusetts
[3] Department of Anesthesiology and Pain Medicine, University of California Davis
[4] Department of Neurobiology, Harvard Medical School, Boston, Massachusetts
[5] Department of Biological Sciences, Dartmouth College, Hanover, New Hampshire
[6] Einstein Center for Neuroscience, Charité Universitätsmedizin Berlin, Germany

Corresponding author email: jsack@ucdavis.edu

Conflict of interest statement: The authors declare no conflicts of interest.

ABSTRACT

KvS proteins are voltage-gated potassium channel subunits that form functional channels when assembled into heterotetramers with Kv2.1 (*KCNB1*) or Kv2.2 (*KCNB2*). Mammals have 10 KvS subunits: Kv5.1 (*KCNF1*), Kv6.1 (*KCNG1*), Kv6.2 (*KCNG2*), Kv6.3 (*KCNG3*), Kv6.4 (*KCNG4*), Kv8.1 (*KCNV1*), Kv8.2 (*KCNV2*), Kv9.1 (*KCNS1*), Kv9.2 (*KCNS2*), and Kv9.3 (*KCNS3*). Electrically excitable cells broadly express channels containing Kv2 subunits and most neurons have substantial Kv2 conductance. However, whether KvS subunits contribute to these conductances has not been clear, leaving the physiological roles of KvS subunits poorly understood. Here, we identify that two potent Kv2 inhibitors, used in combination, can distinguish conductances of Kv2/KvS channels and Kv2-only channels. We find that Kv5, Kv6, Kv8, or Kv9-containing channels are resistant to the Kv2-selective pore-blocker RY785 yet remain sensitive to the Kv2-selective voltage sensor modulator guangxitoxin-1E (GxTX). Using these inhibitors in mouse superior cervical ganglion neurons, we find that little of the Kv2 conductance is carried by KvS-containing channels. In contrast, conductances consistent with KvS-containing channels predominate over Kv2-only channels in mouse and human dorsal root ganglion neurons. These results establish an approach to pharmacologically distinguish conductances of Kv2/KvS heteromers from Kv2-only channels, enabling investigation of the physiological roles of endogenous KvS subunits. These findings suggest that drugs targeting KvS subunits could modulate electrical activity of subsets of Kv2-expressing cell types.

INTRODUCTION

The Kv2 voltage-gated K^+ channel subunits, Kv2.1 and Kv2.2, are broadly expressed in electrically excitable cells throughout the body and have important ion-conducting and non-conducting functions (Liu and Bean, 2014; Bishop et al., 2015; Kirmiz et al., 2018; Vierra et al., 2021; Matsumoto et al., 2023). Consistent with this widespread expression, Kv2 channels have profound impacts on many aspects of our physiology including vision, seizure suppression, stroke recovery, pain signaling, blood pressure, insulin secretion, and reproduction (Bocksteins, 2016). Although modulation of Kv2 channels may seem to hold therapeutic promise, Kv2 subunits are poor drug targets due to their importance in many tissues.

A potential source of molecular diversity for Kv2 channels are a family of Kv2-related proteins referred to as regulatory, silent, or KvS subunits (Bocksteins et al., 2009; Kobertz, 2018). KvS subunits are an understudied class of voltage-gated K^+ channel (Kv) subunits that comprise one fourth of mammalian Kv subunit types. Like all other Kv proteins, the ten KvS proteins (Kv5.1, Kv6.1-6.4, Kv8.1-8.2, and Kv9.1-9.3) have sequences encoding a voltage sensor and pore domain. Distinct from other Kv subunits, KvS have not been found to form functional homomeric channels. Rather, KvS subunits co-assemble with Kv2 subunits to form heterotetrameric Kv2/KvS channels (Salinas et al., 1997a; Kramer et al., 1998) which have biophysical properties distinct from those of homomeric Kv2 channels (Post et al., 1996; Salinas et al., 1997b; Kramer et al., 1998; Richardson and Kaczmarek, 2000; Zhong et al., 2010; Bocksteins et al., 2012; Bocksteins et al., 2017). KvS mRNAs are expressed in tissue and cell-specific manners that overlap with Kv2.1 or Kv2.2 expression (Castellano et al., 1997; Salinas et al., 1997b; Kramer et al., 1998; Bocksteins et al., 2012; Bocksteins and Snyders, 2012; Bocksteins, 2016). These expression patterns and functional effects suggest that Kv2 conductances in many cell types might be Kv2/KvS conductances. Consistent with narrow expression of the many KvS subunits, genetic mutations and gene-targeting studies have linked disruptions in the function of different KvS subunits to defects in distinct organ systems including retinal cone dystrophy (Wu et al., 2006; Hart et al., 2019; Inamdar et al., 2022), male infertility (Regnier et al., 2017), seizures (Jorge et al., 2011), and changes in pain sensitivity (Tsantoulas et al., 2018; Lee et al., 2020b). These organ-specific disruptions suggest that each KvS subunit selectively modulates a subset of the wide-ranging functions of Kv2 channels. However, studies of the physiological roles of KvS subunits have been hindered by a lack of tools to identify native KvS conductances. Due to limited KvS pharmacology, there is little evidence that definitively ascribes native K^+ conductances to KvS-containing channels. While studies have identified native conductances attributed to KvS subunits (reviewed by Bocksteins, 2016), it has not been clear whether the Kv2 conductances that are prominent in many electrically-excitable cell types are carried by Kv2-only channels, or Kv2/KvS heteromeric channels.

No drugs are known to be selective for KvS subunits. However, Kv2/KvS heteromeric channels do have some pharmacology distinct from channels that contain only Kv2 subunits. Quaternary ammonium compounds, 4-aminopyridine, and other broad-spectrum K^+ channel blockers have different potencies against certain KvS-containing channels as compared to Kv2 channels (Post et al., 1996; Thorneloe and Nelson, 2003; Stas et al., 2015). However, these blockers are poorly selective and cannot effectively isolate Kv2/KvS conductances from the many other voltage-gated K^+ conductances of electrically excitable cells.

Highly-selective Kv2 channel inhibitors fall into two mechanistically distinct classes. One class is the inhibitory cystine knot peptides from spiders. An exemplar of this class is the tarantula toxin guangxitoxin-1E (GxTX), which has remarkable specificity for Kv2 channel subunits over other voltage-gated channels (Herrington et al., 2006; Thapa et al., 2021). GxTX binds to the voltage sensor of each Kv2 subunit (Milescu et al., 2009), and stabilizes that voltage sensor in a resting state to prevent channel opening (Tilley et al., 2019). GxTX binding requires a specific sequence of residues, TIFLTES, at the extracellular end of the Kv2 subunit S3 transmembrane helix (Milescu et al., 2013). This GxTX-binding sequence is conserved between Kv2 channels but is not retained by any KvS subunit. A second class of selective Kv2 inhibitors is a family

of small molecules discovered in a high throughput screen for use-dependent Kv2 inhibitors (Herrington et al., 2011). Of these, RY785 is the most selective for Kv2 channels over other channel types. RY785 acts like a pore blocker which binds in the central cavity of Kv2 channels (Marquis and Sack, 2022). The central cavity-lining residues of all KvS subunits have differences from Kv2 subunits. We recently reported that coexpression of Kv5.1 with Kv2.1 led to a conductance that was resistant to RY785 (Ferns et al., 2024).

In this study, we develop a method to isolate conductances of KvS-containing channels. We identify that the combination of GxTX and RY785 can distinguish conductances of Kv2-only channels from channels that contain KvS subunits of the Kv5, Kv6, Kv8, or Kv9 subfamilies. To determine whether cell types enriched with KvS mRNA have functional KvS-containing channels, we use these inhibitors to reveal native neuronal conductances consistent with Kv2/KvS heteromers in mouse and human dorsal root ganglion neurons. These findings suggest that KvS conductances could be targeted to selectively modulate discrete subsets of cell types.

RESULTS

- Kv2.1/Kv8.1 heteromers are resistant to RY785 and sensitive to GxTX

To test whether Kv2 inhibitors also inhibit Kv2/KvS heteromeric channels, we transfected KvS cDNA into a stable cell line which was subsequently induced to express Kv2.1 (Kv2.1-CHO) (Figure 1 Supplement) and later recorded whole cell currents. We previously found that 1 μM RY785 or 100 nM GxTX blocked almost all the voltage-gated K^+ conductance of this Kv2.1-CHO cell line, leaving 1 ± 2% or 0 ± 0.1% (mean ± SEM) current remaining respectively at 0 mV (Tilley et al., 2019; Marquis and Sack, 2022). However, after transfection of Kv8.1 into Kv2.1-CHO cells, we find that a sizable component of the delayed rectifier current became resistant to 1 μM RY785 (Fig 1 A). This RY785-resistant current was inhibited by 100 nM GxTX, suggesting that the GxTX-sensitivity arises from inclusion of Kv2.1 subunits in the channels underlying the RY785-resistant current. A simple interpretation is that RY785-resistant yet GxTX-sensitive currents are carried by Kv2.1/Kv8.1 heteromeric channels. The fraction of RY785-resistant current had pronounced cell-to-cell variability (Fig 1 D). Co-expression of KvS and Kv2 subunits can result in Kv2 homomers and Kv2/KvS heteromers (Pisupati et al., 2018), so variability in the RY785-sensitive fraction could represent cell-to-cell variability in the proportion of Kv8.1-containing channels.

As a control, we transfected Kv2.1-CHO cells with Navβ2, a transmembrane protein not expected to interact with Kv2.1. In Kv2.1-CHO cells transfected with Navβ2, 1 μM RY785 efficiently blocked Kv2.1 conductance, leaving 4 ± 0.6 % (mean ± SEM) of current (Fig 1 B and D). We also transfected Kv2.1-CHO cells with a member of the AMIGO family of Kv2-regulating transmembrane proteins. AMIGO1 promotes voltage sensor activation of Kv2.1 channels in these Kv2.1-CHO cells (Sepela et al., 2022). 1 μM RY785 blocked Kv2.1 conductances in cells transfected with AMIGO1, leaving 0.6 ± 1% (SEM) of current (Fig 1 C and D). These control experiments indicate that transfection of a set of other transmembrane proteins did not confer resistance to RY785, suggesting that the RY785 resistance is not generically induced by overexpression of non-KvS transmembrane proteins.

To determine whether Kv8.1-containing channels are completely resistant to RY785, we performed an RY785 concentration-effect experiment. To pre-block Kv2.1 homomers we began concentration-effect measurements at 0.35 μM RY785, which we expect to block 98% of homomers based on the estimated K_D of 6 nM RY785 for the Kv2.1 currents in these Kv2.1-CHO cells (Marquis and Sack, 2022). Notably, currents resistant to 0.35 μM RY785 were blocked by higher concentrations of RY785, with nearly complete block observed in 35 μM RY785 (Fig 2 A). We quantified block of tail currents at -9 mV following a 200 ms step to +71 mV, and normalized to current from the initial 0.35 μM RY785 treatment. This protocol revealed an IC_{50} of 5 ± 1 μM (SD) (Fig 2 B). The Hill coefficient of 1.2 ± 0.2 is consistent with 1:1 binding to a homogenous population of RY785-inhibited channels.

We had noted that solution exchanges can change current amplitudes, and also interleaved time-matched solution exchange controls. These controls revealed variable current rundown of approximately 30% on average (Fig 2 C). Time-matched control washes were followed by treatment with 35 μM RY785 to confirm that currents in these cells had similar RY785 sensitivity to those in our concentration-effect experiment. Following block by 35 μM RY785, washing with 0.35 μM RY785 caused increases in current amplitudes in every trial (Fig 2 D). The run-down and incomplete wash-out indicate that the 5 μM IC_{50} of RY785 for these resistant channels may be an underestimate. Kv2.1/Kv8.1 currents were unblocked in the first current test following RY785 washout (Fig 2 Supplement). This rapid recovery indicates unblocking of Kv2.1/Kv8.1 heteromers occurred during the less than 3 min wash time at -89 mV, or if RY785 remained trapped in the channels during wash then it unblocked on the millisecond time scale during activating voltage pulses. This is distinct from Kv2.1 homomers, where RY785 becomes trapped in deactivated channels and unblocks much more slowly, with a time constant of about 2 hours

at -92 mV or 100 s at +28 mV (Marquis and Sack, 2022). The dramatically faster unblock from Kv2.1/Kv8.1 is consistent with the weaker affinity observed for RY785. Overall, the results suggest that Kv8.1-containing channels in these Kv2.1-CHO cells form a pharmacologically-homogenous population with an affinity for RY785 ~3 orders of magnitude weaker than for Kv2.1 homomers. Our estimates of the affinities of Kv2.1 homomeric and Kv2.1/Kv8.1 heteromeric channels for RY785 suggest that ~1 µM RY785 elicits nearly complete block of Kv2.1 homomer conductance while blocking little Kv2.1/KvS heteromer conductance.

- Biophysical properties of RY785-resistant conductance are consistent with Kv2.1/Kv8.1 channels.

We wondered whether RY785 block of Kv2 homomers could better reveal the gating of heteromers. While concentrations of RY785 that partially block Kv2.1/Kv8.1 modified the kinetics of voltage-dependent gating, suggesting state-dependent block (Fig 3), we did not observe modification of kinetics with 3.5 µM or lower concentrations of RY785. To study the biophysical properties of the Kv8.1 conductance in the Kv2.1-CHO cells, we analyzed currents in 1 µM RY785 to block the Kv2.1 homomers. For comparison, Kv2.1-CHO cells were transfected with a control plasmid and treated with a vehicle control (Fig 4 Supplement 1). We stepped cells to -9 mV from a holding potential of -89 mV and fit the current rise with an exponential function (equation 1). Cells transfected with Kv8.1 and blocked with 1 µM RY785 had a significantly slower activation time constant and lower sigmoidicity (shorter relative activation delay) than Kv2.1 (Fig 4 A-C). Conductance-voltage relations were fit with a Boltzmann function (equation 2) revealing that the half-maximal conductance of Kv8.1-transfected cells is shifted positive relative to Kv2.1 alone (Fig 4 D and E). We did not detect a significant difference in the steepness (z) of the conductance voltage relation (Fig 4 F). Currents from Kv8.1-transfected cells inactivated less during a 10 s step to -9 mV (Fig 4 G and H). However, the steady-state inactivation of Kv8.1-transfected cells was shifted to more negative voltages and is less steep than Kv2.1-transfected cells (Fig 4 I-K). These biophysical properties are consistent with a previous report which identified that co-expression of Kv8.1 with Kv2.1 in *Xenopus* oocytes slows the rate of activation, reduces inactivation and shifts steady-state inactivation to more negative voltages (Salinas et al., 1997b). This previous report also identified a positive shift in the conductance-voltage relation when Kv8.1 is co-expressed with a Kv2 subunit (Kv2.2), similar to our findings with Kv2.1/Kv8.1. Together these results show that RY785-resistant currents in cells transfected with Kv8.1 are distinct from Kv2.1 and have changes in gating consistent with the prior reports of Kv8.1/Kv2 biophysics. This validates using RY785 block of Kv2 homomers as a method to reveal the biophysics of a Kv8.1-containing population.

- A subunit from each KvS family is resistant to RY785 but sensitive to GxTX.

To test if RY785 resistance is shared broadly by KvS subunits, we studied a subunit from each KvS subfamily. We previously found that the sole Kv5 subunit, Kv5.1, was resistant to RY785 (Ferns et al., 2024). We transfected Kv5.1, Kv6.4, and Kv9.3, to find if they also produced delayed rectifier current resistant to 1 µM RY785 yet sensitive to 100 nM GxTX (Fig 5 A-C). We observed that, in 1 µM RY785, >10% of the voltage-gated current remained in 12/13 Kv5.1, 9/14 Kv6.4, and 5/5 Kv9.3 transfected cells (Fig 5 D). Like Kv8.1, the fraction of RY785-resistant current had pronounced cell-to-cell variability (Fig 5 D) suggesting that the RY785-sensitive fraction could be due to different ratios of functional Kv2.1 homomers to Kv2.1/KvS heteromers. Addition of 100 nM GxTX blocked RY785-resistant current from cells transfected with each of these KvS subunits. A slightly higher fraction of Kv9.3 current remained in 100 nM GxTX, possibly due to Kv9.3 negatively shifting the midpoint of the conductance voltage

relationship (Kerschensteiner and Stocker, 1999). These results show that voltage-gated outward currents in cells transfected with members from each KvS family have decreased sensitivity to RY785 but remain sensitive to GxTX. While we did not test every KvS regulatory subunit, the ubiquitous resistance across all KvS subfamilies results suggest that all KvS subunits may provide resistance to 1 µM RY785 yet remain sensitive to GxTX, and that resistance is a hallmark of KvS-containing channels.

- The Kv2 conductances of mouse superior cervical ganglion neurons do not have KvS-like pharmacology.

We set out to assess whether RY785 together with GxTX could be a means of distinguishing endogenous Kv2/KvS channels from Kv2 channels in native neurons. We first designed experiments to test whether RY785 could inhibit endogenous Kv2 currents in mice, by studying neurons unlikely to express KvS subunits. Rat superior cervical ganglion (SCG) neurons have robust GxTX-sensitive conductances (Liu and Bean, 2014) yet transcriptomics have revealed little evidence of KvS expression (Sapio et al., 2020). We investigated whether SCG neurons have KvS-like conductances by performing whole cell voltage clamp on dissociated mouse neurons. To help isolate Kv2 and Kv2/KvS currents, we bathed SCG neurons in a cocktail of Nav, Kv1, Kv3, and Kv4 inhibitors and recorded voltage-gated currents. We found that exposing SCG neurons to 1 µM RY785 inhibited most of the voltage-gated current, and subsequent addition of 100 nM GxTX inhibited little additional current (Fig 6 A and B). To quantify inhibition, we analyzed tail currents 10 ms after repolarizing to -45 mV, as a hallmark of Kv2 currents is relatively slow deactivation (Thorneloe and Nelson, 2003; Zheng et al., 2019). Tail currents after application of 1 µM RY785 were decreased by 88 $\pm$ 5 % (mean $\pm$ SEM) in SCG neurons (Fig 6 B). Subsequent application of 100 nM GxTX had little further effect. To determine if the RY785-sensitive conductances are consistent with previous reports of Kv2 channels, we examined the biophysical properties of the Kv2-like (RY785-sensitive) currents defined by subtraction (Fig 6 C). Current activation began to be apparent at -45 mV and had a conductance that was half maximal at -11 mV (Fig 6 D). The faster component of deactivation of RY785-sensitive currents in SCG neurons had a time constant of 16 ms $\pm$ 0.6 (mean $\pm$ SEM) at -45 mV (Fig 6 E). These results are consistent with reported biophysical properties of Kv2 channels (Kramer et al., 1998; Liu and Bean, 2014; Tilley et al., 2019; Sepela et al., 2022). Together these results show that 1 µM RY785 almost completely inhibits endogenous Kv2-like conductances in these mouse neurons, suggesting that mouse SCG neurons have few functional Kv2/KvS channels. We cannot rule out that the small amount of current remaining after RY785 (12% of the control) is due to Kv2/KvS channels, but its insensitivity to GxTX suggests that it may instead be current from a non-Kv2 channel remaining in the cocktail of K-channel inhibitors.

- Mouse nociceptors have KvS-like conductances.

To determine if RY785/GxTX pharmacology could reveal endogenous KvS-containing channels, we next studied neurons likely to express KvS subunits. Mouse DRG somatosensory neurons express Kv2 proteins (Stewart et al., 2024), have GxTX-sensitive conductances (Zheng et al., 2019), and express a variety of KvS transcripts (Bocksteins et al., 2009; Zheng et al., 2019). To record from a consistent subpopulation of mouse somatosensory neurons, we used a *Mrgprd*^{GFP} transgenic mouse line which expresses GFP in nonpeptidergic nociceptors (Zylka et al., 2005; Zheng et al., 2019). Deep sequencing identified that mRNA transcripts for Kv5.1, Kv6.2, Kv6.3, and Kv9.1 are present in GFP$^+$ neurons of this mouse line (Zheng et al., 2019) and we confirmed the presence of Kv5.1 and Kv9.1 transcripts in GFP$^+$ neurons from *Mrgprd*^{GFP} mice using RNAscope (Fig 7 Supplement 1). We investigated whether these neurons have KvS-

like conductances by performing whole cell voltage clamp on cultured DRG neurons that had clear GFP fluorescence. Voltage-clamped neurons were bathed in the same cocktail of channel inhibitors used on SCG neurons with the addition of a Nav1.8 inhibitor, A-803467. Application 1 μM RY785 inhibited outward currents somewhat, but unlike in SCG neurons, a prominent delayed-rectifier outward conductance with slow deactivation remained (Fig 7 A left panel). Tail currents in 1 μM RY785 decreased 29 ± 3% (mean ± SEM) (Fig 7 B left panel). Subsequent application of 100 nM GxTX decreased tail currents by 68 ± 5% (mean ± SEM) of their original amplitude before RY785. We observed variable current run-up or run-down but no significant effect of vehicle in blinded, interleaved experiments, while RY785 significantly decreased tail currents relative to vehicle controls (Fig 7 A and B right panel). Concurrent application of 100 nM GxTX and 1 μM RY785 to neurons in vehicle decreased currents by 69 ± 5% (mean ± SEM).

To determine if the RY785- and GxTX-sensitive conductances in GFP$^+$ neurons from *Mrgprd^{GFP}* mice are consistent with previous reports of Kv2- or KvS-containing channels, we examined the biophysical properties of the Kv2-like (RY785-sensitive) and KvS-like (RY785-resistant, GxTX-sensitive) currents defined by subtraction (Fig 7 C). Obvious Kv2-like and KvS-like channel conductances began at -44 mV and had half-maximal conductances around -19 mV (Fig 7 D), consistent with Kv2 and many KvS-containing channels (Kramer et al., 1998; Richardson and Kaczmarek, 2000; Sano et al., 2002; Thorneloe and Nelson, 2003). Moreover, KvS-like, GxTX-sensitive currents deactivated slower than Kv2-like, RY785-sensitive currents (Fig 7 E), consistent with the effects of several KvS subunits whose transcripts are expressed in nociceptor DRG neurons. Kv5.1, Kv6.3, and Kv9.1 all slow deactivation of Kv2 conductances in heterologous cells (Salinas et al., 1997a; Kramer et al., 1998; Sano et al., 2002), and in Kv2.1-CHO cells transfected with Kv5.1, we confirmed that RY785-resistant currents deactivate slower than Kv2.1 controls (Fig 7 Supplement 2). Together, these results indicate that, in these mouse DRG neurons, RY785-sensitive currents are Kv2-like, while RY785-resistant yet GxTX-sensitive currents are KvS-like. Of the total conductance sensitive to RY785 + GxTX, 58 ± 3 % (mean ± SEM) was resistant to RY785 (KvS-like) (Fig 7 F). Overall, these results show that these non-peptidergic nociceptor DRG neurons from mice have KvS transcripts and endogenous voltage-gated currents with KvS-like pharmacology and gating.

- Human somatosensory neurons have KvS-like conductances.

Human DRG neurons express Kv2 proteins (Stewart et al., 2024), and express KvS transcripts (Ray et al., 2018) suggesting that they may have Kv2/KvS conductances. We performed whole-cell voltage clamp on cultured human DRG neurons, choosing smaller-diameter neurons and using the same solutions as mouse DRG neuron recordings. The human DRG neurons had KvS-like delayed-rectifier outward conductances that were sensitive to 100 nM GxTX that were insensitive to 1 μM RY785 (Fig 8 A, B, C). These RY785- or GxTX-sensitive conductances became apparent near -44 mV and were half-maximal between -14 and -4 mV (Fig 8 D). Of the total conductance sensitive to RY785 or GxTX in these human DRG neurons, 76 ± 2 % (mean ± SEM) was KvS-like, being resistant to RY785 but sensitive to GxTX (Fig 8 E). Overall, these results show that human DRG neurons can produce endogenous voltage-gated currents with pharmacology and gating consistent with Kv2/KvS channels.

DISCUSSION

These results identify a method for pharmacologically isolating conductances of Kv2/KvS channels and Kv2-only channels. RY785 blocks homomeric Kv2 channels, and subsequent application of GxTX selectively inhibits Kv2/KvS-containing channels. Such a protocol can aid in identification of Kv2/KvS conductances separately from the Kv2 homomer conductances that are likely to be in the same cell. Characterization of these now separable conductances can reveal impacts of Kv2-only channels and KvS-containing channels on electrophysiological signaling. This is valuable as there are few other tools to probe the contributions of KvS subunits to electrical signaling in native cells and tissues.

It is remarkable that resistance to RY785 is shared across all of the KvS families. We found Kv2.1/Kv8.1 conductances to be ~1000 times less sensitive to RY785 than Kv2.1 homomer conductances in the same cell line. Based on the observation that >50% of Kv current was resistant to 1 µM RY785 in some Kv2.1-CHO cells transfected with Kv5.1, Kv6.4, or Kv9.3, these Kv2.1/KvS channels are expected to have IC_{50} > 1 µM, at least 100-fold less sensitive than the ~10 nM IC_{50} for Kv2.1 in this cell line. This could suggest that the RY785 inhibitory site is substantially disrupted by KvS subunits. Site disruption by KvS subunits could result from steric change in the binding site itself or could be allosteric. In Kv2.1 homomeric channels, intracellular tetraethylammonium competes with RY785 inhibition, and voltage gates RY785 access to its inhibitory site, suggesting that RY785 binds within the voltage-gated intracellular cavity lined by transmembrane segment S6 helices. In all KvS subunits, the S6 residues lining this cavity are distinct (Marquis and Sack, 2022). The precise subunit compositions of KvS-containing channels are debated, with evidence for KvS:Kv2 stoichiometries of either 1:3 (Kerschensteiner et al., 2005; Pisupati et al., 2018) or 2:2 (Moller et al., 2020). If KvS subunits sterically disrupt the RY785 site, this would suggest that the RY785 site spans multiple Kv2 subunits, at least one of which is replaced in the Kv2/KvS heteromers. If the KvS disruption of RY785 inhibition is allosteric, KvS subunits would reduce the occurrence of channel state(s) which bind most tightly to RY785. Allosteric interactions between RY785 inhibition and channel gating are apparent for Kv2.1 homomeric channels as RY785 alters voltage-sensor movement, indicating that RY785 affinity must be state-dependent (Marquis and Sack, 2022). We note that the altered Kv2.1/Kv8.1 conductance kinetics in 35 µM RY785 are consistent with state-dependent binding (Fig. 3). An allosteric mechanism seems generally plausible, as all KvS subunits imbue kinetics and voltage dependencies distinct from Kv2 (Bocksteins, 2016). For example, Kv6.4 alters the voltage-activation of Kv2.1 subunits (Bocksteins et al., 2017), and alters dynamics of the S6 pore-gating apparatus (Pisupati et al., 2018). Notably, the S6 helical bundle crossing of Kv2.1 constricts asymmetrically during channel inactivation in ways that are allosterically modulated by 4-aminopyridine (Fernández-Mariño et al., 2023), and KvS-containing channels allosterically alter interactions with 4-aminopyridine (Stas et al., 2015). These observations suggest KvS subunits could allosterically disrupt RY785 inhibition.

While we have identified a potential means to isolate KvS conductances, it is important to consider the limitations of these findings.

First, although every KvS subunit we tested is resistant to RY785, and these subunits span all the KvS subfamilies (Kv5, Kv6, Kv8, and Kv9), we have not tested all KvS subunits, species variants, cell types, or voltage regimens. Any of these could alter the RY785 IC_{50}. Pharmacology can yield surprises, such as the unexpected resistance of human Nav1.7 to saxitoxin (Walker et al., 2012). The degree of resistance to RY785 may vary among KvS subunits as with other central cavity drugs such as tetraethylammonium and 4-aminopyridine (Post et al., 1996; Thorneloe and Nelson, 2003; Stas et al., 2015). While Kv2.1/Kv8.1 channels appeared to be homogenously susceptible to RY785 (with Hill slope close to 1), other KvS subunits might present multiple pharmacologically-distinct heteromer populations.

Second, it is possible that RY785 can modulate other voltage-gated channels. However, we think

RY785 is unlikely to have substantial off-target effects as RY785 is much less potent against other non-Kv2 voltage-gated potassium channel subtypes as well as voltage-gated sodium and calcium channels (Herrington et al., 2011).

Third, concentrations of RY785 which partially blocked Kv2.1/Kv8.1 modified the gating of the voltage-activated conductance, indicating that RY785 can alter properties of heteromer conductance. Notably, 4-aminopyridine can increase Kv2 or Kv2/KvS conductances under specialized conditions (Stas et al., 2015; Fernández-Mariño et al., 2023). As discussed above, channel state-dependent binding is expected to influence the affinity of RY785.

Fourth, it is possible that other factors could imbue RY785 resistance. While it seems unlikely that pore-forming subunits other than KvS subunits complex with Kv2 subunits, other factors could potentially disrupt the RY785 site. Regulation of Kv2 channel gating could potentially allosterically disrupt RY785 inhibition. Extensive homeostatic regulation of Kv2.1 gating maintains neuronal excitability (Misonou et al., 2006); for example, ischemia (Misonou et al., 2005; Aras et al., 2009), glutamate (Misonou et al., 2008), phosphorylation (Murakoshi et al., 1997), SUMOylation (Plant et al., 2011) and AMIGO auxiliary subunits (Peltola et al., 2011; Maverick et al., 2021) all alter Kv2 gating.

Despite these possibilities, we think the most parsimonious interpretation of RY785-resistant, GxTX-sensitive conductances is that they are produced by heterotetrameric Kv2/KvS channels. However, it is important to consider other possibilities when interpreting RY785 resistance of GxTX-sensitive conductances. With these caveats in mind, we suggest that RY785-resistance combined with GxTX-sensitivity is strong evidence for Kv2/KvS channel currents.

Delayed-rectifier Kv2-like conductances are prominent in many electrically excitable cell types. Our findings in *Mrgprd*-lineage mouse DRG neurons as well as human DRG neurons suggest that the majority of the Kv2 conductance originates from Kv2/KvS channels, while in mouse SCG neurons Kv2-only channels seem to predominate. Beyond these cell types, it is unclear how prevalent KvS-containing conductances are. While Kv2 subunits are broadly expressed in electrically excitable cells throughout the brain and body, transcripts for KvS subunits have unique expression patterns that are specific to each KvS family member (Bocksteins, 2016) which can fluctuate with age (Regnier et al., 2016). However, transcript levels alone are not sufficient to predict protein levels (Liu et al., 2016). We found recently that native Kv2 channels in mouse brain contain KvS subunits, including Kv5.1, Kv8.1. Kv9.1 and Kv9.2. Notably, the KvS mass spectral abundance relative to Kv2.1 ranged from ≈18% for Kv5.1 to 2% for Kv9.1 (Ferns et al., 2024), and Kv5.1 protein expression was largely restricted to cortical neurons. Thus, it seems likely that significant KvS conductances also exist in specific subsets of brain neurons.

The physiological role of Kv2/KvS channels in neurons and other excitable cells remains enigmatic. Previous studies have used knockout mice (Regnier et al., 2017; Miyamae et al., 2021), transient transfection of KvS subunits (Lee et al., 2020b), siRNA knockdown (Tsantoulas et al., 2012), and modeling (Miyamae et al., 2021) to probe the presence of endogenous and functional KvS-containing channels, and these methods can identify phenotypic changes that suggest potential roles of KvS-containing channels. Moreover, genetic mutations and gene targeting studies have linked disruptions in the function of KvS-containing channels to epilepsy (Jorge et al., 2011), neuropathic pain sensitivity (Tsantoulas et al., 2018), labor pain (Lee et al., 2020a) and retinal cone dystrophy (Wu et al., 2006; Hart et al., 2019; Inamdar et al., 2022), stressing their functional importance in specific cell types. The unique pharmacology of KvS-containing channels identified here provides a new and direct method of identifying conductances mediated by KvS-containing channels in native neurons, and establishing what contributions KvS subunits make to electrophysiological signaling.

Finally, these findings also support the potential utility of KvS channels as drug targets. Kv2-targeted drug leads have poor tissue and cell specificity and suffer from pronounced side effects (Li et al., 2013).

KvS transcripts show far greater tissue- and cell-type specific expression relative to Kv2 (Bishop et al., 2015; Bocksteins, 2016), and we identified prominent KvS conductances in mouse nociceptor and human DRG neurons. Consequently, KvS-targeted drugs could offer greater specificity and the ability to modulate neuronal excitability in a variety of pathological contexts, such as neuropathic pain.

MATERIALS AND METHODS

- Mice

Studies were approved by the UC Davis and Harvard Medical School Institutional Animal Care and Use Committees and conform to guidelines established by the NIH. Mice were maintained on a 12 hr light/dark cycle, and food and water were provided ad libitum. The *Mrgprd*^{GFP} mouse line was a generous gift from David Ginty at Harvard (MGI: 3521853).

- Human tissue collection

Human dorsal root ganglia (DRG) were obtained from Sierra Donor Services. The donor was a 58-year-old Asian Indian female and DRG were from the 1st and 2nd lumbar region (cause of death: Stroke). DRG were extracted 6 hours after aortic cross clamp and placed in an ice cold N-methyl-D-glucamine-artificial cerebral spinal fluid (NMDG-aCSF) solution containing in mM: 93 NMDG, 2.5 KCl, 1.25 NaH_2PO_4, 30 $NaHCO_3$, 20 HEPES, 25 Glucose, 5 L-Ascorbic acid, 2 Thiourea, 3 Na pyruvate, 10 $MgSO_4$ and 0.5 $CaCl_2$ pH adjusted to 7.4 with HCl. Human DRG were obtained from the organ donor with full legal consent for use of tissue for research in compliance with procedures approved by Sierra Donor Services.

- Chinese hamster ovary (CHO) cell culture and transfection

The CHO-K1 cell line transfected with a tetracycline-inducible rat Kv2.1 construct (Kv2.1-CHO; Trapani and Korn, 2003) was cultured as described previously (Tilley et al., 2014). Transfections were achieved with Lipofectamine 3000 (Life Technologies, L3000001). 1 µl Lipofectamine was diluted, mixed, and incubated in 25 µl of Opti-MEM (Gibco, 31985062). Concurrently, 0.5 µg of KvS or AMIGO1 or Navβ2, 0.5 µg of pEGFP, 2 µl of P3000 reagent and 25 µl of Opti-MEM were mixed. DNA and Lipofectamine 3000 mixtures were mixed and incubated at room temperature for 15 min. This transfection cocktail was added to 1 ml of culture media in a 24 well cell culture dish containing Kv2.1-CHO cells and incubated at 37 °C in 5% CO_2 for 6 h before the media was replaced. Immediately after media was replaced, Kv2.1 expression was induced in Kv2.1-CHO cells with 1 µg/ml minocycline (Enzo Life Sciences, ALX-380-109-M050), prepared in 70% ethanol at 2 mg/ml. Voltage clamp recordings were performed 12-24 hours later. During recordings, the experimenter was blinded as to whether cells had been transfected with KvS, or Navβ2 or AMIGO1. Human Kv5.1, human Kv6.4 and human Kv8.1, AMIGO1-YFP, and pEGFP plasmids were gifts from James Trimmer (University of California, Davis, Davis, CA). Human Kv9.1 and human Kv9.3 plasmids were purchased from Addgene. Human Navβ2 plasmid was a kind gift from Dr. Alfred George (Lossin et al., 2002).

- Neuron cell culture

  - Mouse

Cervical, thoracic and lumbar dorsal root ganglia (DRGs) were harvested from 7- to 10-week-old *Mrgprd*^{GFP} mice and transferred to Hank's buffered saline solution (HBSS) (Invitrogen). Ganglia were treated with collagenase (2 mg/ml; Type P, Sigma-Aldrich) in HBSS for 15 min at 37 °C followed by 0.05% Trypsin-EDTA (Gibco) for 2.5 min with gentle rotation. Trypsin was neutralized with culture media (MEM, with l-glutamine, Phenol Red, without sodium pyruvate) supplemented with 10% horse serum (heat-inactivated; Gibco), 10 U/ml penicillin, 10 µg/ml streptomycin, MEM vitamin solution (Gibco), and B-27 supplement (Gibco). Serum-containing media was decanted and cells were triturated using a fire-polished Pasteur pipette in MEM culture media containing the supplements listed above. Cells were

plated on laminin-treated (0.05 mg/ml, Sigma-Aldrich) 5 mm German glass coverslips (Bellco Glass, 1943-00005), which had previously been washed in 70% ethanol and sterilized with ultraviolet light. Cells were then incubated at 37 °C in 5% CO_2. Cells were used for electrophysiological experiments 24–38 hr after plating.

Superior cervical ganglia (SCG) were harvested from Swiss Webster (CFW) mice (postnatal day 13-15, either sex) and treated for 20 min at room temperature (RT) with 20 U/ml papain (Worthington Biochemical), 5 mM dl-cysteine, 1.25 mM EDTA, and 67 μM β-mercaptoethanol in a Ca^{2+}, Mg^{2+}-free (CMF) Hank's solution (Gibco) supplemented with 1 mM Sodium Pyruvate (Sigma-Aldrich, St. Louis, MO), and 5 mM HEPES (Sigma-Aldrich, St. Louis, MO). Ganglia were then treated for 20 min at 37 °C with 3 mg/ml collagenase (type I; Roche Diagnostics) and 3 mg/ml dispase II (Roche Diagnostics) in CMF Hank's solution. Cells were dispersed by trituration with fire-polished Pasteur pipettes in a solution composed of two media combined in a 1:1 ratio: Leibovitz's L-15 (Invitrogen) supplemented with 5 mM HEPES, and DMEM/F12 medium (Invitrogen). Cells were then plated on glass coverslips and incubated at 37 °C (95% O_2, 5% CO_2) for 1 hr, after which Neurobasal medium (Invitrogen) with B-27 supplement (Invitrogen), penicillin and streptomycin (Sigma) was added to the dish. Cells were incubated at 25 °C (95% O_2, 5% CO_2) and used within 10 hr.

- Human

Dura were removed from human DRG with a scalpel in ice cold NMDG-aCSF solution (Valtcheva et al., 2016). Human DRG were then cut into approximately 1 mm thick sections and were placed in 1.7 mg/mL Stemxyme (Worthington Biochemical, LS004107) and 6.7 mg/mL DNAse I (Worthington Biochemical, LSOO2139) diluted in HBSS (Thermo Fisher Scientific, 14170161) for 12 hr at 37 °C. DRG were then triturated with a fire-polished Pasteur pipette and passed through a 100 μm cell strainer. Cells were then spun at 900 g through 10% BSA. The supernatant was removed, and cells were resuspended in human DRG culturing media that contained 1% penicillin/streptomycin, 1% GlutaMAX (Gibco, 35050-061), 2% NeuroCult SM1 (05711, Stemcell technologies), 1% N2 Supplement (Thermo Scientific, 17502048), 2% FBS (Gibco, 26140-079) diluted in BrainPhys media (Stemcell tehnologies, 05790). DRG neurons were plated on poly-D-lysine treated (0.01 mg/mL) 5 mm German glass coverslips, which had previously been washed in 70% ethanol and sterilized with ultraviolet light. DRG neurons were then incubated at 37 °C in 5% CO_2. Human DRG neuron experiments were performed up to 7 days after plating.

- Whole cell voltage clamp of CHO cells

Voltage clamp was achieved with a dPatch amplifier (Sutter Instruments) run by SutterPatch software (Sutter Instruments). Solutions for Kv2.1-CHO cell voltage-clamp recordings: CHO-internal (in mM) 120 K-methylsulfonate, 10 KCl, 10 NaCl, 5 EGTA, 0.5 CaCl2, 10 HEPES, 2.5 MgATP pH adjusted to 7.2 with KOH, 289 mOsm. CHO-external (in mM) 145 NaCl, 5 KCl, 2 CaCl2, 2 MgCl2, 10 HEPES pH adjusted to 7.3 with NaOH, 298 mOsm. Osmolality was measured with a vapor pressure osmometer (Wescor, 5520). The liquid junction potential of -9 mV between these solutions was accounted for. The liquid junction potential was calculated according to the stationary Nernst–Planck equation (Marino. et al., 2014) using LJPcalc (RRID:SCR_025044). For voltage-clamp recordings, Kv2.1-CHO cells were detached in a PBS-EDTA solution (Gibco, 15040-066), spun at 500 g for 2 minutes and then resuspended in 50% cell culture media and 50% CHO-external recording solution. Cells were then added to a recording chamber (Warner, 64–0381) and were rinsed with the CHO-external patching solution after adhering to the bottom of the recording chamber. Transfected Kv2.1-CHO cells were identified by GFP fluorescence and were selected for whole cell voltage clamp. Thin-wall borosilicate glass recording pipettes (Sutter,

BF150-110-10) were pulled with blunt tips, coated with silicone elastomer (Sylgard 184, Dow Corning), heat cured, and tip fire-polished to resistances less than 4 MΩ. Series resistance of 2–14 MΩ was estimated from the Sutterpatch whole-cell parameters routine. Series resistance compensation between 13 and 90% was used to constrain voltage error to less than 15 mV; compensation feedback lag was 6 µs for most experiments or 100 µs for concentration-effect experiments. Capacitance and ohmic leak were subtracted using a P/4 protocol. Output was low-pass filtered at 5 kHz using the amplifier's built-in Bessel and digitized at 25 kHz or, for concentration-effect experiments, 1 and 10 kHz. Experiments were performed on Kv2.1-CHO cells with membrane resistance greater than 1 GΩ assessed prior to running voltage clamp protocols while cells were held at a membrane potential of –89 mV. RY785 (gift from Bruce Bean, Harvard, or Cayman, 19813) was prepared in DMSO as a 1 mM stock for dilutions to 1 µM or a 35 mM stock for concentration-effect experiments. Stocks of GxTX-1E Met35Nle (Tilley et al., 2014) in water were 10 µM. Stocks were stored frozen and diluted in recording solution just prior to application to cells. Solutions were flushed over cells at a rate of approximately 1 mL/min. Concentrated RY785 and GxTX stocks were stored at -20 °C. Kv2.1-CHO cells were given voltage steps from -89 mV to -9 mV for 200 ms every 6 seconds during application of RY785 until currents stabilized. When vehicle control was applied to cells, -9 mV steps were given for a similar duration. The DMSO concentration in RY785 and vehicle control solutions was 0.1%. Perfusion lines were cleaned with 70% ethanol then doubly-deionized water. For concentration-effect experiments, changes in current amplitude due to solution exchange were controlled for by treating every other tested cell with multiple washes of the same, 0.35 µM RY785 solution instead of increasing concentrations of RY785. The timing and duration of these control washes was similar to that of the washes in concentration-effect experiments.

- Whole cell voltage clamp of mouse and human dorsal root ganglion neurons

Whole cell recordings from mouse and human neurons were performed using the same methods as CHO cell recordings with the following exceptions. Voltage clamp was achieved with a dPatch amplifier run by SutterPatch software or an AxoPatch 200B amplifier (Molecular Devices) controlled by PatchMaster software (v2x91, HEKA Elektronik) via an ITC-18 A/D board (HEKA Instruments Inc). Solutions for voltage-clamp recordings: internal (in mM) 140 KCl, 13.5 NaCl, 1.8 $MgCl_2$ 0.09 EGTA, 4 MgATP, 0.3 Na_2GTP, 9 HEPES pH adjusted to 7.2 with KOH, 326 mOsm. The external solution contained (in mM) 3.5 KCl, 155 NaCl, 1 $MgCl_2$, 1.5 $CaCl_2$, 0.01 $CdCl_2$, 10 HEPES, 10 glucose pH adjusted to 7.4 with NaOH, 325 mOsm. The calculated liquid junction potential of -4 mV between these solutions was accounted for. For voltage-clamp recordings, neurons on cover slips were placed in the same recording chamber used for CHO cell recordings and were rinsed with an external patching solution. Neurons from *Mrgprd*^{GFP} mice with green fluorescence were selected for recordings. Human DRG neurons with cell capacitances between 22.5 and 60 pF were used. After whole-cell voltage clamp was established, Kv2/KvS conductances were isolated by exchanging the external solution with external solution containing 100 nM alpha-dendrotoxin (Alomone) to block Kv1, 3 µM AmmTX3 (Alomone) to block Kv4, 100 µM 4-aminopyridine to block Kv3, 1 µM TTX to block TTX sensitive Nav channels, and 10 µM A-803467 (Tocris) to block Nav1.8. After addition of 1 µM RY785 neurons were given 10 steps to -24 mV for 500 ms to allow for voltage dependent block of RY785. Thin-wall borosilicate glass recording pipettes were pulled with blunt tips, coated with silicone elastomer, heat cured, and tip fire-polished to resistances less than 2 MΩ. Series resistance of 1–4 MΩ was estimated from the whole-cell parameters circuit. Series resistance compensation between 55 and 98% was used to constrain voltage error to less than 15 mV. Ohmic leak was not subtracted. Neurons were held at a membrane potential of –74 mV.

- Whole cell voltage clamp of mouse superior cervical ganglion neurons

Whole cell recordings from mouse superior cervical ganglion neurons were performed using an Axon Instruments Multiclamp 700B Amplifier (Molecular Devices). Electrodes were pulled on a Sutter P-97 puller (Sutter Instruments) and shanks were wrapped with Parafilm (American National Can Company) to allow optimal series resistance compensation without oscillation. Voltage or current commands were delivered and signals were recorded using a Digidata 1321A data acquisition system (Molecular Devices) controlled by pCLAMP 9.2 software (Molecular Devices). The internal solution was (in mM): 140 mM K aspartate, 13.5 mM NaCl, 1.8 mM MgCl2, 0.09 mM EGTA, 9 mM HEPES, 14 mM creatine phosphate (Tris salt), 4 mM MgATP, 0.3 mM Tris-GTP, pH 7.2 adjusted with KOH. The base external solution was the same as for DRG recordings: (in mM) 3.5 KCl, 155 NaCl, 1 MgCl2, 1.5 CaCl2, and 0.01 CdCl2, 10 HEPES 10 glucose pH adjusted to 7.4 with NaOH, 325 mOsm. The calculated liquid junction potential of -15 mV between these solutions was accounted for. After establishing whole-cell recording, cell capacitance was nulled and series resistance was partially (60%) compensated to constrain voltage error to less than 2 mV. The cell was then lifted and placed in front of a series of quartz fiber flow pipes for rapid solution exchange and application of RY785 and GxTX. The external solution used for recording Kv2 currents used the same cocktail of inhibitors for sodium channels and other potassium channels as for the DRG recordings except that A-803467 was omitted because the sodium current in SCG neurons is all TTX sensitive (Toledo-Aral et al., 1997): 100 nM alpha-dendrotoxin (Alomone), 1 µM TTX, 3 µM AmmTX3 (Alomone), and 100 µM 4-aminopyridine.

- Voltage clamp analysis

Activation kinetics were fit from 10-90% of current (I_K) rise with the power of an exponential function:

Equation 1

$$I_K = A\left(1 - e^{\frac{-t}{\tau_{act}}}\right)^{\sigma}$$

where A is the maximum current amplitude, $\tau_{act}$is the time constant of activation, σ is sigmoidicity, and t is time. The t = 0 mark was adjusted to 100 µs after the start of the voltage step from the holding potential to correct for filter delay and cell charging.

Conductance values were determined from tail current levels at -9 mV after 200 ms steps to the indicated voltage. Tail currents were the mean current amplitude from 1 to 5 ms into the -9 mV step. Conductance–voltage relations were fit with the Boltzmann function:

Equation 2

$$f(V) = A\left(1 + e^{-\left(V - V_{\frac{1}{2}}\right)\frac{zF}{RT}}\right)^{-1}$$

where V is voltage, A is amplitude, z is the number of elementary charges, F is Faraday's constant, R is the universal gas constant, and T is temperature (held at 295 K).

Deactivation kinetics were fit with a double exponential:

Equation 3

$$f(x) = y_0 + A_1 e^{\frac{-(t-t_0)}{\tau_1}} + A_2 e^{\frac{-(t-t_0)}{\tau_2}}$$

Where t is time, y_0 is the initial current amplitude, t_0 is the start time of the exponential decay, τ_1 and τ_2 are the time constants, and A_1 and A_2 are the amplitudes of each component.

- Immunofluorescence

Kv2.1-CHO cells were fixed for 15 minutes at 4 °C in 4% formaldehyde prepared fresh from paraformaldehyde in PBS buffer pH 7.4. Cells were then washed 3 x 5 minutes in PBS, followed by blocking in blotto-PBS (PBS, pH 7.4 with 4% (w/v) non-fat milk powder and 0.1% (v/v) Triton-X100) for 1 hr. Cells were incubated for 1 hr with primary antibodies diluted in blotto-PBS and subsequently washed 3 x 5 minutes in PBS. Antibodies used were mAb K89/34 for Kv2.1 (NeuroMab, RRID:AB_1067225), rabbit pAb 5.1C for Kv5.1 (in-house, RRID:AB_3076240), and rabbit anti-V5 for Kv9.3-V5 (Rockland, 600-401-378). For surface labeling of Kv5.1, non-permeabilized cells were incubated with Kv5.1 mAb (Santa Cruz Biotech, 81881) in blotto-PBS lacking Triton-X100. The cells were then incubated with mouse IgG subclass- and/or species-specific Alexa-conjugated fluorescent secondary antibodies (Invitrogen) diluted in blotto-PBS for 45 min and washed 3 x 5 min in PBS. Cover glasses were mounted on microscope slides with Prolong Gold mounting medium (ThermoFisher, P36930) according to the manufacturer's instructions. Widefield fluorescence images were acquired with an AxioCam MRm digital camera installed on a Zeiss AxioImager M2 microscope with a 63×/1.40 NA Plan-Apochromat oil immersion objective and an ApoTome coupled to Axiovision software version 4.8.2.0 (Zeiss, Oberkochen, Germany).

- Multiplex in situ hybridization

A 6-week-old *Mrgprd*^{GFP} mouse was briefly anesthetized with 3–5% isoflurane and then decapitated. The spinal column was dissected, and the left and right L1 DRG were removed and drop fixed for 12 minutes in ice cold 4% paraformaldehyde in 0.1 M phosphate buffer (PB) pH adjusted to 7.4. The L1 vertebrae was identified by the 13th rib. The DRG was washed 3 × 10 minutes each in PB and cryoprotected at 4 °C in 30% sucrose diluted in PB for 2 hr. The DRG were then frozen in Optimal Cutting Temperature (OCT) compound (Fisher, 4585) and stored at –80 °C until sectioning. Samples were cut into 20 µm sections on a freezing stage sliding microtome and were collected on Colorfrost Plus microscope slides (Fisher Scientific, 12-550-19). Sections were processed for RNA *in situ* detection using an RNAscope Fluorescent Detection Kit according to the manufacturer's instructions (Advanced Cell Diagnostics) with the following probes: *KCNF1* (508731, mouse) or *KCNS1* (525941, mouse). TSA Vivid 650 Fluorophore was used to label probes (TSA Vivid, 7527) Following in situ hybridization, immunohistochemistry to label GFP was performed. Sections were incubated in vehicle solution (4% milk, 0.2% triton diluted in PB) for 1 hr at RT. Tissue was then incubated in a rabbit polyclonal anti-GFP antibody (Rockland 600-401-215S) diluted 1:1000 in vehicle overnight at 4 °C. Sections were washed three times in vehicle for 5 minutes per wash and then incubated in a goat anti-rabbit secondary antibody (Invitrogen, A-11008) diluted 1:1500 in vehicle. Sections were then mounted with Prolong Gold (Thermo Fisher, P36930) and #1.5 cover glass (Fisher Scientific, NC1776158).

- Imaging

Images were acquired with an inverted scanning confocal and airy disk imaging system (Zeiss LSM 880 Airyscan, 410900-247-075) run by ZEN black v2.1. Laser lines were 488 nm and 633 nm. Images were acquired with a 0.8 NA 20x objective (Zeiss, 420650-9901) details in figure legends.

- Statistics

All statistical tests were performed in Igor Pro software version 8 (Wavemetrics, Lake Oswego, OR). Independent replicates (n) are individual cells/neurons while biological replicates (N) are individual mice. All tests were two-tailed. Wilcoxon rank tests were used for two-sample comparisons. Dunnett tests were used for multiple comparisons.

ACKNOWLEDGMENTS

We thank the human tissue donors and their families for their generous donations. We thank Sierra Donor Services for recovering human dorsal root ganglia, as well as Sean Van Slyck, Marnae Salampessy, and Theanne Griffith for helping arrange for human tissue. We thank Bryan Copits, Ted Price, and Juliet Mwirigi for advice on culturing human neurons. We thank Cyrrus Espino, Hai Nguyen, Sitong Zhu, and Geir Hareland for preparation of human tissues. We thank Josh Tulman for illustrations. We thank Bruce Bean for scientific discussions and feedback on the manuscript. GxTx-Nle35 was synthesized at the Molecular Foundry of the Lawrence Berkeley National Laboratory under U.S. Department of Energy contract DE-AC02-05CH11231. Research at the University of California Davis was supported by the University of California Davis and U.S. National Institutes of Health grant R03-TR004200. Research at Harvard was supported by National Institutes of Health grant R35-NS127216. The Neurobiology Course at the Marine Biological Laboratory is supported by National Institutes of Health grant R25-NS063307.

REFERENCES

Aras MA, Saadi RA, Aizenman E (2009) Zn2+ regulates Kv2.1 voltage-dependent gating and localization following ischemia. Eur J Neurosci 30:2250-2257.

Bishop HI, Guan D, Bocksteins E, Parajuli LK, Murray KD, Cobb MM, Misonou H, Zito K, Foehring RC, Trimmer JS (2015) Distinct cell- and layer-specific expression patterns and independent regulation of Kv2 channel subtypes in cortical pyramidal neurons. J Neurosci 35:14922-14942.

Bocksteins E (2016) Kv5, Kv6, Kv8, and Kv9 subunits: No simple silent bystanders. J Gen Physiol 147:105-125.

Bocksteins E, Snyders DJ (2012) Electrically silent Kv subunits: their molecular and functional characteristics. Physiology (Bethesda) 27:73-84.

Bocksteins E, Snyders DJ, Holmgren M (2017) Independent movement of the voltage sensors in K(V)2.1/K(V)6.4 heterotetramers. Sci Rep 7:41646.

Bocksteins E, Labro AJ, Snyders DJ, Mohapatra DP (2012) The electrically silent Kv6.4 subunit confers hyperpolarized gating charge movement in Kv2.1/Kv6.4 heterotetrameric channels. PLoS One 7:e37143.

Bocksteins E, Raes AL, Van de Vijver G, Bruyns T, Van Bogaert PP, Snyders DJ (2009) Kv2.1 and silent Kv subunits underlie the delayed rectifier K+ current in cultured small mouse DRG neurons. Am J Physiol Cell Physiol 296:C1271-1278.

Castellano A, Chiara MD, Mellstrom B, Molina A, Monje F, Naranjo JR, Lopez-Barneo J (1997) Identification and functional characterization of a K+ channel alpha-subunit with regulatory properties specific to brain. J Neurosci 17:4652-4661.

Fernández-Mariño AI, Tan XF, Bae C, Huffer K, Jiang J, Swartz KJ (2023) Inactivation of the Kv2.1 channel through electromechanical coupling. Nature 622:410-417.

Ferns M, Van der List D, Vierra NC, Lacey T, Murray KD, Kirmiz M, Stewart RG, Sack JT, Trimmer JS (2024) Electrically silent KvS subunits associate with native Kv2 channels in brain and impact diverse properties of channel function. bioRxiv:2024.2001.2025.577135.

Hart NS, Mountford JK, Voigt V, Fuller-Carter P, Barth M, Nerbonne JM, Hunt DM, Carvalho LS (2019) The Role of the Voltage-Gated Potassium Channel Proteins Kv8.2 and Kv2.1 in Vision and Retinal Disease: Insights from the Study of Mouse Gene Knock-Out Mutations. eNeuro 6.

Herrington J, Solly K, Ratliff KS, Li N, Zhou YP, Howard A, Kiss L, Garcia ML, McManus OB, Deng Q, Desai R, Xiong Y, Kaczorowski GJ (2011) Identification of novel and selective Kv2 channel inhibitors. Mol Pharmacol 80:959-964.

Herrington J et al. (2006) Blockers of the delayed-rectifier potassium current in pancreatic beta-cells enhance glucose-dependent insulin secretion. Diabetes 55:1034-1042.

Inamdar SM, Lankford CK, Poria D, Laird JG, Solessio E, Kefalov VJ, Baker SA (2022) Differential impact of Kv8.2 loss on rod and cone signaling and degeneration. Hum Mol Genet 31:1035-1050.

Jorge BS, Campbell CM, Miller AR, Rutter ED, Gurnett CA, Vanoye CG, George AL, Jr., Kearney JA (2011) Voltage-gated potassium channel KCNV2 (Kv8.2) contributes to epilepsy susceptibility. Proc Natl Acad Sci U S A 108:5443-5448.

Kerschensteiner D, Stocker M (1999) Heteromeric assembly of Kv2.1 with Kv9.3: effect on the state dependence of inactivation. Biophys J 77:248-257.

Kerschensteiner D, Soto F, Stocker M (2005) Fluorescence measurements reveal stoichiometry of K+ channels formed by modulatory and delayed rectifier alpha-subunits. Proc Natl Acad Sci U S A 102:6160-6165.

Kirmiz M, Palacio S, Thapa P, King AN, Sack JT, Trimmer JS (2018) Remodeling neuronal ER-PM junctions is a conserved nonconducting function of Kv2 plasma membrane ion channels. Mol Biol Cell:mbcE18050337.

Kobertz WR (2018) Oddballs in the Shaker family: Kv2-related regulatory subunits. J Gen Physiol 150:1599-1601.
Kramer JW, Post MA, Brown AM, Kirsch GE (1998) Modulation of potassium channel gating by coexpression of Kv2.1 with regulatory Kv5.1 or Kv6.1 alpha-subunits. Am J Physiol 274:C1501-1510.
Lee MC, Nahorski MS, Hockley JRF, Lu VB, Ison G, Pattison LA, Callejo G, Stouffer K, Fletcher E, Brown C, Drissi I, Wheeler D, Ernfors P, Menon D, Reimann F, Smith ESJ, Woods CG (2020a) Human Labor Pain Is Influenced by the Voltage-Gated Potassium Channel K(V)6.4 Subunit. Cell Rep 32:107941.
Lee MC, Nahorski MS, Hockley JRF, Lu VB, Ison G, Pattison LA, Callejo G, Stouffer K, Fletcher E, Brown C, Drissi I, Wheeler D, Ernfors P, Menon D, Reimann F, Smith ESJ, Woods CG (2020b) Human labor pain is influenced by the voltage-gated potassium channel Kv 6.4 subunit. Cell Rep 32:107941.
Li XN, Herrington J, Petrov A, Ge L, Eiermann G, Xiong Y, Jensen MV, Hohmeier HE, Newgard CB, Garcia ML, Wagner M, Zhang BB, Thornberry NA, Howard AD, Kaczorowski GJ, Zhou YP (2013) The role of voltage-gated potassium channels Kv2.1 and Kv2.2 in the regulation of insulin and somatostatin release from pancreatic islets. J Pharmacol Exp Ther 344:407-416.
Liu PW, Bean BP (2014) Kv2 channel regulation of action potential repolarization and firing patterns in superior cervical ganglion neurons and hippocampal CA1 pyramidal neurons. J Neurosci 34:4991-5002.
Liu Y, Beyer A, Aebersold R (2016) On the Dependency of Cellular Protein Levels on mRNA Abundance. Cell 165:535-550.
Lossin C, Wang DW, Rhodes TH, Vanoye CG, George AL, Jr. (2002) Molecular basis of an inherited epilepsy. Neuron 34:877-884.
Marino. M, Misuri. L, Brogioli. D (2014) A new open source software for the calculation of the liquid junction potential between two solutions according to the stationary Nernst-Planck equation. arXiv.
Marquis MJ, Sack JT (2022) Mechanism of use-dependent Kv2 channel inhibition by RY785. J Gen Physiol 154.
Matsumoto C, O'Dwyer SC, Manning D, Hernandez-Hernandez G, Rhana P, Fong Z, Sato D, Clancy CE, Vierra NC, Trimmer JS, Fernando Santana L (2023) The formation of K(V)2.1 macro-clusters is required for sex-specific differences in L-type Ca(V)1.2 clustering and function in arterial myocytes. Commun Biol 6:1165.
Maverick EE, Leek AN, Tamkun MM (2021) Kv2 channel-AMIGO β-subunit assembly modulates both channel function and cell adhesion molecule surface trafficking. J Cell Sci 134.
Milescu M, Lee HC, Bae CH, Kim JI, Swartz KJ (2013) Opening the shaker K+ channel with hanatoxin. J Gen Physiol 141:203-216.
Milescu M, Bosmans F, Lee S, Alabi AA, Kim JI, Swartz KJ (2009) Interactions between lipids and voltage sensor paddles detected with tarantula toxins. Nat Struct Mol Biol 16:1080-1085.
Misonou H, Thompson SM, Cai X (2008) Dynamic regulation of the Kv2.1 voltage-gated potassium channel during brain ischemia through neuroglial interaction. J Neurosci 28:8529-8538.
Misonou H, Mohapatra DP, Menegola M, Trimmer JS (2005) Calcium- and metabolic state-dependent modulation of the voltage-dependent Kv2.1 channel regulates neuronal excitability in response to ischemia. J Neurosci 25:11184-11193.
Misonou H, Menegola M, Mohapatra DP, Guy LK, Park KS, Trimmer JS (2006) Bidirectional activity-dependent regulation of neuronal ion channel phosphorylation. J Neurosci 26:13505-13514.
Miyamae T, Hashimoto T, Abraham M, Kawabata R, Koshikizawa S, Bian Y, Nishihata Y, Kikuchi M, Ermentrout GB, Lewis DA, Gonzalez-Burgos G (2021) Kcns3 deficiency disrupts Parvalbumin neuron physiology in mouse prefrontal cortex: Implications for the pathophysiology of schizophrenia. Neurobiol Dis 155:105382.

Moller L, Regnier G, Labro AJ, Blunck R, Snyders DJ (2020) Determining the correct stoichiometry of Kv2.1/Kv6.4 heterotetramers, functional in multiple stoichiometrical configurations. Proc Natl Acad Sci U S A 117:9365-9376.
Murakoshi H, Shi G, Scannevin RH, Trimmer JS (1997) Phosphorylation of the Kv2.1 K+ channel alters voltage-dependent activation. Mol Pharmacol 52:821-828.
Peltola MA, Kuja-Panula J, Lauri SE, Taira T, Rauvala H (2011) AMIGO is an auxiliary subunit of the Kv2.1 potassium channel. EMBO Rep 12:1293-1299.
Pisupati A, Mickolajczyk KJ, Horton W, van Rossum DB, Anishkin A, Chintapalli SV, Li X, Chu-Luo J, Busey G, Hancock WO, Jegla T (2018) The S6 gate in regulatory Kv6 subunits restricts heteromeric K. J Gen Physiol 150:1702-1721.
Plant LD, Dowdell EJ, Dementieva IS, Marks JD, Goldstein SA (2011) SUMO modification of cell surface Kv2.1 potassium channels regulates the activity of rat hippocampal neurons. J Gen Physiol 137:441-454.
Post MA, Kirsch GE, Brown AM (1996) Kv2.1 and electrically silent Kv6.1 potassium channel subunits combine and express a novel current. FEBS Lett 399:177-182.
Ray P, Torck A, Quigley L, Wangzhou A, Neiman M, Rao C, Lam T, Kim JY, Kim TH, Zhang MQ, Dussor G, Price TJ (2018) Comparative transcriptome profiling of the human and mouse dorsal root ganglia: an RNA-seq-based resource for pain and sensory neuroscience research. Pain 159:1325-1345.
Regnier G, Bocksteins E, Van de Vijver G, Snyders DJ, van Bogaert PP (2016) The contribution of Kv2.2-mediated currents decreases during the postnatal development of mouse dorsal root ganglion neurons. Physiol Rep 4.
Regnier G, Bocksteins E, Marei WF, Pintelon I, Timmermans JP, Leroy JLMR, Snyders DJ (2017) Targeted deletion of the Kv6.4 subunit causes male sterility due to disturbed spermiogenesis. Reprod Fertil Dev 29:1567-1575.
Richardson FC, Kaczmarek LK (2000) Modification of delayed rectifier potassium currents by the Kv9.1 potassium channel subunit. Hear Res 147:21-30.
Salinas M, Duprat F, Heurteaux C, Hugnot JP, Lazdunski M (1997a) New modulatory alpha subunits for mammalian Shab K+ channels. The Journal of biological chemistry 272:24371-24379.
Salinas M, de Weille J, Guillemare E, Lazdunski M, Hugnot JP (1997b) Modes of regulation of shab K+ channel activity by the Kv8.1 subunit. J Biol Chem 272:8774-8780.
Sano Y, Mochizuki S, Miyake A, Kitada C, Inamura K, Yokoi H, Nozawa K, Matsushime H, Furuichi K (2002) Molecular cloning and characterization of Kv6.3, a novel modulatory subunit for voltage-gated K(+) channel Kv2.1. FEBS Lett 512:230-234.
Sapio MR, Vazquez FA, Loydpierson AJ, Maric D, Kim JJ, LaPaglia DM, Puhl HL, Lu VB, Ikeda SR, Mannes AJ, Iadarola MJ (2020) Comparative Analysis of Dorsal Root, Nodose and Sympathetic Ganglia for the Development of New Analgesics. Front Neurosci 14:615362.
Sepela RJ, Stewart RG, Valencia LA, Thapa P, Wang Z, Cohen BE, Sack JT (2022) The AMIGO1 adhesion protein activates Kv2.1 voltage sensors. Biophys J 121:1395-1416.
Stas JI, Bocksteins E, Labro AJ, Snyders DJ (2015) Modulation of Closed-State Inactivation in Kv2.1/Kv6.4 Heterotetramers as Mechanism for 4-AP Induced Potentiation. PLoS One 10:e0141349.
Stewart RG, Camacena M, Copits BA, Sack JT (2024) Distinct cellular expression and subcellular localization of Kv2 voltage-gated K(+) channel subtypes in dorsal root ganglion neurons conserved between mice and humans. The Journal of comparative neurology 532:e25575.
Thapa P, Stewart R, Sepela RJ, Vivas O, Parajuli LK, Lillya M, Fletcher-Taylor S, Cohen BE, Zito K, Sack JT (2021) EVAP: A two-photon imaging tool to study conformational changes in endogenous Kv2 channels in live tissues. J Gen Physiol 153.

Thorneloe KS, Nelson MT (2003) Properties and molecular basis of the mouse urinary bladder voltage-gated K+ current. J Physiol 549:65-74.
Tilley DC, Angueyra JM, Eum KS, Kim H, Chao LH, Peng AW, Sack JT (2019) The tarantula toxin GxTx detains K. J Gen Physiol 151:292-315.
Tilley DC, Eum KS, Fletcher-Taylor S, Austin DC, Dupré C, Patrón LA, Garcia RL, Lam K, Yarov-Yarovoy V, Cohen BE, Sack JT (2014) Chemoselective tarantula toxins report voltage activation of wild-type ion channels in live cells. Proceedings of the National Academy of Sciences of the United States of America 111:E4789-E4796.
Toledo-Aral JJ, Moss BL, He ZJ, Koszowski AG, Whisenand T, Levinson SR, Wolf JJ, Silos-Santiago I, Halegoua S, Mandel G (1997) Identification of PN1, a predominant voltage-dependent sodium channel expressed principally in peripheral neurons. Proc Natl Acad Sci U S A 94:1527-1532.
Tsantoulas C, Denk F, Signore M, Nassar MA, Futai K, McMahon SB (2018) Mice lacking Kcns1 in peripheral neurons show increased basal and neuropathic pain sensitivity. Pain 159:1641-1651.
Tsantoulas C, Zhu L, Shaifta Y, Grist J, Ward JP, Raouf R, Michael GJ, McMahon SB (2012) Sensory neuron downregulation of the Kv9.1 potassium channel subunit mediates neuropathic pain following nerve injury. J Neurosci 32:17502-17513.
Valtcheva MV, Copits BA, Davidson S, Sheahan TD, Pullen MY, McCall JG, Dikranian K, Gereau RWt (2016) Surgical extraction of human dorsal root ganglia from organ donors and preparation of primary sensory neuron cultures. Nat Protoc 11:1877-1888.
Vierra NC, O'Dwyer SC, Matsumoto C, Santana LF, Trimmer JS (2021) Regulation of neuronal excitation-transcription coupling by Kv2.1-induced clustering of somatic L-type Ca(2+) channels at ER-PM junctions. Proc Natl Acad Sci U S A 118.
Walker JR, Novick PA, Parsons WH, McGregor M, Zablocki J, Pande VS, Du Bois J (2012) Marked difference in saxitoxin and tetrodotoxin affinity for the human nociceptive voltage-gated sodium channel (Nav1.7) [corrected]. Proc Natl Acad Sci U S A 109:18102-18107.
Wu H, Cowing JA, Michaelides M, Wilkie SE, Jeffery G, Jenkins SA, Mester V, Bird AC, Robson AG, Holder GE, Moore AT, Hunt DM, Webster AR (2006) Mutations in the gene KCNV2 encoding a voltage-gated potassium channel subunit cause "cone dystrophy with supernormal rod electroretinogram" in humans. Am J Hum Genet 79:574-579.
Zheng Y, Liu P, Bai L, Trimmer JS, Bean BP, Ginty DD (2019) Deep sequencing of somatosensory neurons reveals molecular determinants of intrinsic physiological properties. Neuron 103:598-616.e597.
Zhong XZ, Abd-Elrahman KS, Liao CH, El-Yazbi AF, Walsh EJ, Walsh MP, Cole WC (2010) Stromatoxin-sensitive, heteromultimeric Kv2.1/Kv9.3 channels contribute to myogenic control of cerebral arterial diameter. J Physiol 588:4519-4537.
Zylka MJ, Rice FL, Anderson DJ (2005) Topographically distinct epidermal nociceptive circuits revealed by axonal tracers targeted to Mrgprd. Neuron 45:17-25.

FIGURES AND LEGENDS

Figure 1

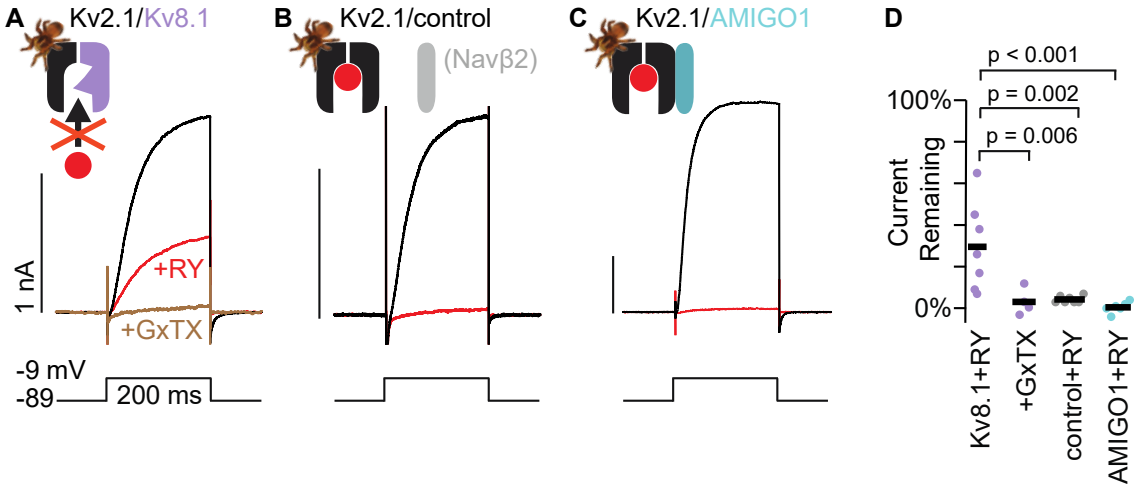

Figure 1. Kv2.1/Kv8.1 heteromers are resistant to RY785 and sensitive to GxTX

A) Exemplar traces from a voltage-clamped Kv2.1-CHO cell transfected with Kv8.1. Black and red traces are currents before and after application of 1 µM RY785 respectively. Brown trace is current after subsequent application of 1 µM RY785 and 100 nM GxTX.
B) Exemplar traces from a Kv2.1-CHO cell transfected with Navβ2.
C) Exemplar traces from a Kv2.1-CHO cell transfected with AMIGO1.
D) Current remaining after application of 1 µM RY785 or 1 µM RY785 + 100 nM GxTX. Black bars represent mean. Each point represents current from one cell at the end of a 200 ms voltage step to -9 mV. Dunnett tests with Kv8.1 + RY785 as control.

Figure 1 Supplement

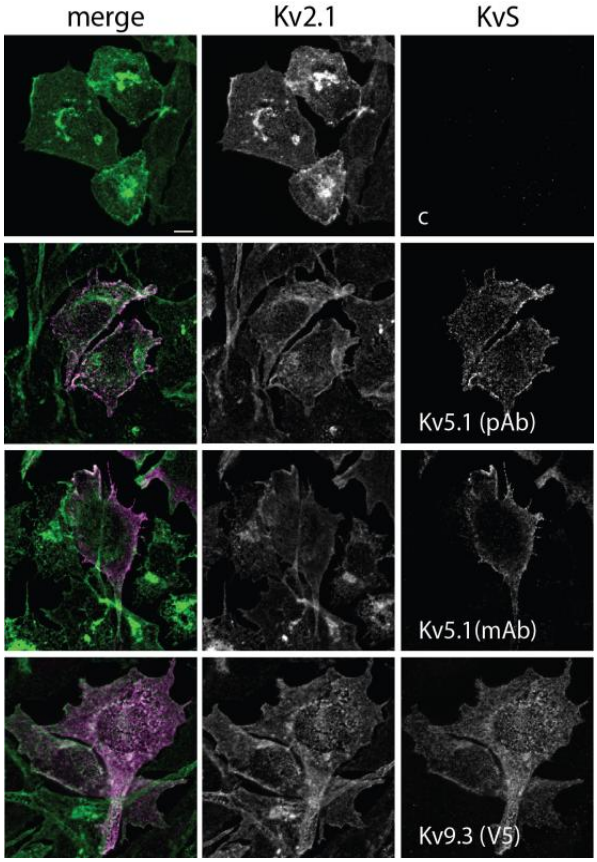

Figure 1 Supplement. KvS subunits colocalize with Kv2.1 on the surface of CHO cells.

Kv2.1-CHO cells transfected with the designated KvS subunits (c = no KvS transfection) were immunolabeled for Kv2.1 (green) and Kv5.1 or Kv9.3 (magenta). Immunolabeling for Kv5.1 and Kv9.3 were detected both intracellularly and on the apparent cell surface where they colocalized with Kv2.1 labeling. The anti-Kv5.1 mAb recognizes an extracellular epitope and was used on non-permeabilized cells, confirming surface expression of Kv5.1. Scale bars = 5 μm.

Figure 2

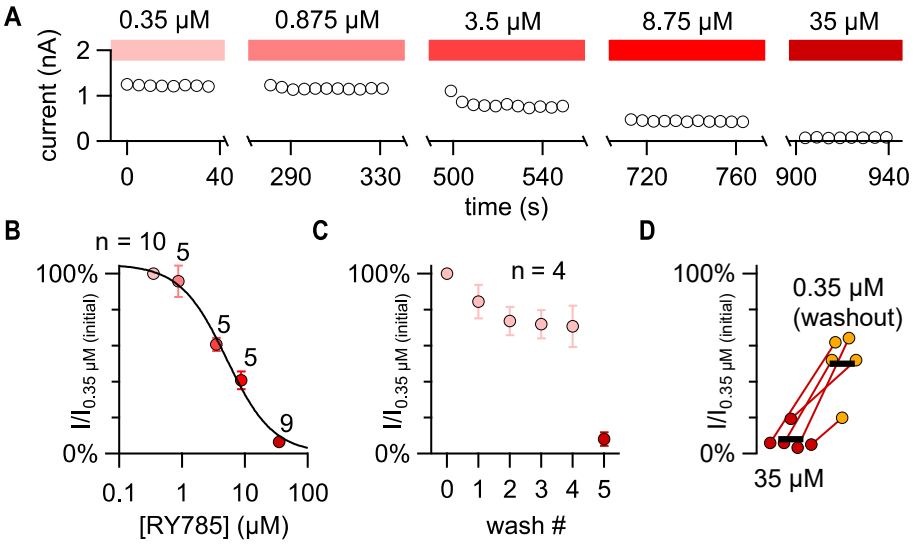

Figure 2. RY785 blocks Kv2.1/Kv8.1 heteromers in a concentration-dependent manner.

A) Current amplitudes during an RY785 concentration-effect experiment on a Kv2.1-CHO cell transfected with Kv8.1. Circles represent tail current amplitudes 2-4 ms into a step to –9 mV following a 200 ms activating step to 71 mV. Voltage protocol was repeated in 5 s intervals. Solution exchanges occurred during the gaps in the time axis. For exemplar current traces, see Figure 2 Supplement and Figure 3.

B) Mean normalized tail current amplitudes with increasing concentrations of RY785. Error bars represent SEMs. Black curve is a fitted Hill function with $n_H = 1$ (IC_{50} = 5.1 ± 1.0 µM, base = 1.0 ± 0.1 %).

C) Vehicle control tail current with repeated solution exchanges (washes) into 0.35 µM RY785, mimicking solution exchanges in panel B. Vehicle control solution exchanges were followed by exchange into 35 µM RY785 (wash #5). Error bars represent SEMs from n = 4 cells.

D) Tail current recovery following solution exchange from 35 µM RY785 into 0.35 µM RY785 (washout). Bars represent mean current amplitudes from n = 5 cells.

Figure 2 Supplement

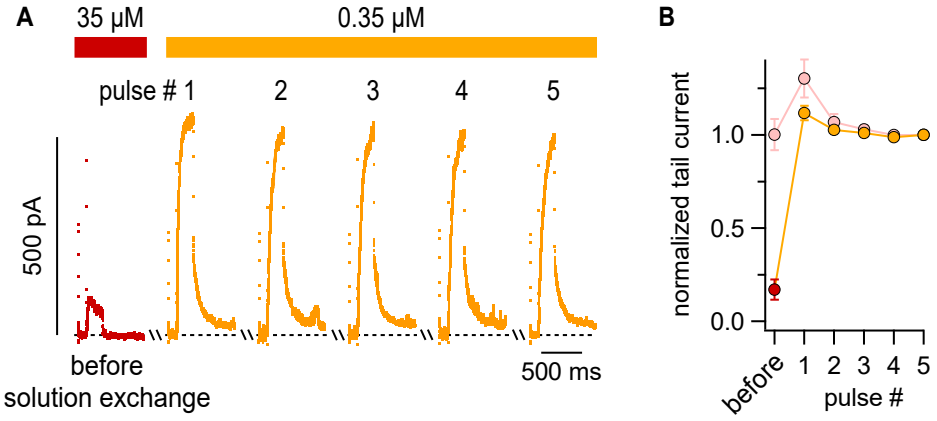

Figure 2 Supplement. Rapid unblock of RY785 from Kv2.1/Kv8.1 heteromers

A) Exemplar traces showing current recovery following solution exchange from 35 µM RY785 into 0.35 µM RY785. Voltage protocol is the same as in Figure 2. Cells were held at -89 mV without pulsing during solution exchange.

B) Tail current amplitudes, as in Figure 2, normalized to pulse #5. n = 5 cells treated first with 35 µM RY785 (dark red) then 0.35 µM RY785 (orange). n = 4 control cells treated first with 0.35 µM RY785 and washed again with 0.35 µM RY785 (pink). The transient increase in current amplitudes upon solution exchange also occurs with Kv2.1 (Marquis and Sack, 2022).

Figure 3

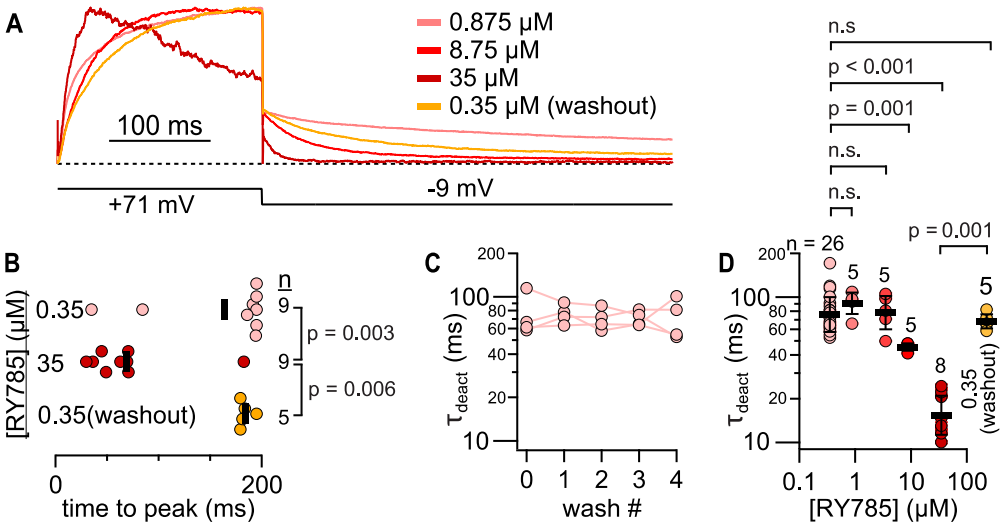

Figure 3. RY785 can affect Kv2.1/Kv8.1 current kinetics.

A) Kinetics of currents from a Kv2.1-CHO cell transfected with Kv8.1 are altered by RY785. Traces normalized to max.

B) Latency to peak current during steps to +71 mV. The time axis of this plot is aligned with that of Panel A. Bars represent means. Unpaired Wilcoxon rank tests.

C) Time constant of deactivation at -9 mV is constant after washes with 0.35 µM RY785. Time constants are derived from fits of a monoexponential function (Equation 3 with A_2 set equal to 0) to tail currents like those shown in Panel A. Fits were from the peak of each tail current to 200 ms after the voltage step. Brown and Forsythe test p = 0.98. ANOVA p = 0.98. Statistics were performed on natural logarithms of time constants. n = 4 cells.

D) RY785 can alter time constant of deactivation. Brown and Forsythe test p = 3×10^{-12}. Unpaired Welch test p = 1×10^{-7}. Dunnett tests with 0.35 µM RY785 (initial) as control. Unpaired Wilcoxon rank test comparing 35 µM RY785 to 0.35 µM RY785 (washout) p = 0.001. Statistics were performed on natural logarithms of time constants.

Figure 4

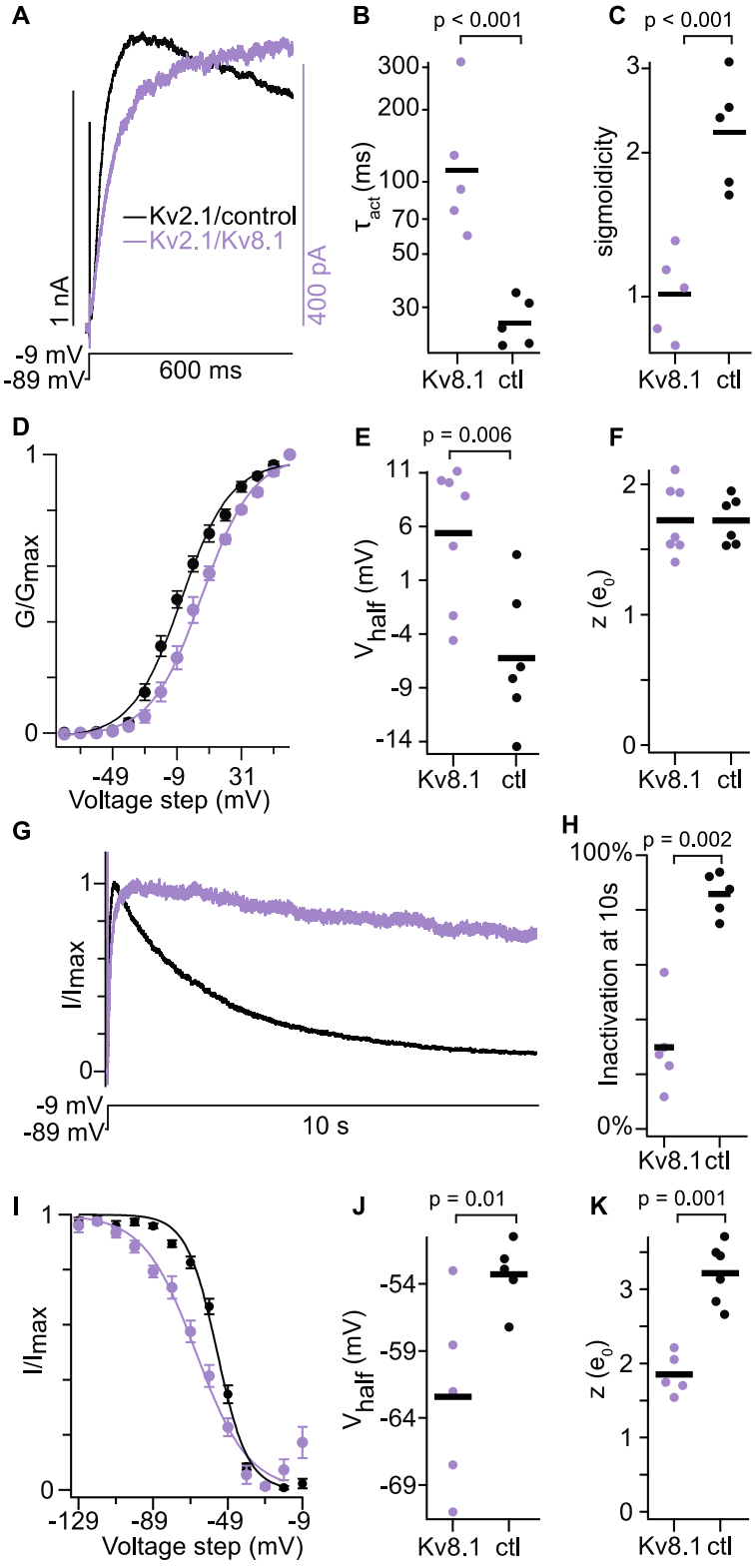
A
—Kv2.1/control
—Kv2.1/Kv8.1
1 nA
400 pA
-9 mV
-89 mV
600 ms
B
p < 0.001
τact (ms)
300
200
100
70
50
30
Kv8.1
ctl
C
p < 0.001
sigmoidicity
3
2
1
Kv8.1
ctl
D
G/Gmax
1
0
-49
-9
31
Voltage step (mV)
E
p = 0.006
Vhalf (mV)
11
6
1
-4
-9
-14
Kv8.1
ctl
F
z (e0)
2
1
0
Kv8.1
ctl
G
I/Imax
1
0
-9 mV
-89 mV
10 s
H
p = 0.002
Inactivation at 10s
100%
0%
Kv8.1
ctl
I
I/Imax
1
0
-129
-89
-49
-9
Voltage step (mV)
J
p = 0.01
Vhalf (mV)
-54
-59
-64
-69
Kv8.1
ctl
K
p = 0.001
z (e0)
3
2
1
0
Kv8.1
ctl

Figure 4. RY785-resistant current is consistent with Kv2.1/Kv8.1 heteromers

Kv2.1/8.1 data (purple) are from Kv2.1-CHO cells transfected with Kv8.1, and are in 1 µM RY785. Kv2.1/control (black) were transfected with Navβ2, and are in vehicle control solution. Before measurements, repeated voltage steps to -9 mV were given until currents stabilized. p values are from two-tailed unpaired Wilcoxon rank test.

A) Exemplar currents during a step to -9 mV.
B) Time constants from exponential fit (Equation 1). Geometric mean.
C) Sigmoidicity from exponential fit (Equation 1). Geometric mean.
D) Conductance-voltage activation relation. Conductance was measured from initial tail currents at -9 mV. Mean ± SEM. Kv2.1/Kv8.1 n = 7 cells Kv2.1 n = 6 cells. Lines are Boltzmann fits (Equation 2) (Kv2.1/Kv8.1: $V_{1/2}$ = 6 ± 1 mV, z = 1.6 ± 0.1 e_0; Kv2.1/control: $V_{1/2}$ = -6.3 ± 1 mV, z = 1.7 ± 0.1 e_0).
E) Activation $V_{1/2}$ values from individual cells.
F) Activation z values.
G) Exemplar currents during a 10 s step to -9 mV.
H) Percent of current inactivated after 10 seconds at -9 mV.
I) Steady state currents at -9 mV after holding at indicated voltages for 10 seconds. Normalized to the max and min. Mean ± SEM. Kv2.1/Kv8.1 n = 5 cells Kv2.1 n = 5 cells. Lines are Boltzmann fits (Equation 2) (Kv2.1/Kv8.1: $V_{1/2}$ = -66 ± 1 mV, z = 1.8 ± 0.1 e_0; Kv2.1/control: $V_{1/2}$ = -54.7 ± 0.8 mV, z = 3.1 ± 0.3 e_0).
J) Inactivation $V_{1/2}$ values from individual cells.
K) Inactivation z values.

Figure 4 Supplement

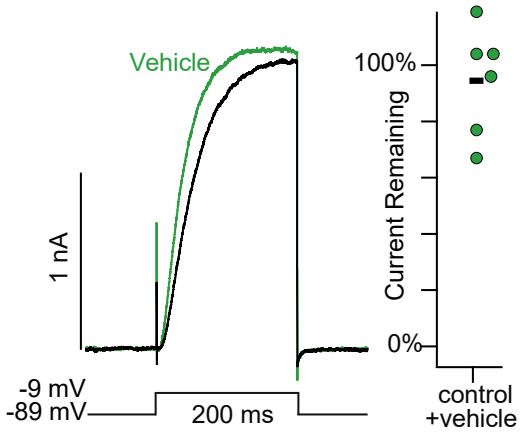

Figure 4 Supplement. Effect of vehicle control on Kv2.1.

Left: Exemplar traces from a Kv2.1-CHO cell transfected with Navβ2. Black and green traces are currents before and after application of vehicle control respectively. Right: Current remaining after application of vehicle control. Black bar represents mean. Each point represents current from one cell at the end of a 200 ms -9 mV voltage step.

Figure 5

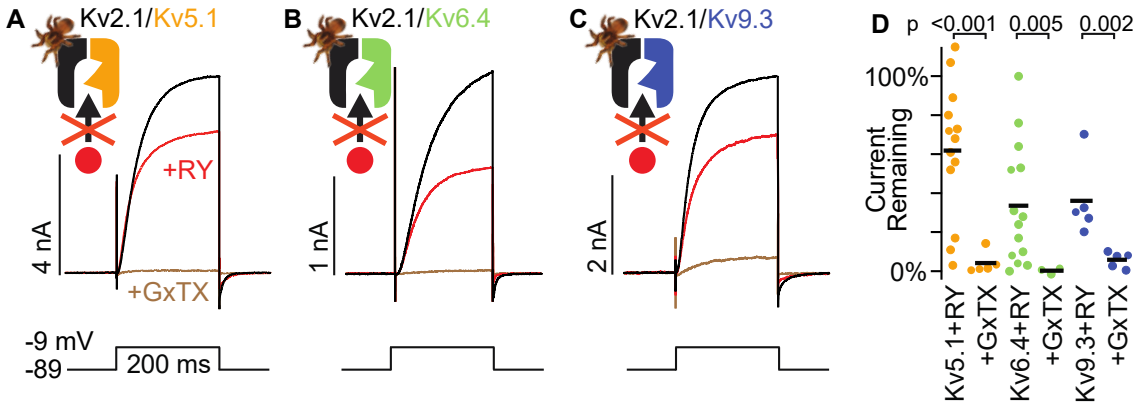

Figure 5. A subunit from each KvS family is resistant to RY785

A) Exemplar traces from a voltage-clamped Kv2.1-CHO cell transfected with Kv5.1. Black and red traces are currents before and after application of 1 µM RY785 respectively. Brown trace is current after subsequent application of 1 µM RY785 + 100 nM GxTX
B) Exemplar traces from a Kv2.1-CHO cell transfected with Kv6.4.
C) Exemplar traces from a Kv2.1-CHO cell transfected with Kv9.3.
D) Current remaining after application of 1 µM RY785 or 1 µM RY785 + 100 nM GxTX. Black bars represent mean. Each point represents current from one cell at the end of a 200 ms voltage step to -9 mV. Unpaired Wilcoxon rank tests.

Figure 6

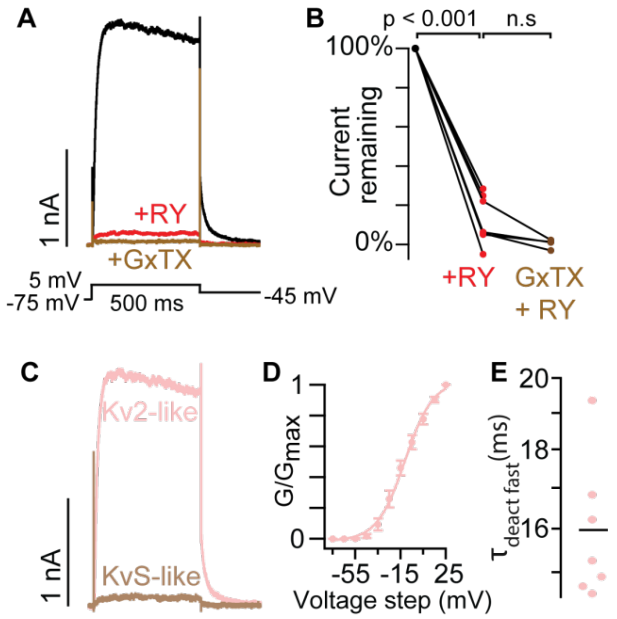

Figure 6. Mouse superior cervical ganglion neurons lack substantial KvS-like currents.

A) Exemplar currents from a voltage-clamped SCG neuron. Black and red traces are currents before and after application of 1 µM RY785 respectively. Brown trace is current after subsequent application of 1 µM RY785 + 100 nM GxTX.

B) Tail current amplitude 10 ms after voltage was stepped from +5 mV to -45 mV normalized to current amplitude before RY785. Paired Wilcoxon rank tests, n = 7 neurons, N = 3 mice.

C) Subtracted currents from A. Kv2-like current is the RY785-sensitive current (black trace minus red in A). KvS-like current is the GxTX-sensitive current remaining in RY785 (red trace minus brown in A).

D) Conductance-voltage activation relation of Kv2-like current in SCG neurons. Conductance was measured from tail currents at -45 mV. $V_{1/2}$ = -11 ± 1 mV, z = 2.1 ± 0.2 e_0 Mean ± SEM. n = 7 neurons, N = 3 mice.

E) The faster time constant of a double exponential (Equation 3) fit to channel deactivation at -45 mV.

Figure 7

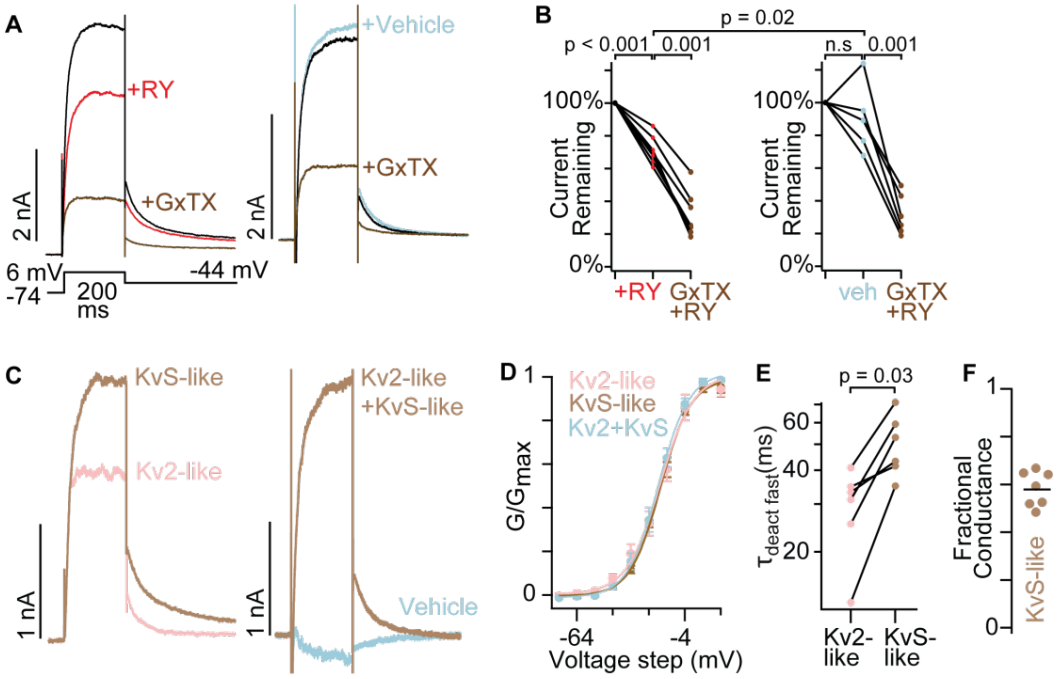

Figure 7. Mouse nociceptors have RY785-resistant KvS-like currents.

A) Exemplar currents from nonpeptidergic nociceptors, GFP$^+$ neurons from *Mrgprd^{GFP}* mice.

B) Tail current amplitude 10 ms after voltage was stepped from +6 mV to -44 mV normalized to current amplitude before RY785 or vehicle treatment. Wilcoxon rank tests were paired, except the comparison of RY785 to vehicle which was unpaired. RY785 then GxTX: n = 7 neurons, N = 4 mice. Vehicle then GxTX: n = 6 neurons, N = 4 mice.

C) Exemplar subtracted currents from A. Kv2-like is the initial current minus RY785 (black trace minus red in A left panel). KvS-like is the current in RY785 minus GxTX (red trace minus brown in A left panel). Kv2-like+KvS-like is the current in vehicle minus RY785 + GxTX (blue trace minus brown in A right panel).

D) Voltage dependance of activation of subtraction currents in *Mrgprd^{GFP+}* neurons. Pink points represent Kv2-like currents, brown points represent KvS like currents, and light blue points represent Kv2+KvS-like currents after vehicle treatment. Conductance was measured from initial tail currents at -44 mV. Kv2-like: $V_{1/2}$ = -18 ± 1 mV, z = 2.7 ± 0.3 e_0, KvS-like: $V_{1/2}$ = -18 ± 1 mV, z = 3 ± 0.2 e_0, Kv2 + KvS-like: $V_{1/2}$ = -19 ± 1 mV, z = 2.9 ± 0.1 e_0. Mean ± SEM. KvS-like and Kv2-like n = 7 neurons N = 4 mice, Kv2+KvS-like n = 6 neurons N = 4 mice.

E) The faster time constant of a double exponential fit (Equation 3) to channel deactivation at -44 mV. p value represents paired Wilcoxon rank test.

F) Fractional KvS-like conductance relative to the total RY785 + GxTX-sensitive conductance. KvS-like is only sensitive to GxTX.

Figure 7 Supplement 1

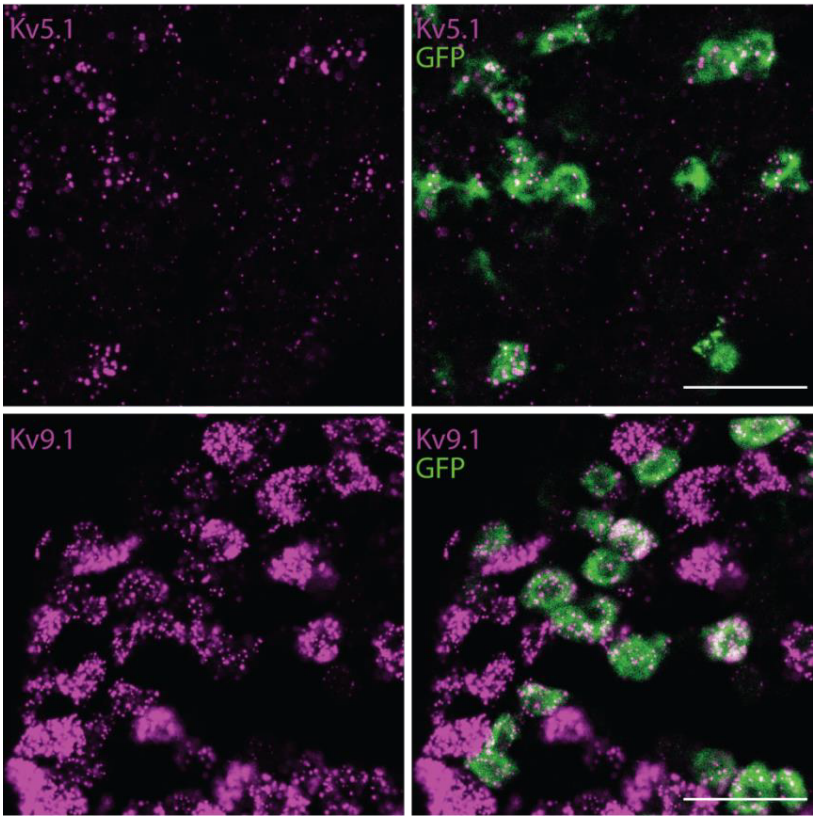

Figure 7 Supplement 1. Nonpeptidergic nociceptors express Kv5.1 and Kv9.1 mRNA transcripts.

Exemplar images of DRG sections from a *Mrgprd*^{GFP} mouse labeled with RNAscope *in situ* hybridization for *KCNF1* (Kv5.1) (top magenta) or *KCNS1* (Kv9.1) (bottom magenta). Scale bars are 50 µm.

Fig 7 Supplement 2

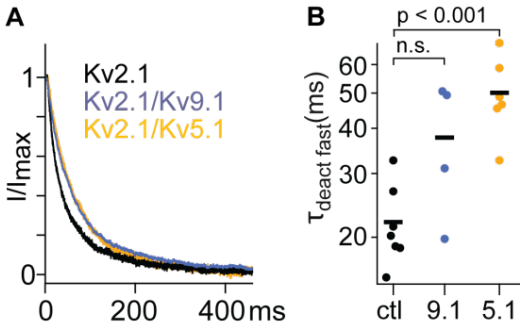

Figure 7 Supplement 2. RY785 resistant currents from Kv2.1-CHO cells transfected with Kv5.1 or Kv9.1 deactivate slower than currents from untransfected Kv2.1-CHO cell.

A) Exemplar traces of channel deactivation at -49 mV after a 50 ms step to +11 mV. Traces are normalized to max current during the -49 mV step.
B) The faster time constant of a double exponential fit (Equation 3) to channel deactivation. Dunnett tests versus control (ctl). Ctl n = 7. Kv9.1 n = 4. Kv5.1 n = 6.

Figure 8

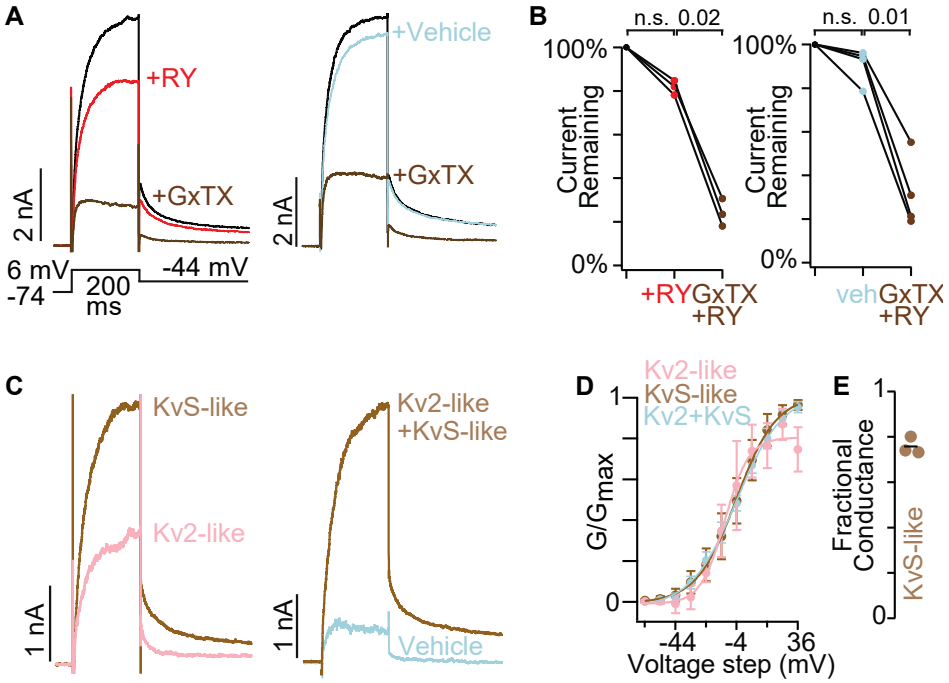

Figure 8. Human somatosensory neurons have RY785-resistant KvS-like currents.

A) Exemplar currents from human dorsal root ganglion neurons.

B) Tail current amplitude 10 ms after voltage was stepped from +6 mV to -44 mV normalized to current amplitude before RY785 or vehicle treatment. Paired Wilcoxon rank tests. RY785 then GxTX: n = 3 neurons. Vehicle then GxTX: n = 4 neurons. All neurons from same human.

C) Exemplar subtracted currents from A. Kv2-like is the initial current minus RY785 (black trace minus red in A left panel). KvS-like is the current in RY785 minus GxTX (red trace minus brown in A left panel). Kv2+KvS-like is the current in vehicle minus RY785 + GxTX (blue trace minus brown in A right panel).

D) Voltage dependence of activation of subtraction currents in human dorsal root ganglion neurons. Pink points represent Kv2-like currents, brown points represent KvS like currents, and blue points represent Kv2 + KvS-like currents after vehicle treatment. Conductance was measured from initial tail currents at -44 mV. Mean ± SEM. Kv2 + KvS-like n = 3 neurons N = 1 human, KvS+Kv2-like n = 4 neurons N = 1 human.

E) Fractional KvS-like conductance relative to the total RY785 + GxTX-sensitive conductance. KvS-like is only sensitive to GxTX.

Summary and Conclusions

My work revealed a mechanism in which ion channel blocker activity is impacted both by gated access to a blocking site and by state-biased affinity. RY785 can be used as a research tool to selectively block homomeric $K_V2.1$ channels without affecting the gating of $K_V8.1$-containing channels. I speculate that this selectivity is due to $K_V2.1/K_V8.1$ channels having weak closed-state affinity for RY785, unlike homomeric channels. Open-state bias could account for the apparent open channel block and recovery between pulses of $K_V2.1/K_V8.1$ channels. This topic could be further explored by assessing how RY785 affinity is affected by channel inactivation, which closes the pore[6]. Future efforts might also explore on the medicinal chemistry of state-bias.

References

1. Zheng, J., & Trudeau, M.C. (Eds.). (2023). Textbook of Ion Channels Volume I: Fundamental Mechanisms and Methodologies (1st ed.). CRC Press. https://doi.org/10.1201/9781003096214

2. Zheng, J., & Trudeau, M.C. (Eds.). (2015). Handbook of Ion Channels (1st ed.). CRC Press. https://doi.org/10.1201/b18027

3. Matthew James Marquis, Jon T. Sack; Mechanism of use-dependent Kv2 channel inhibition by RY785. J Gen Physiol 6 June 2022; 154 (6): e202112981. doi: https://doi.org/10.1085/jgp.202112981

4. Ben Short; A Kv2 inhibitor traps itself in place. J Gen Physiol 6 June 2022; 154 (6): e202213181. doi: https://doi.org/10.1085/jgp.202213181

5. Robert G. Stewart, Matthew James Marquis, Sooyeon Jo, Michael Ferns, & Jon T. Sack. KvS regulatory subunits confer drug resistance to Kv2 channels *bioRxiv* 2024.01.31.578214; doi: https://doi.org/10.1101/2024.01.31.578214

6. Fernández-Mariño, A. I., Tan, X. F., Bae, C., Huffer, K., Jiang, J., & Swartz, K. J. (2023). Inactivation of the Kv2.1 channel through electromechanical coupling. Nature, 622(7982), 410–417. https://doi.org/10.1038/s41586-023-06582-8

Appendix I: Undergraduate Seminar Design

Foreword

This chapter is an insubstantially edited reproduction of a reflection that I composed as a requirement of FSE392, "Teaching Practicum in the Sciences", which is a requirement of the Future Undergraduate Science Educators (FUSE) graduate academic certificate program. The purpose of this practicum was to implement evidence-based pedagogical practices that I developed in other FUSE courses in a real classroom setting. My work produced concrete evidence of student learning in a highly rated seminar and an open-access archive of reusable course materials. Course materials and related documents are necessary to understand the reflection and can be found at https://ucdavis.app.box.com/folder/171458095272?s=nugjtye11y8yi2j64b7z3k1kr38qxfi7.

Matthew James Marquis
Ph.D. candidate
University of California, Davis
Dept. of Physiology & Membrane Biology
14 May 2024

On my professional development prior to the practicum - I began tutoring peers in general chemistry in my freshman year of college. My first official teaching role was as the UCSC Chemistry Club's chief tutor. I tutored fellow undergraduates in chemistry, in individual or group sessions, approximately once per week for five academic quarters. As a chemistry club member, I also helped organize and present at several science fairs at two local elementary schools. In my senior year, I worked for one quarter as a learning assistant in the UCSC Modified Supplemental Instruction program. I led weekly study sessions of fewer than 12 Chemistry 1A students and tutored small groups (<4) of students requesting additional help. A 1-unit seminar on education theory was the required training for peer tutors. In the second year of my Ph.D. program, I used principles learned in that seminar to design and co-teach a 1-unit CURE (Auchincloss *et al*., 2014) titled "The Physical Basis of Biological Electricity". FRS003-016 is a major redesign of that course focused on independent knowledge acquisition to address observed problems with cognitive load. I served for 2 quarters as a teaching assistant for a 3-unit, junior-level class, "Structure and Function of Biomolecules". As one of two TAs for approximately 250 students, I helped facilitate in-class learning activities, led discussion sections, and graded exams. I served for 2 quarters as a teaching assistant for

another 3-unit, junior-level class, "Bioenergetics and Metabolism". As the only TA for approximately 250 students, I facilitated in-class learning activities, led discussion sections, made supplemental instructional videos, and graded exams and projects. Face-to-face interaction with students differed while serving as a teaching assistant compared to a tutor and provided valuable practice, especially in communicating course expectations, that prepared me for FRS003-016. In a series of workshops offered by the Graduate Teaching Community at the Center for Educational Effectiveness I engaged in roundtable discussions on topics related to diversity in education and received a certificate of participation. Coursework I have completed for the FUSE program has covered pedagogical techniques, course design, and the epistemology of modern education theory. The redesign of "The Physical Basis of Biological Electricity" into FRS003-016 began as an exercise in one of the FUSE courses. Most recently, I coauthored a chapter of a graduate-level reference text in my field of study.

On my process developing the materials for this course - Conceptualization of FRS003-016 began with four areas for improvement in traditional undergraduate biology education: (1) coverage of the molecular mechanisms of ion homeostasis and electrical signaling, (2) opportunities to explore scientific literature, (3) encouragement of metacognitive career planning, and (4) development of open-ended communication skills. The broad learning goals for FRS003-016 were thus for students to gain knowledge on an ion-channel related topic of their choosing, become proficient at navigating a

literature database (*e.g.* PubMed, UniProt, the PDB), articulate their career goals and plans, and practice critical reasoning/scientific communication. Specific learning objectives and indicators of instructor success were articulated (see the appendix of the course application https://ucdavis.app.box.com/file/1031673715529). Lecture learning objectives are in the speaker's notes in each deck of lecture slides (https://ucdavis.app.box.com/folder/189689799319). In deference to the students' time, and to give them agency over their own learning, the learning activities for FRS003-016 centered on a scaffolded, independent research project on modern ion channel research. The point distribution of the course by Bloom's taxonomy level (Allen and Tanner, 2002; Crowe, Dirks, and Wenderoth, 2008) was: 14% knowledge, 34% comprehension, 9% application, 18% analysis, 11% synthesis, and 9% evaluation (and 5% participation). The assignments (https://ucdavis.app.box.com/folder/189690074636) comprising the research project were presented in a standard format to minimize the class time needed to explain them. This format consisted of an assignment title, a description of its purpose, a brief summary of its requirements, a list of recommended steps, an annotated example of an "A"-level submission, and a detailed rubric. An exercise in career planning was also assigned. Lectures and additional resources (https://ucdavis.app.box.com/folder/189692873076) were subsequently designed to provide critical background knowledge. Some lecture content was tailored to self-reported student interests solicited on the first day of class. The meeting schedule (see the

syllabus https://ucdavis.app.box.com/file/1111827681760) was largely determined by the needs of the research project. The project required students to summarize current knowledge on a topic of their choosing (assignment 2), ask an unanswered question on that topic (assignment 3), devise a hypothesis answering that question (assignment 4), design an experiment addressing that hypothesis (assignment 5), and condense their thoughts into a research proposal and presentation (final assignment). Consequently, lectures were concentrated in the first half of the quarter and learning activities in the second. To limit lecture time, I created a visual guide to finding and reading literature on PubMed. The course syllabus was designed according to principles described in a guide from Vanderbilt University's Center for Teaching (Riviere, Picard, and Coble, 2014). My experience co-teaching FRS003-016 revealed key deficiencies in the formatting of the assignment handouts and the requirements of the research project. Lessons learned during this experience are described below.

On my experience teaching this course - The following observations constitute a case study of student reactions to FRS003-016 and the logistics of implementing its materials. They will be interpreted in the following sections. A miscommunication with administrative staff resulted in a last-minute room change causing at least 2 students to miss the first day of class. Although 18 were enrolled at the start of the quarter, class size quickly dwindled to 7 and typical attendance was only 2-3 students. Due to a personal emergency, my co-instructor was only able to attend 5 out of 10 class sessions. Session 1

introductions yielded information about student class-levels and interests. As expected of a first-year seminar, most students were freshmen. However, one student was a senior. All students were considering or determined to attend medical school. Student interests included Alzheimer's disease, sensation, cancer, gastrointestinal inflammation, counterbioterrorism, and muscle physiology. During lecturing, students seemed generally attentive and were not too hesitant to ask or answer questions. I tended to run overtime in my lecturing which led to one planned learning activity, an exercise using PubMed, being skipped. Session 5 included a roundtable discussion in which students asked my co-instructor and I career questions. Students were eager to participate in this activity and the discussion easily filled the 20 minutes allotted for it. Participation was generally high in the course's other learning activities. However, during some less-structured paired discussions, students chose to work alone rather than speak to a classmate. The final two class sessions were reserved for student slideshow presentations. Students reserved presentation times on a first-come, first-serve basis via a Google spreadsheet announced over our institution's course management site, Canvas. Two students chose to present on the first day and four on the second. One did not give a presentation (or perform any of the work for this course). Presentations were required to last 3-6 minutes with 7-4 minutes for questions: a total of 10 minutes. There were enough questions from students that, despite all presentations staying under 6 minutes, all question-and-answer sessions reached the 10-minute mark. This contributed to the last

session feeling rushed because administrative staff requested, just days before the last session, that 10 minutes of class time be used for a course evaluation that they designed. In addition to the presentation, the final assignment included a written summary of thoughts developed during the course. This summary was due 1 week after the last class session, however, most students submitted theirs prior to their presentations.

On the successful aspects of this course - Multiple lines of evidence suggest that the workload for this course was appropriate for a 1-unit seminar. Students generally turned assignments in on or ahead of their due dates and the quality of work performed matched rubric expectations. Furthermore, students verbally indicated that assignment completion time estimates were approximately correct on multiple occasions. Student abilities to navigate scientific literature varied widely. However, all students eventually located and extracted salient information from apparently trustworthy research or review articles. Students exhibited confidence while presenting and discussing their original thoughts and expressed gratitude towards my co-instructor and me at the end of the course.

On ways to improve the course - Despite students performing admirably in this course, I believe some aspects could be scaled back and more emphasis should be placed on database exploration and reading. Due in part to omission of a learning activity (mentioned above), database exploration and reading skills were not thoroughly assessed. A careful analysis of submissions for assignments 2 and 3 may offer some clues

as to students' search tactics and comprehension. But, it is unclear whether students used available resources (such as the PubMed guide), learned systematically, or simply got lucky with their search results. Notably, PubMed appears to be the only database that students utilized, despite 4 others being discussed in class (see slide 6 of lecture 3). On a similar note, significant lecture time was spent on ion channel physiology and experimental methods, but students largely avoided this material in their research projects. In future installments of this course, I will strongly consider omitting Assignments 3-5 in favor of deeper and broader coverage of databases and science-specific reading skills. Proper assessment of reading skills will probably require an assignment in which students are given specific passages to analyze. Preferably these would come from articles the students found themselves but, practically, they would probably need to be hand-picked by the instructor based on her/his expertise. The most critical area for improvement in this course appears to be communication of course expectations. Very detailed assignment handouts were crafted to create structure and thereby promote equity, however, this strategy clearly failed for one student who spoke English as a second language. "Student 4" clearly misunderstood the expectations of Assignments 2-5 and the final writing assignment even after multiple in-person discussions of how their drafts needed improvement. Student 4 likely would have benefitted from more regular attendance but I believe the major barrier to Student 4's

success was the phrasing and formatting of my assignment handouts (see comments on assignment 2). These will require simplification.

On unexpected revelations of this course - One unexpected interaction occurred during a brief learning activity presented in slide 8 of lecture 3. Students were shown two publications and asked to spot the untrustworthy one and explain their reasoning. One student correctly identified the bogus article. That student's reasoning, politely conveyed, was essentially that the authors were all Indian. I was saved from this potentially awkward situation by another student, an Indian immigrant, who wholeheartedly agreed with the first student's reasoning, to everyone's amusement. This event heightened my awareness of the pervasiveness of ethnic/cultural bias. Just as unexpected was the aforementioned prevalence of early assignment submissions. Most work collected in this course was received well ahead of its deadline, with only one student consistently submitting work late. That student, Student 4, was struggling to understand the assignments (as described above) accounting for their tardiness. I do not know whether to interpret early submission as an indicator of student confidence or apathy. Hence, I think it premature to conclude that students were not sufficiently challenged. I am also puzzled by the case of Student 5 who came to my otherwise empty office hours halfway through the quarter to discuss the requirements of the class. Student 5 had already missed the first 2 assignment due dates and apparently had not viewed the course materials. Student 5 explained that an oversized courseload had distracted from FRS003-016 and I

reassured them that a passing grade was still achievable without too much effort. I never heard from Student 5 again and I wonder whether I should have suggested that they drop the course.

On pedagogical knowledge and awareness that I gained from the practicum - Although I had already designed a teachable unit as part of my FUSE coursework, this was my first experience implementing backwards design in a real course (Handelsman, Miller, and Pfund, 2007, pgs. 19-21). I found that having predefined learning goals helped me design learning activities more quickly and easily. I think that, without the logical framework of backwards course design, developing scaffolded assignments would have been prohibitively time-consuming. This course was also my first time employing a "matching game" in the classroom. My matching game is a reduced form of a memory matrix (Columbia University CTL) which encourages student-to-student interaction and acts as an open-ended formative assessment of student knowledge. Although the game was overambitious for a 50-minute class session, I found that it was a very effective means of EnGaugement (Handelsman, Miller, and Pfund, 2007, pg. 20). Prior to teaching this course, I had not encouraged students to perform metacognition in any formal learning activity. Although I did not measure the consequences of the metacognitive career planning assignment, students did verbally indicate that they expected to benefit from it prior to starting the assignment and, afterwards, that they appreciated the attention given

to their personal goals. In summary, backward design, memory matrices, and metacognitive exercises were all worth the time invested in exploring them.

On what I have learned and how I will approach future teaching - To summarize the lessons I learned while teaching FRS003-016: (i) the administration works in mysterious ways, (ii) you catch more participation with structure than with freedom, (iii) undergraduates can use PubMed, (iv) students are strongly disinclined to explore new material without an obvious benefit, (v) my instructions sacrificed too much clarity for the sake of detail, (vi) inequities are everywhere, and (vii) procrastination is not inevitable. In my future teaching, I will make greater effort to communicate with administrative staff to determine my bureaucratic obligations. My observations suggest that structure is important for generating engagement, especially in group activities. I will try to always incorporate concrete goals into paired discussions such that students do not need to navigate the awkwardness of deciding exactly what to talk about. I am excited by my students' now proven ability to navigate graduate-level literature and conclude that original research articles do belong in the undergraduate curriculum. FRS003-016 was overambitious in several ways and, moving forward, I will be more cautious to lecture on content that is not directly aligned with a summative assessment. Tightening alignment will have the added benefit of reducing the details necessary to explain assignments, enhancing clarity and restricting cognitive load. Thoughtful backward course design is perhaps my best tool for promoting diversity and equity in

the classroom. Finally, despite its flaws, this course gave my students an opportunity to demonstrate their initiative, creativity, and independence in ways seldom seen in the traditional science curriculum and my students delivered.

Sources Cited

Allen, Deborah and Kimberly Tanner. 2002. "Approaches to Cell Biology Teaching: Questions about Questions". *Cell Biology Education* Vol. 1, 63–67, Fall 2002

Auchincloss, Lisa Corwin; Sandra L. Laursen; Janet L. Branchaw; Kevin Eagan, Mark Graham; David I. Hanauer; Gwendolyn Lawrie; Colleen M. McLinn, Nancy Pelaez; Susan Rowland; Marcy Towns; Nancy M. Trautmann; Pratibha Varma-Nelson; Timothy J. Weston; and Erin L. Dolan. 2014. "Assessment of Course-Based Undergraduate Research Experiences: A Meeting Report". *Cell Biology Education* Vol. 13:1, 29-40

Columbia University, Center for Teaching and Learning. Webpage accessed May 7, 2023. https://ctl.columbia.edu/resources-and-technology/resources/assess-active-learning/

Crowe, Alison; Clarissa Dirks; and Mary Pat Wenderoth. 2008. "Biology in Bloom: Implementing Bloom's Taxonomy to Enhance Student Learning in Biology". *Cell Biology Education* Vol. 7, 368 –381

Handelsman, Jo; Sarah Miller; and Christine Pfund. 2007. "Scientific Teaching". W. H. Freeman and Company. 41 Madison Ave. New York, NY 10010. ISBN-10: 1-4292-0188-6

Riviere, Jessica; Danielle Picard; and Richard Coble. 2014. "Syllabus Design". Vanderbilt University Center for Teaching. Retrieved May 6, 2023 https://cft.vanderbilt.edu/guides-sub-pages/syllabus-design/

Appendix II: Licenses

PARTIES:

1. **Taylor and Francis Group LLC (Books) US** (Licensor); and
2. **Matthew Marquis** (Licensee).

Thank you for your recent permission request. Some permission requests for use of material published by the Licensor, such as this one, are now being facilitated by PLSclear.

Set out in this licence cover sheet (the **Licence Cover Sheet**) are the principal terms under which Licensor has agreed to license certain Licensed Material (as defined below) to Licensee. The terms in this Licence Cover Sheet are subject to the attached General Terms and Conditions, which together with this Licence Cover Sheet constitute the licence agreement (the **Licence**) between Licensor and Licensee as regards the Licensed Material. The terms set out in this Licence Cover Sheet take precedence over any conflicting provision in the General Terms and Conditions.

Free Of Charge Licence Terms

Licence Date:	05/02/2024
PLSclear Ref No:	90545

The Licensor

Company name:	Taylor and Francis Group LLC (Books) US
Address:	711 3rd Avenue New York 10017 United States US

The Licensee

Licensee Contact Name:	Matthew Marquis
Licensee Address:	507 Hudson Ct Davis 95616 United States

Licensed Material

title:	Textbook of Ion Channels Volume I
ISBN:	9780367538156
publisher:	Taylor and Francis Group LLC (Books) US

Chapter name or number	6
Number of words	7650
Page numbers	101-117
Number of pages	17
Identifier / First few words	Mechanisms of Inhibition
Author of original work	Matthew J. Marquis and Jon T. Sack
Are you the author of the content that you are requesting to reuse?	Yes
Will you be changing or editing the text?	No

For Use In Licensee's Publication(s)

usage type	Book, Journal, Magazine or Academic Paper-Thesis or Dissertation
Will your dissertation be placed in an online repository?	Yes
Author	Matthew J. Marquis
Estimated publication date	2024-06-20
Language	English
Title of dissertation/thesis	State-Dependent Binding of Small-Molecules to the Central Cavities of Voltage-Gated Potassium Channels
University or institution	University of California, Davis
Unlimited circulation?	Yes

Rights Granted

Exclusivity:	Non-Exclusive
Format:	Thesis or Dissertation
Language:	English
Territory:	World
Duration:	Lifetime of Licensee's Edition
Maximum Circulation:	Unlimited

GENERAL TERMS AND CONDITIONS

1. Definitions and Interpretation

1.1 Capitalised words and expressions in these General Terms and Conditions have the meanings given to them in the Licence Cover Sheet.

1.2 In this Licence any references (express or implied) to statutes or provisions are references to those statutes or provisions as amended or re-enacted from time to time. The term including will be construed as illustrative, without limiting the sense or scope of the words preceding it. A reference to in writing or written includes faxes and email. The singular includes the plural and vice versa.

2. Grant of Rights

2.1 The Licensor grants to Licensee the non-exclusive right to use the Licensed Material as specified in the Licence Cover Sheet.

2.2 The rights licensed to Licensee under this Licence do not include the right to use any third party copyright material incorporated in the Licensed Material. Licensee should check the Licensed Material carefully and seek permission for the use of any such third party copyright material from the relevant copyright owner(s).

2.3 Unless otherwise stated in the Licence Cover Sheet, the Licensed Material may be:

2.3.1 subjected to minor editing, including for the purposes of creating alternative formats to provide access for a beneficiary person (provided that any such editing does not amount to derogatory treatment); and/or

2.3.2 used for incidental promotional use (such as online retail providers' search facilities).

2.4 Save as expressly permitted in this Licence or as otherwise permitted by law, no use or modification of the Licensed Material may be made by Licensee without Licensor's prior written permission.

3. Copyright Notice and Acknowledgement

3.1 Licensee must ensure that the following notices and acknowledgements are reproduced prominently alongside each reproduction by Licensee of the Licensed Material:

3.1.1 the title and author of the Licensed Material;

3.1.2 the copyright notice included in the Licensed Material; and

3.1.3 the statement "Reproduced with permission of The Licensor through PLSclear."

4. Reversion of Rights

4.1 The rights licensed to Licensee under this Licence will terminate immediately and automatically upon the earliest of the following events to occur:

4.1.1 the Licensed Material not being used by Licensee within 18 months of the Licence Date;

4.1.2 expiry of the Licence Duration; or

4.1.3 the Maximum Circulation being reached.

5. Miscellaneous

5.1 By using the Licensed Material, Licensee will be deemed to have accepted all the terms and conditions contained in this Licence.

5.2 This Licence contains the entire understanding and agreement of the parties relating to its subject matter and supersedes in all respects any previous or other existing arrangements, agreements or understandings between the parties whether oral or written in relation to its subject matter.

5.3 Licensee may not assign this Licence or any of its rights or obligations hereunder to any third party without Licensor's prior written consent.

5.4 This Licence is governed by and shall be construed in accordance with the laws of England and Wales and the parties hereby irrevocably submit to the non-exclusive jurisdiction of the Courts of England and Wales as regards any claim, dispute or matter arising under or in relation to this Licence.

CCC Marketplace

Order Date	06-Feb-2024	Type of Use	Republish in a thesis/dissertation
Order License ID	1447780-1		
ISSN	1540-7748	Publisher	ROCKEFELLER UNIVERSITY PRESS
		Portion	Chapter/article

LICENSED CONTENT

Publication Title	JOURNAL OF GENERAL PHYSIOLOGY. ONLINE	Country	United States of America
		Rightsholder	Rockefeller University Press
Article Title	Mechanism of use-dependent Kv2 channel inhibition by RY785.	Publication Type	Journal
		Issue	6
Author/Editor	Society of General Physiologists.	Volume	154
Date	01/01/1918		
Language	English		

REQUEST DETAILS

Portion Type	Chapter/article	Rights Requested	Main product
Page Range(s)	1-14	Distribution	Worldwide
Total Number of Pages	14	Translation	Original language of publication
Format (select all that apply)	Electronic	Copies for the Disabled?	No
Who Will Republish the Content?	Academic institution	Minor Editing Privileges?	Yes
		Incidental Promotional Use?	No
Duration of Use	Life of current and all future editions	Currency	USD
Lifetime Unit Quantity	Up to 499		

NEW WORK DETAILS

Title	State-Dependent Binding of Small-Molecules to the Central Cavities of Voltage-Gated Potassium Channels	Institution Name	University of California, Davis
		Expected Presentation Date	2024-06-20
Instructor Name	Matthew Marquis		

ADDITIONAL DETAILS

Order Reference Number	N/A	**The Requesting Person / Organization to Appear on the License**	Matthew Marquis

REQUESTED CONTENT DETAILS

Title, Description or Numeric Reference of the Portion(s)	Mechanism of use-dependent Kv2 channel inhibition by RY785	**Title of the Article / Chapter the Portion Is From**	Mechanism of use-dependent Kv2 channel inhibition by RY785.
Editor of Portion(s)	Marquis, Matthew James; Sack, Jon T	**Author of Portion(s)**	Marquis, Matthew James; Sack, Jon T
Volume / Edition	154	**Issue, if Republishing an Article From a Serial**	6
Page or Page Range of Portion	1-14	**Publication Date of Portion**	2022-06-05

Marketplace Permissions General Terms and Conditions

The following terms and conditions ("General Terms"), together with any applicable Publisher Terms and Conditions, govern User's use of Works pursuant to the Licenses granted by Copyright Clearance Center, Inc. ("CCC") on behalf of the applicable Rightsholders of such Works through CCC's applicable Marketplace transactional licensing services (each, a "Service").

1) **Definitions.** For purposes of these General Terms, the following definitions apply:

"License" is the licensed use the User obtains via the Marketplace platform in a particular licensing transaction, as set forth in the Order Confirmation.

"Order Confirmation" is the confirmation CCC provides to the User at the conclusion of each Marketplace transaction. "Order Confirmation Terms" are additional terms set forth on specific Order Confirmations not set forth in the General Terms that can include terms applicable to a particular CCC transactional licensing service and/or any Rightsholder-specific terms.

"Rightsholder(s)" are the holders of copyright rights in the Works for which a User obtains licenses via the Marketplace platform, which are displayed on specific Order Confirmations.

"Terms" means the terms and conditions set forth in these General Terms and any additional Order Confirmation Terms collectively.

"User" or "you" is the person or entity making the use granted under the relevant License. Where the person accepting the Terms on behalf of a User is a freelancer or other third party who the User authorized to accept the General Terms on the User's behalf, such person shall be deemed jointly a User for purposes of such Terms.

"Work(s)" are the copyright protected works described in relevant Order Confirmations.

2) **Description of Service.** CCC's Marketplace enables Users to obtain Licenses to use one or more Works in accordance with all relevant Terms. CCC grants Licenses as an agent on behalf of the copyright rightsholder identified in the relevant Order Confirmation.

3) **Applicability of Terms.** The Terms govern User's use of Works in connection with the relevant License. In the event of any conflict between General Terms and Order Confirmation Terms, the latter shall govern. User acknowledges that Rightsholders have complete discretion whether to grant any permission, and whether to place any limitations on any grant, and that CCC has no right to supersede or to modify any such discretionary act by a Rightsholder.

4) **Representations; Acceptance.** By using the Service, User represents and warrants that User has been duly authorized by the User to accept, and hereby does accept, all Terms.

5) **Scope of License; Limitations and Obligations.** All Works and all rights therein, including copyright rights, remain the sole and exclusive property of the Rightsholder. The License provides only those rights expressly set forth in the terms and conveys no other rights in any Works

6) **General Payment Terms.** User may pay at time of checkout by credit card or choose to be invoiced. If the User chooses to be invoiced, the User shall: (i) remit payments in the manner identified on specific invoices, (ii) unless otherwise specifically stated in an Order Confirmation or separate written agreement, Users shall remit payments upon receipt of the relevant invoice from CCC, either by delivery or notification of availability of the invoice via the Marketplace platform, and (iii) if the User does not pay the invoice within 30 days of receipt, the User may incur a service charge of 1.5% per month or the maximum rate allowed by applicable law, whichever is less. While User may exercise the rights in the License immediately upon receiving the Order Confirmation, the License is automatically revoked and is null and void, as if it had never been issued, if CCC does not receive complete payment on a timely basis.

7) **General Limits on Use.** Unless otherwise provided in the Order Confirmation, any grant of rights to User (i) involves only the rights set forth in the Terms and does not include subsequent or additional uses, (ii) is non-exclusive and non-transferable, and (iii) is subject to any and all limitations and restrictions (such as, but not limited to, limitations on duration of use or circulation) included in the Terms. Upon completion of the licensed use as set forth in the Order Confirmation, User shall either secure a new permission for further use of the Work(s) or immediately cease any new use of the Work(s) and shall render inaccessible (such as by deleting or by removing or severing links or other locators) any further copies of the Work. User may only make alterations to the Work if and as expressly set forth in the Order Confirmation. No Work may be used in any way that is unlawful, including without limitation if such use would violate applicable sanctions laws or regulations, would be defamatory, violate the rights of third parties (including such third parties' rights of copyright, privacy, publicity, or other tangible or intangible property), or is otherwise illegal, sexually explicit, or obscene. In addition, User may not conjoin a Work with any other material that may result in damage to the reputation of the Rightsholder. Any unlawful use will render any licenses hereunder null and void. User agrees to inform CCC if it becomes aware of any infringement of any rights in a Work and to cooperate with any reasonable request of CCC or the Rightsholder in connection therewith.

8) **Third Party Materials.** In the event that the material for which a License is sought includes third party materials (such as photographs, illustrations, graphs, inserts and similar materials) that are identified in such material as having been used by permission (or a similar indicator), User is responsible for identifying, and seeking separate licenses (under this Service, if available, or otherwise) for any of such third party materials; without a separate license, User may not use such third party materials via the License.

9) **Copyright Notice.** Use of proper copyright notice for a Work is required as a condition of any License granted under the Service. Unless otherwise provided in the Order Confirmation, a proper copyright notice will read substantially as follows: "Used with permission of [Rightsholder's name], from [Work's title, author, volume, edition number and year of copyright]; permission conveyed through Copyright Clearance Center, Inc." Such notice must be provided in a reasonably legible font size and must be placed either on a cover page or in another location that any person, upon gaining access to the material which is the subject of a permission, shall see, or in the case of republication Licenses, immediately adjacent to the Work as used (for example, as part of a by-line or footnote) or in the place where substantially all other credits or notices for the new work containing the republished Work are located. Failure to include the required notice results in loss to the Rightsholder and CCC, and the User shall be liable to pay liquidated damages for each such failure equal to twice the use fee specified in the Order Confirmation, in addition to the use fee itself and any other fees and charges specified.

10) **Indemnity.** User hereby indemnifies and agrees to defend the Rightsholder and CCC, and their respective employees and directors, against all claims, liability, damages, costs, and expenses, including legal fees and expenses, arising out of any use of a Work beyond the scope of the rights granted herein and in the Order Confirmation, or any use of a Work which has been altered in any unauthorized way by User, including claims of defamation or infringement of rights of copyright, publicity, privacy, or other tangible or intangible property.

11) **Limitation of Liability.** UNDER NO CIRCUMSTANCES WILL CCC OR THE RIGHTSHOLDER BE LIABLE FOR ANY DIRECT, INDIRECT, CONSEQUENTIAL, OR INCIDENTAL DAMAGES (INCLUDING WITHOUT LIMITATION DAMAGES FOR LOSS OF BUSINESS PROFITS OR INFORMATION, OR FOR BUSINESS INTERRUPTION) ARISING OUT OF THE USE OR INABILITY TO USE A WORK, EVEN IF ONE OR BOTH OF THEM HAS BEEN ADVISED OF THE POSSIBILITY OF SUCH DAMAGES. In any event, the total liability of the Rightsholder and CCC (including their respective employees and directors) shall not exceed the total amount actually paid by User for the relevant License. User assumes full liability for the actions and omissions of its principals, employees, agents, affiliates, successors, and assigns.

12) **Limited Warranties.** THE WORK(S) AND RIGHT(S) ARE PROVIDED "AS IS." CCC HAS THE RIGHT TO GRANT TO USER THE RIGHTS GRANTED IN THE ORDER CONFIRMATION DOCUMENT. CCC AND THE RIGHTSHOLDER DISCLAIM ALL OTHER WARRANTIES RELATING TO THE WORK(S) AND RIGHT(S), EITHER EXPRESS OR IMPLIED, INCLUDING WITHOUT LIMITATION IMPLIED WARRANTIES OF MERCHANTABILITY OR FITNESS FOR A PARTICULAR PURPOSE. ADDITIONAL RIGHTS MAY BE REQUIRED TO USE ILLUSTRATIONS, GRAPHS, PHOTOGRAPHS, ABSTRACTS, INSERTS, OR OTHER PORTIONS OF THE WORK (AS OPPOSED TO THE ENTIRE WORK) IN A MANNER CONTEMPLATED BY USER; USER UNDERSTANDS AND AGREES THAT NEITHER CCC NOR THE RIGHTSHOLDER MAY HAVE SUCH ADDITIONAL RIGHTS TO GRANT.

13) **Effect of Breach.** Any failure by User to pay any amount when due, or any use by User of a Work beyond the scope of the License set forth in the Order Confirmation and/or the Terms, shall be a material breach of such License. Any breach not cured within 10 days of written notice thereof shall result in immediate termination of such License without further notice. Any unauthorized (but licensable) use of a Work that is terminated immediately upon notice thereof may be liquidated by payment of the Rightsholder's ordinary license price therefor; any unauthorized (and unlicensable) use that is not terminated immediately for any reason (including, for example, because materials containing the Work cannot reasonably be recalled) will be subject to all remedies available at law or in equity, but in no event to a payment of less than three times the Rightsholder's ordinary license price for the most closely analogous licensable use plus Rightsholder's and/or CCC's costs and expenses incurred in collecting such payment.

14) **Additional Terms for Specific Products and Services.** If a User is making one of the uses described in this Section 14, the additional terms and conditions apply:

a) ***Print Uses of Academic Course Content and Materials (photocopies for academic coursepacks or classroom handouts).*** For photocopies for academic coursepacks or classroom handouts the following additional terms apply:

i) The copies and anthologies created under this License may be made and assembled by faculty members individually or at their request by on-campus bookstores or copy centers, or by off-campus copy shops and other similar entities.

ii) No License granted shall in any way: (i) include any right by User to create a substantively non-identical copy of the Work or to edit or in any other way modify the Work (except by means of deleting material immediately preceding or following the entire portion of the Work copied) (ii) permit "publishing ventures" where any particular anthology would be systematically marketed at multiple institutions.

iii) Subject to any Publisher Terms (and notwithstanding any apparent contradiction in the Order Confirmation arising from data provided by User), any use authorized under the academic pay-per-use service is limited as follows:

A) any License granted shall apply to only one class (bearing a unique identifier as assigned by the institution, and thereby including all sections or other subparts of the class) at one institution;

B) use is limited to not more than 25% of the text of a book or of the items in a published collection of essays, poems or articles;

C) use is limited to no more than the greater of (a) 25% of the text of an issue of a journal or other periodical or (b) two articles from such an issue;

D) no User may sell or distribute any particular anthology, whether photocopied or electronic, at more than one institution of learning;

E) in the case of a photocopy permission, no materials may be entered into electronic memory by User except in order to produce an identical copy of a Work before or during the academic term (or analogous period) as to which any particular permission is granted. In the event that User shall choose to retain materials that are the subject of a photocopy permission in electronic memory for purposes of producing identical copies more than one day after such retention (but still within the scope of any permission granted), User must notify CCC of such fact in the applicable permission request and such retention shall constitute one copy actually sold for purposes of calculating permission fees due; and

F) any permission granted shall expire at the end of the class. No permission granted shall in any way include any right by User to create a substantively non-identical copy of the Work or to edit or in any other way modify the Work (except by means of deleting material immediately preceding or following the entire portion of the Work copied).

iv) Books and Records; Right to Audit. As to each permission granted under the academic pay-per-use Service, User shall maintain for at least four full calendar years books and records sufficient for CCC to determine the numbers of copies made by User under such permission. CCC and any representatives it may designate shall have the right to audit such books and records at any time during User's ordinary business hours, upon two days' prior notice. If any such audit shall determine that User shall have underpaid for, or underreported, any photocopies sold or by three percent (3%) or more, then User shall bear all the costs of any such audit; otherwise, CCC shall bear the costs of any such audit. Any amount determined by such audit to have been underpaid by User shall immediately be paid to CCC by User, together with interest thereon at the rate of 10% per annum from the date such amount was originally due. The provisions of this paragraph shall survive the termination of this License for any reason.

b) ***Digital Pay-Per-Uses of Academic Course Content and Materials (e-coursepacks, electronic reserves, learning management systems, academic institution intranets).*** For uses in e-coursepacks, posts in electronic reserves, posts in learning management systems, or posts on academic institution intranets, the following additional terms apply:

i) The pay-per-uses subject to this Section 14(b) include:

A) **Posting e-reserves, course management systems, e-coursepacks for text-based content,** which grants authorizations to import requested material in electronic format, and allows electronic access to this material to members of a designated college or university class, under the direction of an instructor designated by the college or university, accessible only under appropriate electronic controls (e.g., password);

B) **Posting e-reserves, course management systems, e-coursepacks for material consisting of photographs or other still images not embedded in text,** which grants not only the authorizations described in Section 14(b)(i)(A) above, but also the following authorization: to include the requested material in course materials for use consistent with Section 14(b)(i)(A) above, including any necessary resizing, reformatting or modification of the resolution of such requested material (provided that such modification does not alter the underlying editorial content or meaning of the requested material, and provided that the resulting modified content is used solely within the scope of, and in a manner consistent with, the particular authorization described in the Order Confirmation and the Terms), but not including any other form of manipulation, alteration or editing of the requested material;

C) **Posting e-reserves, course management systems, e-coursepacks or other academic distribution for audiovisual content,** which grants not only the authorizations described in Section 14(b)(i)(A) above, but also the following authorizations: (i) to include the requested material in course materials for use consistent with Section 14(b)(i)(A) above; (ii) to display and perform the requested material to such members of such class in the physical classroom or remotely by means of streaming media or other video formats; and (iii) to "clip" or reformat the requested material for purposes of time or content management or ease of delivery, provided that such "clipping" or reformatting does not alter the underlying editorial content or meaning of the requested material and that the resulting material is used solely within the scope of, and in a manner consistent with, the particular authorization described in the Order Confirmation and the Terms. Unless expressly set forth in the relevant Order Conformation, the License does not authorize any other form of manipulation, alteration or editing of the requested material.

ii) Unless expressly set forth in the relevant Order Confirmation, no License granted shall in any way: (i) include any right by User to create a substantively non-identical copy of the Work or to edit or in any other way modify the Work (except by means of deleting material immediately preceding or following the entire portion of the Work copied or, in the case of Works subject to Sections 14(b)(1)(B) or (C) above, as described in such Sections) (ii) permit "publishing ventures" where any particular course materials would be systematically marketed at multiple institutions.

iii) Subject to any further limitations determined in the Rightsholder Terms (and notwithstanding any apparent contradiction in the Order Confirmation arising from data provided by User), any use authorized under the electronic course content pay-per-use service is limited as follows:

A) any License granted shall apply to only one class (bearing a unique identifier as assigned by the institution, and thereby including all sections or other subparts of the class) at one institution;

B) use is limited to not more than 25% of the text of a book or of the items in a published collection of essays, poems or articles;

C) use is limited to not more than the greater of (a) 25% of the text of an issue of a journal or other periodical or (b) two articles from such an issue;

D) no User may sell or distribute any particular materials, whether photocopied or electronic, at more than one institution of learning;

E) electronic access to material which is the subject of an electronic-use permission must be limited by means of electronic password, student identification or other control permitting access solely to students and instructors in the class;

F) User must ensure (through use of an electronic cover page or other appropriate means) that any person, upon gaining electronic access to the material, which is the subject of a permission, shall see:

- a proper copyright notice, identifying the Rightsholder in whose name CCC has granted permission,
- a statement to the effect that such copy was made pursuant to permission,
- a statement identifying the class to which the material applies and notifying the reader that the material has been made available electronically solely for use in the class, and
- a statement to the effect that the material may not be further distributed to any person outside the class, whether by copying or by transmission and whether electronically or in paper form, and User must also ensure that such cover page or other means will print out in the event that the person accessing the material chooses to print out the material or any part thereof.

G) any permission granted shall expire at the end of the class and, absent some other form of authorization, User is thereupon required to delete the applicable material from any electronic storage or to block electronic access to the applicable material.

iv) Uses of separate portions of a Work, even if they are to be included in the same course material or the same university or college class, require separate permissions under the electronic course content pay-per-use Service. Unless otherwise provided in the Order Confirmation, any grant of rights to User is limited to use completed no later than the end of the academic term (or analogous period) as to which any particular permission is granted.

v) Books and Records; Right to Audit. As to each permission granted under the electronic course content Service, User shall maintain for at least four full calendar years books and records sufficient for CCC to determine the numbers of copies made by User under such permission. CCC and any representatives it may designate shall have the right to audit such books and records at any time during User's ordinary business hours, upon two days' prior notice. If any such audit shall determine that User shall have underpaid for, or underreported, any electronic copies used by three percent (3%) or more, then User shall bear all the costs of any such audit; otherwise, CCC shall bear the costs of any such audit. Any amount determined by such audit to have been underpaid by User shall immediately be paid to CCC by User, together with interest thereon at the rate of 10% per annum from the date such amount was originally due. The provisions of this paragraph shall survive the termination of this license for any reason.

c) ***Pay-Per-Use Permissions for Certain Reproductions (Academic photocopies for library reserves and interlibrary loan reporting) (Non-academic internal/external business uses and commercial document delivery).*** The License expressly excludes the uses listed in Section (c)(i)-(v) below (which must be subject to separate license from the applicable Rightsholder) for: academic photocopies for library reserves and interlibrary loan reporting; and non-academic internal/external business uses and commercial document delivery.

i) electronic storage of any reproduction (whether in plain-text, PDF, or any other format) other than on a transitory basis;

ii) the input of Works or reproductions thereof into any computerized database;

iii) reproduction of an entire Work (cover-to-cover copying) except where the Work is a single article;

iv) reproduction for resale to anyone other than a specific customer of User;

v) republication in any different form. Please obtain authorizations for these uses through other CCC services or directly from the rightsholder.

Any license granted is further limited as set forth in any restrictions included in the Order Confirmation and/or in these Terms.

d) ***Electronic Reproductions in Online Environments (Non-Academic-email, intranet, internet and extranet).*** For "electronic reproductions", which generally includes e-mail use (including instant messaging or other electronic transmission to a defined group of recipients) or posting on an intranet, extranet or Intranet site (including any display or performance incidental thereto), the following additional terms apply:

i) Unless otherwise set forth in the Order Confirmation, the License is limited to use completed within 30 days for any use on the Internet, 60 days for any use on an intranet or extranet and one year for any other use, all as measured from the "republication date" as identified in the Order Confirmation, if any, and otherwise from the date of the Order Confirmation.

ii) User may not make or permit any alterations to the Work, unless expressly set forth in the Order Confirmation (after request by User and approval by Rightsholder); provided, however, that a Work consisting of photographs or other still images not embedded in text may, if necessary, be resized, reformatted or have its resolution modified without additional express permission, and a Work consisting of audiovisual content may, if necessary, be "clipped" or reformatted for purposes of time or content management or ease of delivery (provided that any such resizing, reformatting, resolution modification or "clipping" does not alter the underlying editorial content or meaning of the Work used, and that the resulting material is used solely within the scope of, and in a manner consistent with, the particular License described in the Order Confirmation and the Terms.

15) **Miscellaneous.**

a) User acknowledges that CCC may, from time to time, make changes or additions to the Service or to the Terms, and that Rightsholder may make changes or additions to the Rightsholder Terms. Such updated Terms will replace the prior terms and conditions in the order workflow and shall be effective as to any subsequent Licenses but shall not apply to Licenses already granted and paid for under a prior set of terms.

b) Use of User-related information collected through the Service is governed by CCC's privacy policy, available online at www.copyright.com/about/privacy-policy/.

c) The License is personal to User. Therefore, User may not assign or transfer to any other person (whether a natural person or an organization of any kind) the License or any rights granted thereunder; provided, however, that, where applicable, User may assign such License in its entirety on written notice to CCC in the event of a transfer of all or substantially all of User's rights in any new material which includes the Work(s) licensed under this Service.

d) No amendment or waiver of any Terms is binding unless set forth in writing and signed by the appropriate parties, including, where applicable, the Rightsholder. The Rightsholder and CCC hereby object to any terms contained in any writing prepared by or on behalf of the User or its principals, employees, agents or affiliates and purporting to govern or otherwise relate to the License described in the Order Confirmation, which terms are in any way inconsistent with any Terms set forth in the Order Confirmation, and/or in CCC's standard operating procedures, whether such writing is prepared prior to, simultaneously with or subsequent to the Order Confirmation, and whether such writing appears on a copy of the Order Confirmation or in a separate instrument.

e) The License described in the Order Confirmation shall be governed by and construed under the law of the State of New York, USA, without regard to the principles thereof of conflicts of law. Any case, controversy, suit, action, or proceeding arising out of, in connection with, or related to such License shall be brought, at CCC's sole discretion, in any federal or state court located in the County of New York, State of New York, USA, or in any federal or state court whose geographical jurisdiction covers the location of the Rightsholder set forth in the Order Confirmation. The parties expressly submit to the personal jurisdiction and venue of each such federal or state court.

Last updated October 2022